Novel Aspects in the Microphase Separation of Block Copolymers

Thesis by

Wei Zheng

In Partial Fulfillment of the Requirements

for the Degree of

Doctor of Philosophy

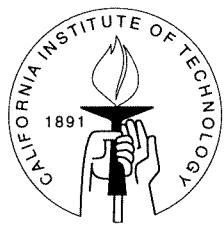

California Institute of Technology

Pasadena, California

1997

(Submitted August 24, 1996)

Acknowledgements

Many people have helped me a great deal during my time at Caltech, and it is impossible to thank everyone to whom I am indebted. Several people stand out, however, and I will endeavor to thank them here.

First and foremost, I am deeply indebted to my advisor, Professor Zhen-Gang Wang for guiding me to a new and exciting field, polymer physics, and for his encouragement and support. His inspiration and guidance have been invaluable to me during my graduate school career. I would also like to thank my former advisor Professor Peter Weichman for helping me understand many issues in critical phenomena.

I would like to thank my fellow graduate students Jeremy Martin and Shu-Yan Qi for many useful discussions in polymer physics and lending a helping hand when I had computer problems. I would also like to thank Suresh Guptha for providing sorely needed computer support.

Among all the friends whose friendship I have cherished, I particularly wish to thank my former officemate, Eugenia Kuo for many wonderful moments that we spent together. Her great friendship had added color and joy to my graduate student life.

There are no words in the world to express my deepest gratitude to my family for their love, support, sacrifices, and unfailing confidence in my ability to succeed. They are the sources of every single achievement that I have had in the past thirty years.

Abstract

Several novel aspects of the microphase separation transition of block copolymers have been studied. These aspects are exemplified by the following three systems:

(1) ABC triblock copolymers;

(2) Weakly charged diblock copolymers;

(3) Diblock copolymers in confined geometries.

For ABC triblock copolymers, results from theoretical calculations of the morphological phase diagrams in the strong segregation limit are presented. The chain conformation free energy is approximated following an approach proposed by Ohta and Kawasaki. Our study focuses on two unique features of the ABC triblock copolymers, namely, the dependence of the morphology on the sequence of the triblock chain and the relative strength of the various interaction parameters. Our results compare favorably with experimental observations. In addition, we predict the existence of some new structures that have yet to be observed experimentally.

For weakly charged diblock copolymers, a theoretical framework is developed. This framework combines the Random Phase Approximation and the Poisson-Boltzmann equation in order to consistently treat the electrostatic interactions between all charged species and the free energy contributions from the connectivity of the diblock copolymers. A Landau-Ginzburg effective free energy is derived and is used to study the microphase separation of charged-neutral block copolymers with an arbitrary amount of added salt in the weak segregation limit. Study of the spinodal limit of the system shows not only greatly enhanced compatibility between A and B blocks in comparison with the corresponding neutral system, but also inhibition of microphase separation under certain conditions. A criterion for microphase separation is derived and phase diagrams under various conditions are presented. Study of concentration fluctuation near the order-disorder transition demonstrates that the breaking of the interchange symmetry leads to new scaling of fluctuation corrections

at a fixed value of monomer charge density α.

The morphology of diblock copolymer melt confined between two solid walls in the strong segregation limit is studied by extending the method developed by Ohta and Kawasaki to include surface effects. We focus on two new features which are absent in simple diblock copolymers: the competition between the surface interactions and the confinement effects, and the breaking of the rotational and translational symmetry. The first new feature is demonstrated by studying the equilibrium properties of symmetric/nearly symmetric diblock copolymers confined between two identical walls with a small preferential surface affinity. The second feature is illustrated by studying the phase behavior of diblock copolymers with arbitrary value of volume fraction. For phase transition involves morphologies with three dimensional structure, the broken rotational and translational symmetry leads to the dependence of the transition volume fraction on the distance between the two plates. The influence of surface effects on diblock copolymers confined between two distinct plates is also studied by presenting phase diagrams for two special cases.

Contents

List of Figures

Chapter 1 Introduction

1.1 Motivation

A polymer is a large molecule composed of many fundamental units, called monomers, connected by chemical bonds. If these monomers are identical, the result is a "homopolymer"; if the monomers are of two or more kinds, the product is a hetero- or copolymer that can be either random or have a well-defined sequence.

Polymers are the most commonly encountered complex material in the world. With the exception of metals and inorganic compounds, most of the materials that we come into contact with everyday are polymeric. These include proteins and nucleic acids in our bodies; the fibers we use for clothing; the protein and starch we eat; the elastomers in our automobile tires, paints, plastic wall and floor coverings, foam insulation, and so forth, in our house.

Although there are many varieties of polymers, they all have some common features. The rapid growth of polymer science over the past few decades has been due in large part to deepening understanding of the relationship between the physical characteristics of polymers and the structure of the polymer molecules. It has become apparent that molecular properties such as chain length, chain stiffness, degree of branching, molecular architecture, and the number of charge groups are more significant than the detailed chemical make-up of polymers in determining their physical characteristics [1]. An understanding of the relationship between such molecular properties and the physical characteristics can help efficiently direct the synthesis of new materials with useful properties.

One of the more interesting and extensively studied class of polymers are the block copolymers. A block copolymer is a polymer composed of two or more sequences of monomers joined together by chemical bonds. Several commonly encountered block copolymers are depicted in Figure 1.1. Block copolymers are fascinating materials with unique mechanical, optical, and structural properties. They can be used as surfactants, as compatibilizing agents in polymer blends, and as adhesives. The

most important property of block copolymers is their ability to self-assemble. Due to the incompatibility between different polymer species in a block copolymer, the very low value of entropy of mixing for macromolecules, and the fact that the different polymer blocks are connected by chemical bonds, block copolymers undergo a microphase separation and assemble into various ordered structures [8]- [18]. Recently, self-assembled ordered polymer structures with periodicities on the nanometer scale have become an important area of study because of their potential applications in nano-technology. For instance, it has been suggested that block copolymers can be used in the development of new classes of electronic devices [19] , [20] and in the synthesis of mesoporous solids which can be used as catalysts and sorption media [21], [22]. An important factor contributing to the block copolymers' widespread popularity is the controllability of the size and morphology of the microstructure, and hence the material properties, by varying the molecular weight, molecular architecture, and composition of the copolymers.

1.2 Definition and Background

The equilibrium phase behavior of block copolymer is controlled by four factors: (1) molecular architecture (see Figure 1.1), (2) degree of polymerization, (3) composition, and (4) choice of monomers. The number of molecular configurations available to connect chemically distinct polymer species is almost unlimited. Some of the commonly encounted molecular architectures in block copolymers are shown in Figure 1.1. The degree of polymerization is the total number of repeat units (i.e., monomers) that make up a polymer chain, and is denoted as N. Composition generally refers to the overall volume fraction of a component. In a diblock copolymer $A-B$, if A and B have monomer volumes v_A and v_B, respectively, and the degree of polymerization of blocks A and B are N_A and N_B, respectively, then the composition of the diblock copolymer $f = N_A v_A/(N_A v_A + N_B v_B)$. If monomer A and B have the same volume, then $f = N_A/(N_A + N_B)$. The choice of a particular pair of monomers establishes the sign and magnitude of the mixing energy. This can, in general, be approximated by the Flory-Huggins segment-segment interaction parameter χ,

$$\chi = \frac{1}{k_B T}\left[\epsilon_{AB} - \frac{1}{2}(\epsilon_{AA} + \epsilon_{BB})\right] \tag{1.1}$$

where ϵ_{ij} represents the contact energy bewteen i and j segments. A negative value of χ results in a favorable energy of mixing, i.e., $A-B$ contacts on average produce a lower system energy than the sum of $A-A$ and $B-B$ contacts. Certain types of $A-B$ interactions, such as hydrogen bonding, can result in a negative χ. Positive values of χ occur when the system energy increases upon forming $A-B$ contacts from unmixed components. Most nonpolar polymers such as polyethylene, polystyrene, and polyisoprene have a positive χ. Experiments show that χ is of order $10^{-3}-10^{-1}$ for most polymer mixtures. (It should be pointed out that in reality, many factors such as the compressibility of the system, anisotropic monomer structures can cause deviation of χ from the simple form expressed in Eq.(1.1) [7]. However, most block copolymer melt can be treated as incompressible and nearly isotropic, we therefore ignore this complication.)

The simplest and best understood block copolymer is an incompressible diblock copolymer melt. In order to establish some of the common concepts for all block copolymers and to provide a natural basis against which the new features of the systems that we are going to study can be best illustrated and appreciated, we will review the microphase separation of diblock copolymers.

The free energy density of diblock copolymers contains both enthalpic and entropic contributions. The enthalpic energy density is proportional to χ, while the entropic energy scales as $S \sim 1/N$. For positive χ, monomers A and B repel each other. Therefore, there is a tendency to decrease the numbers of contacts between monomer A and B in order to lower the contribution of the interaction energy (equal to the enthalpic energy in an incompressible system) to the free energy. However, a decrease in the number of contacts between monomers A and B decreases the entropy of the system and consequently increases the free energy. The equilibrium state of diblock copolymers is the result of a "competition" between these two opposite trends. Hence it is the product χN that controls the state of segregation [8]. For $\chi N \ll 10$, the entropic factor dominates and diblock copolymers exist in a homogeneous state [8]. Increasing χN shifts the free energy balance and leads to local composition fluctuations on a scale proportional to the polymer radius of gyration ($R^2 = R_A^2 + R_B^2$). When $\chi N \simeq 10$, a delicate balance exists between the entropic and enthalpic energy. Increasing χN further induces a first order transition to an ordered state. This phase transition, known as the order-disorder transition (ODT), is analogous to the

solidification of liquids, although the periodicity of the ordered structure of diblock copolymers (of nanometer scale) is much larger than the periodicity of crystal lattice. When $\chi N \gg 10$, the microdomain boundaries become sharp as the number of $A-B$ contacts decreases at the expense of additional chain stretching. In this limit, called the strong segregation limit, the enthalpic factor is dominant and ordered structures have narrow interfaces. Figure 1.2 is a schematic representation of the evolution of the structure of symmetic diblock copolymers from a disordered state to an ordered state with increasing χN.

Changes in the composition, f, of diblock copolymers, primarily affect the shape and packing symmetry of the ordered structure. In order to determine the equilibrium properties, and in particular, the dependency of the morphology on f and χN, many theories have been developed. These theories can be broadly grouped into two categories: (i) the weak segregation limit ($\chi N \geq 10$) [8], [3], and (ii) the strong segregation limit ($\chi N \gg 10$) [10]-[18].

The weak segregation theories are based on the assumption that composition fluctuations are small and the effective free energy can be written in the Landau-Ginzburg form. The strong segregation theories assume that the microdomain structures are well developed with very narrow interfaces and account for chain stretching. Although both the weak and strong segregation theories have involved various approximations, by combining results from the different methods the general behavior of diblock copolymers has been revealed. Recently, with the help of modern computers, Matson and Schick [17], Matsen and Bates [9] were able to use the full self-consistent field theory without approximations to study the equilibrium properties of diblock copolymers at the mean field level. The calculation traverses from the weak to the strong segregation regimes [9]. Their results can be summarized as follows. In the weak and intermediate segregation regime, the diblock copolymer melts exhibit the following ordered morphologies upon increasing the volume fraction f: $BCC \rightarrow HEX \rightarrow Gyroid \rightarrow LAM \rightarrow Gyroid \rightarrow HEX \rightarrow BCC$. Here BCC denotes body-centered-cubic packed spheres, HEX is hexagonally packed cylinders, LAM is alternating lamellar structures, and the Gyroid phase is a bicontinuous cubic phase characterized by $Ia\bar{3}d$ space group symmetry. The gyroid phase terminates at a triple point, with a lamellar to hexagonal transition in the weak segregation limit. The stable regions of the gyroid phase pinch off as the strong segregation regime is entered.

Therefore, in the strong segregation limit, the sequence of ordered morphologies upon increasing the volume fraction f is: $BCC \rightarrow HEX \rightarrow LAM \rightarrow HEX \rightarrow BCC$.

1.3 Objectives and Outlines

The purpose of this thesis is to investigate the novel aspects in microphase separation transition of three distinct block copolymer systems resulting from modifications of the simple diblock copolymers:

(1) ABC triblock copolymers,

(2) Weakly charged diblock copolymers,

(3) Diblock copolymers in confined geometries.

An ABC triblock copolymer consists of three different polymer segments A, B, and C joined together by chemical bonds. There are three interaction parameters, χ_{AB}, χ_{BC}, and χ_{CA}, in ABC triblock copolymers, as opposed to one interaction parameter, χ_{AB}, in AB diblock copolymers. The morphological structure of triblock copolymers depends not only on the temperature, the overall molecular weight, and the fraction of each block, but also crucially on the sequence of the blocks in the chain (i.e., whether it is sequenced $A-B-C$, $B-C-A$, or $C-A-B$). Furthermore, there are more ways for ABC triblock copolymers to segregate, thus richer and more complex morphological behaviors are expected in ABC triblock copolymers than in AB diblocks. Indeed,several intriguing new morphologies have been reported in recent experiments [23], [24].

In chapter 2, the morphological phase diagrams for ABC triblock copolymers are calculated in the strong segregation limit. The chain conformation free energy is approximated following an approach proposed by Ohta and Kawasaki [12]. The study focuses on two unique features of the ABC triblock copolymers, namely, the dependence of the morphology on the sequence of the triblock chain, and the relative strength of the various interaction parameters. The results are compared with experimental observations. In addition, the existence of some new structures is predicted.

A charged-neutral diblock copolymer is a block copolymer composed of a charged block A joined to a neutral block B. The system that we are going to study consists of charged-neutral diblock copolymers and some salt ions. This system combines the celebrated microphase separation properties of uncharged diblocks with the properties of

charged polymers. In charged-neutral diblock copolymer systems, the long-range electrostatic interactions and increased mixing entropy due to free ions are influential in determining the microphase separation transition (MST), where the system changes from a disordered state to a periodic structure. Studies of the spinodal instability in charged-neutral diblock copolymers by Marko and Rabin [10], and Mozuelos and de la Cruz [13] show that charged-neutral blocks have greatly enhanced compatibility between A and B in comparison with the corresponding neutral system. However, these works did not study the effects of the charge on the relative stability of the various ordered structures; and the full equilibrium properties of charged-neutral diblock copolymers remained an open question.

In chapter 3, a theoretical framework is developed for charged-neutral diblock copolymers which combines the Random Phase Approximation and the Poisson-Boltzmann equation. This approach allows a consistent treatment of the electrostatic interactions between all charged species and the free energy contributions due to the connectivity of the polymer chains. A Landau-Ginzburg effective free energy is derived and is used to study the microphase separation and the equilibrium properties of charged-neutral block copolymers with an arbitrary amount of added salt in the weak segregation limit. The concentration fluctuation effect near the critical point is studied by extending the method of Fredrickson and Helfand [3]. The scaling of fluctuation corrections is studied in various situations.

As block copolymers are finding increasing applications as thin-film adhesives and surfactants, surface effects on the microphase separation of diblock copolymers has attracted widespread attention. The system consisting of a diblock copolymer melt confined between two solid walls combines both the surface interactions and confinement effects. Recent experimental and theoretical studies show that the presence of surface interactions, in an otherwise homogeneous diblock copolymer melt, yields various interesting surface induced ordering phenomena [17]- [23]. In addition, the existence of two walls introduces a new length scale L (the distance between the two plates) and breaks the rotational and translational symmmetry present in the isotropic bulk system. Therefore, the equilibrium state of confined diblock copolymer melts is a result of competition among the surface interactions, the confinement effects, and the intrinsic driving force for microphase separation in diblock copolymers.

In chapter 4, the morphology of diblock copolymer melts confined between two rigid plates in the strong segregation limit is studied by extending the method developed by Ohta and Kawasaki [12] to include surface effects. By studying the equilibrium properties of symmetric/nearly symmetric diblock copolymers confined between two identical walls with small preferential affinity for one of the blocks, we want to explicitly demonstrate the effect of the competition between the surface interactions and the confinements. In order to explore the surface effects on the stability of various morphologies (lamellar, cylinder, and sphere), we study the phase behavior of diblock copolymers with arbitrary volume fraction f and illustrate the effect of the broken rotational and translational symmmetry on the phase transition.

1.4 Figures

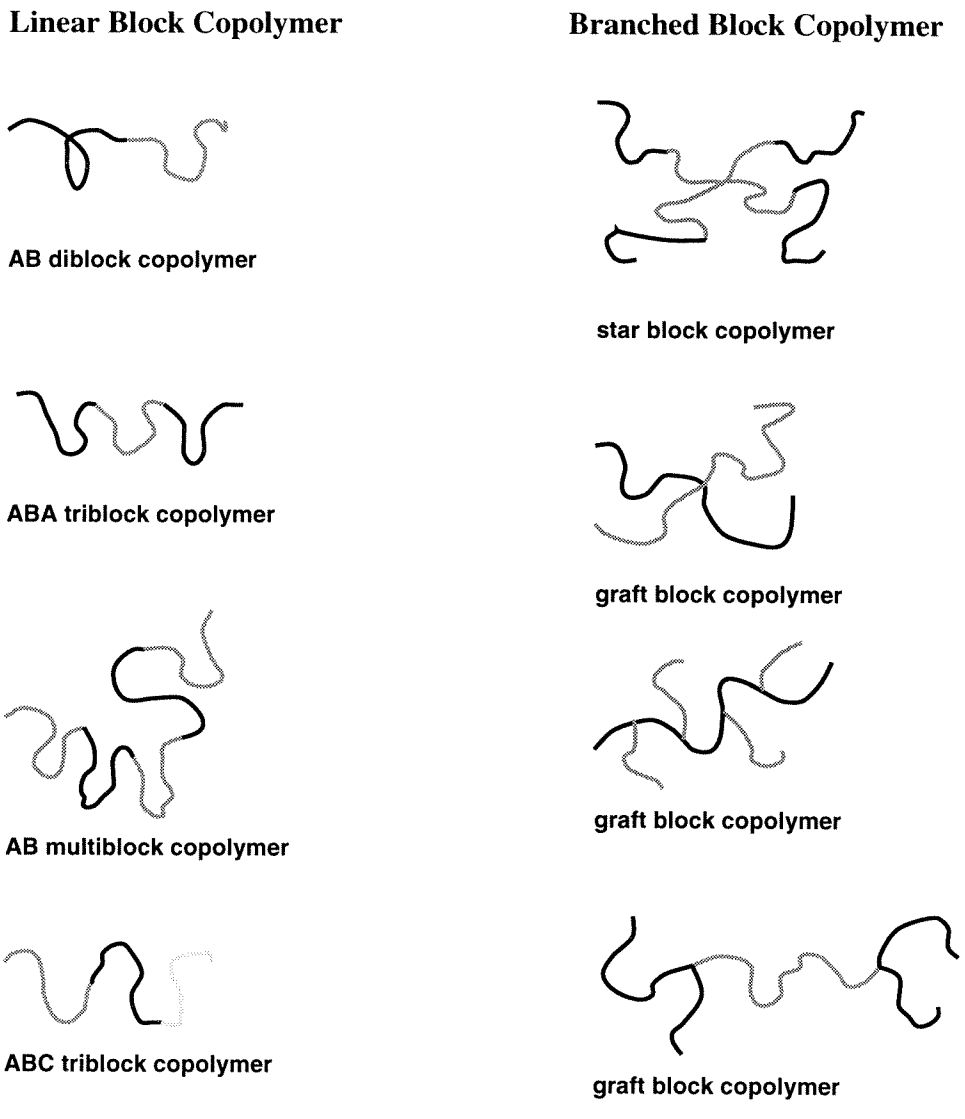

Figure 1.1: Typical block copolymers

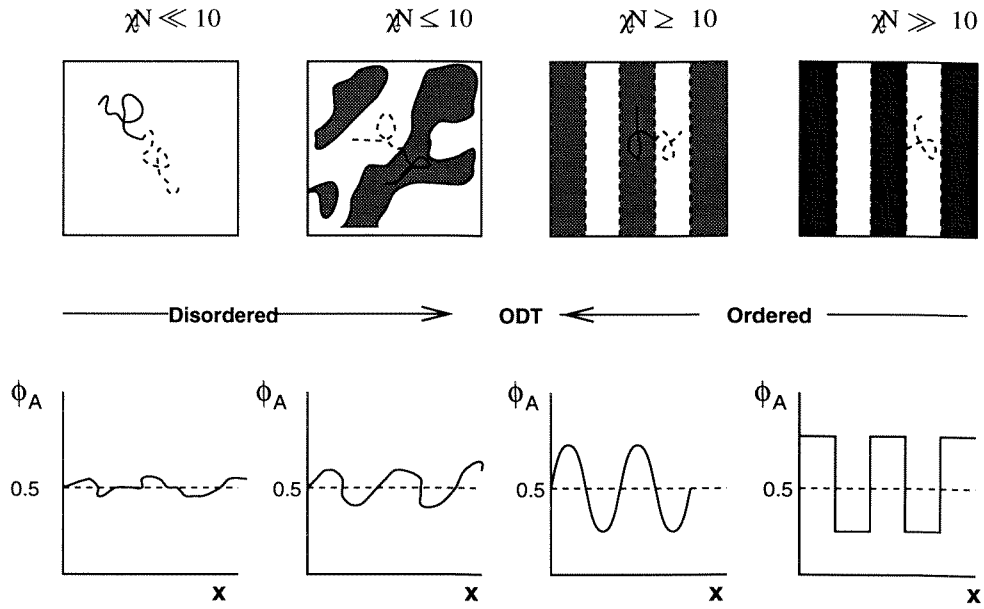

Figure 1.2: Evolution of structure of diblock copolymers with volume fraction $f = 0.5$ as χN increases. The figures on the second row illustrate the change of composition profile.

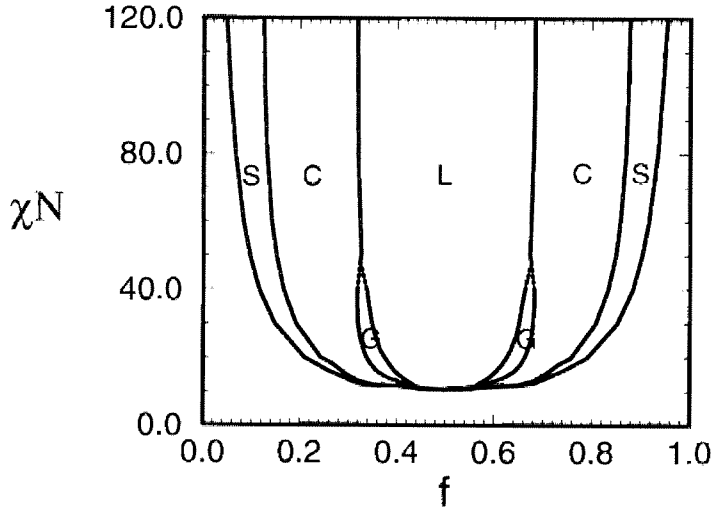

(a)

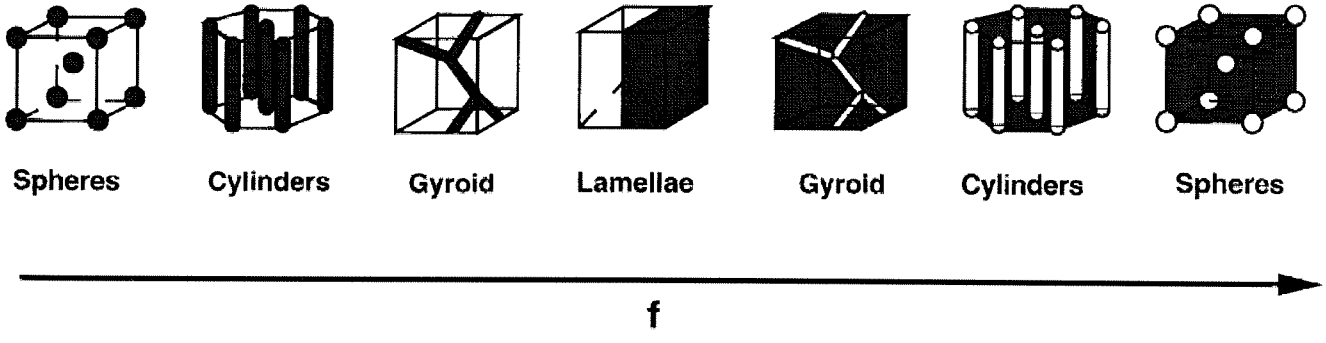

(b)

Figure 1.3: (a) Schematic illustration of phase diagram for $A-B$ diblock copolmers. (b) Schematic representation of morphologies formed in diblock copolymers. Dark: A-rich domains, white: B-rich domains.

Bibliography

[1] Flory, P. *Principles of Polymer Chemistry*; Cornell University Press; Ithaca, NY, 1953

[2] Leibler, L. *Macromolecules 13.* 1602 (1980)

[3] Fredrickson, G.H. and Helfand, E. *J. Chem. Phys* **1987**, *87*, 697

[4] Brazovskii, A. *Sov. Phys. JETP* **1975**, *41*, 85

[5] Bates, F.S. and Fredrickson, G. *Ann. Rev. Phys. Chem. 41.* 525 (1990)

[6] Fried H. and Binder, K. *J. Chem. Phys 94.* 8349 (1991)

[7] Bates, F. S. *Science 251.* 898 1991

[8] Leibler, L. *Macromolecules 13.* 1602 (1980)

[9] Matsen, M. W. and Bates, F. S. *Macromolecules 29.* 1092 (1996), and refrences cited therein

[10] Helfand, E.; Wasserman, Z.R. *Macromolecules* **1980**, *13*, 994 and the earlier refeerences cited therein.

[11] Semenov, A. N. *Sov. Phys. JETP* **1985**, *61*, 733.

[12] Ohta, T., Kawasaki, K. *Macromolecules* **1986**, *19*, 2621

[13] Ohta, T., Kawasaki, K. *Macromolecules* **1990**, *23*, 2413

[14] Hong, K. M. and Noolandi, J. *Macromolecules* **1981**, *14*, 727; ibid **1981**, *14*, 736; Hong, K. M. and Noolandi, J., ibid **1982**, *15*, 482; ibid **1984**, *17*, 1531; Whitmore, M. D., and Noolandi, J., ibid **1988**, *21*, 2972.

[15] Muthukumar, M., Melenkevitz, J., *Macromolecules* **1991**, *24*, 4199

[16] Muthukumar, M., *Macromolecules* **1993**, *26*, 5259

[17] Matsen, M. W., Schick, M., *Macromolecules* **1994**, *27*, 7157

[18] Olmsted , P. D., Milner, S. T., *Phys. Rev. L* **1994**, *72*, 936; ibid **1995**, *74*, 829

[19] Morkved, T. L. Wiltzius, P. Jaege, H. M., Grier, D. C., and Witten, T. A., *Appl. Phys. Lett.* **64**, 422 (1994)

[20] Kirk, W. P., and Reed, M. A., eds. *Nanostructures and Mesoscopic Systems* (Academic, New York, 1992)

[21] Archibald, D. D., and Mann, S., *Nature* **364**, 430(1993)

[22] Krege, C. K., Leonowitcz, M. E., Roth, W. L., Vartuli, J. C., and Beck, J. S., *Nature* **359**, 710 (1992)

[23] Auschra, C., Stadler, R., *Macromolecules* **1993**, *26*, 2171

[24] Auschra, C., Stadler, R., *Macromolecules Rapid Communication* **1994**, *15*, 67

[25] Marko, J. F. and Rabin , Y. *Macromolecules 25.* 1503 (1992)

[26] P. González-Mozuelos and M. O. de la Cruz *J. Chem. Phys 100.* 507 (1994)

[27] Hasegawa, H. and Hashimoto, T., *Macromolecules* **1985**, *18*, 589.

[28] Henkee, C. S., Thomas, E. L., and Fetters, L. J., *J. Mat. Sci.* **1988**, *23*, 1685

[29] Coulon, G., Russell, T. P., Deline, V. R., and Green, P. F., *Macromolecules* **1989**, *22*, 2581.

[30] Russell T. P., Coulon, G., Deline, V. R., and Miller, D. C., *Macromolecules* **1989**, *22*, 4600.

[31] Anastasiadis, S. H., Russell, T. P., Satija, S. K. and Majkkrzak, C. F., *Phys. Rev. Lett.* **1989**, *62*, 1852

[32] Anastasiadis, S. H., Russell, T. P., Satija, S. K. and Majkkrzak, C. F., *J. Chem. Phys.* **1990**, *92*, 5677

Chapter 2 Morphology of ABC Triblock Copolymers

2.1 Introduction

Block copolymers have received considerable attention, both experimentally and theoretically, due to their fascinating ability to self-assemble into a variety of ordered nanoscale morphologies. Recently, self-assembled ordered structures with periodicities on the nanometer scale have become an important area of study because of their applications in nano-technology. For instance, it has been suggested that block copolymers can be used in the development of new classes of electronic devices [1] , [2]; and in the synthesis of mesoporous solids, which can be used as catalysts and sorption media [3], [4]. One of the distinct advantages of block copolymers is the controllability of the size and morphology of the nanostructures by changing the molecular weight, molecular architecture, and composition of the copolymers.

Ordered morphologies and phase transitions in linear AB-type diblock copolymers have been studied for many years. Helfand et. al [5], Semenov [6], and Ohta and Kawasaki [7], [8] developed approaches for studying the strong segregation limit, while Leibler studied the case of the weak segregation limit by using an order parameter Landau mean field theory [9]. Fredrickson and Helfand [10] incorporated the effects of concentration fluctuations in the order-disorder transition by reducing the effective Hamiltonian of block copolymers to a form previously studied by Brazovskii [11]. Noolandi et al. developed a self-consistent mean-field theory for studying both the strong and weak segregation limits [12]. Recently, Melenkevitz and Muthukumar [13], Muthukumar [14], Matsen and Schick [15], and Olmsted and Milner [16] have made important contributions to the further development of theory of diblock copolymers.

It is now well recognized that the phase behavior of AB diblock copolymers is determined by three factors: the overall degree of polymerization, $N = N_A + N_B$; the composition of the copolymer characterized by $f = N_A/N$; and the temperature expressed in terms of the Flory-Huggins interaction parameter χ. For symmetric

diblocks (f=0.5), an order-disorder transition takes place at $\chi N \sim 10$ [9]. Depending on the composition and/or temperature, b.c.c ordered spheres, hexagonally ordered cylinders, lamellae, and more complex bicontinuous structures have been obtained below the order-disorder transition temperature [17].

While the equilibrium morphologies of AB diblock copolymers have been relatively well understood theoretically (except for some uncertainties with regard to the bicontinuous phases [16], [18]-[20]), considerably less theoretical work exists for the ABC type triblock copolymers [21]-[24]. The recent experimental discovery of exotic new morphologies in ABC triblocks, as well as a growing interest in using these copolymers to synthesize new nanoscale structures have increased the need for the theoretical study of these systems.

ABC triblock copolymers consist of three different polymer segments A, B, and C, that are chemically bonded together, as illustrated in Figure 2.1. Since there are three interaction parameters, χ_{AB}, χ_{BC}, and χ_{CA}, in ABC triblock copolymers, as opposed to one interaction parameter, χ_{AB}, in AB diblock copolymers, the microphase separation of ABC triblock copolymers is much more complicated than that in diblock copolymers. More importantly, some distinctively new features arise in triblock copolymers that are absent in the diblock counterpart. For example, the morphological structure of triblock copolymers depends not only on the temperature, the overall molecular weight, and the fraction of each block, but also crucially on the sequence of the blocks in the chain (i.e., whether it is sequenced $A-B-C$, $B-C-A$, or $C-A-B$). Indeed, recent experiments have shown that the lamellar morphology is formed in the system of poly(isoprene-b-styrene-b-2-vinylpyridine)(ISP) with volume fraction 1:1:1 [25], whereas the hexagonally ordered co-axial cylinder phase was obtained in the system of SIP with the same composition [26]. The schematic representations of the lamellar phase and the co-axial cylinder phase are shown in Figure 2.2(a) and 2.2(b) respectively.

Even for a given sequence, say $A-B-C$, one can obtain different morphologies, depending on the relative magnitudes of the three Flory-Huggins parameters and the composition. Thus, richer and more complex morphological behaviors are expected in ABC triblock copolymers than in AB diblocks. In addition to the discovery of ordered spherical, cylindrical , lamellar, and ordered tricontinuous double-diamond structures (OTDD) [25]-[27] which bear the same basic structural features as the corresponding

structures in AB diblock copolymers, several intriguing new morphologies have been reported in recent experiments. Auschra et al. [28] , [29] demonstrated the formation of three new phases: a lamella-cylinder combination phase, a lamella-sphere combination phase, and a cylinder-ring combination phase. The schematic representation of the three new phases are given in Figure 2.2(c), (d), and (e) respectively. The possibility of forming morphologies which were combination of the lamellar, cylinder, and sphere phases in triblock copolymers was first predicted by Riess et al.[22], [23]. These combination morphologies, which often have characteristics of one, two, and three dimensional order simultaneously, can have unique mechanical properties. Nanostructures templated after these morphologies are also expected to have unusual electronic and transport properties.

Considering the novel features which are alluded to above, we feel that the study of triblock copolymers represents a significantly new direction in self-assembling polymers. In this paper, we map out the three-component phase diagrams of ABC triblock copolymers in the entire range of f_A, f_B, and f_C in the strong segregation limit by applying a simple, approximate theory put forth by Ohta, Kawasaki and Nakazawa [7] , [8] , [21] to the most general cases in which χ_{AB}, χ_{BC}, and χ_{CA} are not necessarily equal to each other. By varying the interaction parameters and the composition of copolymers, we seek to establish relationship between the molecular characteristics of the system and its morphologies.

The key simplification in the Ohta and Kawasaki theory is the separation of the free energy of the copolymer system into a short range interaction, which accounts for the interfacial free energy of the system, and a long range interaction, which accounts for the chain conformation energy. In addition, these authors assume that the long range interaction can be approximated by a term proportional to $1/k^2$, as suggested by the small k behavior of the structure factor calculated in the random phase approximation. A similar approximation was proposed by Stillinger [30] in his study of miceller self-assembly. Although the validity of this last assumption is difficult to justify theoretically, previous results of Ohta and Kawasaki [7], Nakazawa and Ohta [21], and Muthukumar and Melenkevitz [13] on block copolymers, and of Stillinger [30] and Chandler and co-workers [31] on short surfactant systems suggest that such a representation seems to be capable of capturing many of the essential features of the microphase separation of block copolymer systems. Here we adopt this approximate

approach for its simplicity in implementation. More accurate approaches, such as the method of electrostatic analogy developed by Semenov [6], and the "wedge" approach developed by Milner and Olmsted [16] can be employed in principle, as demonstrated in the recent work of Kane and Spontak [32], who has extented Semenov's approach to strongly-segregated lamellar phase of ABC triblock copolymers; however, extensive computational efforts will be required if these methods are to be applied to the complicated morphologies studied in this paper. Although the results presented herein are subject to the inherent approximation in the approach, and hence may not be quantitatively accurate, we believe that the features of the phase diagrams presented can be useful in providing a guide for further experimental and theoretical studies. More precise results can be obtained by the self-consistent method.

The organization of the paper is as follows: In section II, we discuss the general formulation of the free energy of a triblock copolymer system, by following the Ohta-Kawasaki approach. In section III, we present and discuss phase diagrams of triblock copolymer systems; these phase diagrams are classified according to the relative strength of the interaction parameters. In section IV, we compare our calculations with some available experimental results. Section V is the conclusion. The Appendix contains a detailed calculation of the free energy of lamella-sphere phase, which illustrate the method we employed.

2.2 Model and Free Energy

We consider a model system containing n monodisperse triblock copolymer chains with an overall degree of polymerization N. Each chain consists of three types of monomers, a, b, and c, with interaction parameters χ_{ab}, χ_{bc}, and χ_{ac}. Henceforth, we will use the lower-case " a", "b", and "c" to designate the segmental position of the three blocks such that "a" and "c" are the outer blocks while "b" is the middle block. The upper-case letters refer to the chemical makeup of the blocks. Thus we will always designate a triblock copolymer as $a-b-c$, even though there can be three chemically distinct sequences $A-B-C$, $B-C-A$, and $B-A-C$. For the sake of simplicity, we will assume that all three blocks have the same Kuhn statistical segment length, which we take to be unity, and the same monomeric volume v_o. The

volume fraction of blocks a, b and c in a chain are f_a, f_b, and f_c respectively, which satisfy $f_a + f_b + f_c = 1$. We assume that the system is incompressible.

In the strong segregation limit, the microdomains form a regular arrangement, giving rise to periodic structures with the interfacial width much smaller than the lattice dimensions. The free energy of the system can be separated into two parts: an entropic chain-conformational free energy, and an interfacial free energy, whose strength is characterized by the Flory-Huggins parameters. We define a characteristic length scale (or one of the characteristic length scales) of a periodic structure to be l. For example, l can be the period in the lamellar phase, or the lattice constant of the square lattice in the cylinder phase, or one of the periods in the lamella-cylinder phase.

The free energy per chain can be written as

$$F = \frac{l^2}{2N}\,\Phi(f_a, f_c) + \frac{\sigma_{av} N v_o}{l} \tag{2.1}$$

where $\Phi(f_a, f_c)$ is a scaling function which depends on the morphology of the system, v_o is the volume of a monomer, and σ_{av} is an average interfacial tension to be explained later.

While Equation (2.1) is formally exact in the strong segregation limit, further progress requires an explicit expression for the scaling function $\Phi(f_a, f_c)$. Here we use the approximation suggested by Nakazawa and Ohta [21]. In this approximation, $\Phi(f_a, f_c)$ is calculated from the asymptotic behavior of the structure factor in the long wave length limit. More specifically, $\Phi(f_a, f_c)$ is written as

$$\Phi(f_a, f_c) = \sum_{\alpha\beta=a,c} \sum_{\hat{Q}} \frac{1}{\hat{Q}^2}\, A_L^{\alpha\beta}(f_a, f_c)\Psi_\alpha(\hat{Q})\Psi_\beta^*(\hat{Q}) \tag{2.2}$$

where $\Psi_\alpha(\hat{Q})$ is the Fourier Transform of $\Psi_\alpha(\vec{r})$, which is the local volume fraction deviation of monomers α from its uniform distribution, ie.

$$\Psi_\alpha(\hat{Q}) = \frac{1}{V_{cell}} \int d\vec{r}\Psi_\alpha(\vec{r}) exp(i\vec{Q}\vec{r}) \tag{2.3}$$

with V_{cell} being the volume of the unit cell. The quantity $\hat{Q}$ is the reciprocal lattice vector scaled by l, i.e. $\hat{Q} = \vec{Q}l$. In Equation (2.2), $\Psi_b(\hat{Q})$ has been eliminated by the

use of incompressibility. The coefficient $A_L^{\alpha\beta}(f_a, f_c)$ is given by

$$A_L^{aa} = B\,\frac{2(1-f_c)^2}{f_a^2} \tag{2.4}$$

$$A_L^{ac} = A_L^{ca} = B\,\frac{1-f_a^2-f_c^2}{f_a f_c} \tag{2.5}$$

$$A_L^{cc} = B\,\frac{2(1-f_a)^2}{f_c^2} \tag{2.6}$$

with

$$B = \frac{6}{\{3-2(f_a+f_c)-(f_a-f_c)^2\}(1-f_a-f_c)^2} \tag{2.7}$$

The average interfacial tension is given by

$$\sigma_{av} = \sum_{\alpha\beta} \hat{S}_{\alpha\beta}\,\sigma_{\alpha\beta}/\hat{V}_{cell} \tag{2.8}$$

where $\hat{V}_{cell}$ is the volume of the unit cell scaled by l^3, and $\hat{S}_{\alpha\beta}$ is the interfacial area between α andβ domains in a unit cell scaled by l^2. If there is more than one disconnected interface between the α and β domains in a unit cell, the interfacial area is the sum of all the disconnected interfacial areas. The variable $\sigma_{\alpha\beta}$ is the interfacial tension between the α and β domains. In the strong segregation limit, if we ignore the presence of the third component in the interfacial region between α and β, $\sigma_{\alpha\beta}$ is proportional to $\chi_{\alpha\beta}^{1/2}$ and independent of the block ratio [8], [33].

Minimization of F with respect to l yields the length scale l^* and the corresponding free energy F^*

$$l^* = [\sigma_{av}\,N^2 v_o/\Phi(f_a, f_c)]^{1/3} \tag{2.9}$$

$$F^* = C^*[\hat{\sigma}_{av}^2\,\Phi(f_a, f_c)]^{1/3} \tag{2.10}$$

where $C^* = 3(\sigma_{ab}^2 v_o^2 N/2)^{1/3}$ is the free energy of a three-phase four-layer lamellar phase (see Figure 2.2(a)) with interfacial tension σ_{ab}=σ_{bc}. The quantity $\hat{\sigma}_{av}$ is given by

$$\hat{\sigma}_{av} = \frac{1}{2}[\hat{S}_{ab} + \hat{S}_{bc}(\sigma_{bc}/\sigma_{ab}) + \hat{S}_{ac}(\sigma_{ac}/\sigma_{ab})]/\hat{V}_{cell} \tag{2.11}$$

Thus the equilibrium state of the system, which is determined by the minimum value of F, depends on the relative strength of interfacial tensions σ_{bc}/σ_{ab} and σ_{ac}/σ_{ab}, in

addition to the composition.

For some simple morphologies such as the lamellar, cylinder, and spherical phases, where there is only one characteristic length, the obtained F^* is the minimum free energy of the morphology. However, for the more complex morphologies such as the lamella-cylinder phase in which there are two characteristic length scales, F^* depends on the ratio of the two length scales through $\Phi(f_a, f_c)$ and $\hat{\sigma}_{av}$, and the minimum free energy is obtained by further minimization of F^* with respect to this ratio. The detailed calculation of the free energy of the lamella-cylinder phase is presented in the Appendix; the calculation of the free energies of the other morphologies are carried out in a similar fashion. Although of great current interest, we do not consider the ordered tricontinuous phases in this paper. Our preliminary analysis shows that the ordered tricontinuous phases in triblocks are much more complex and subtle than the corresponding bicontinuous phases in diblocks. Furthermore, even for diblocks, there is controversy as to the stability of these phases in the strong segregation limit [16], [18]-[20].

2.3 Phase Diagrams of ABC Triblock Copolymers

Three different types of homopolymers A, B, and C, with interaction parameters χ_{AB}, χ_{BC}, and χ_{CA}, can be bonded together to form $A-B-C$, or $A-C-B$, or $B-C-A$ copolymers. If χ_{AB}, χ_{BC} and χ_{CA} are not equal to one another, the different sequences will have different phase behaviors. For a system with a given sequence and volume fractions, using "a", "b", and "c" to label the three blocks as explained in the section II, we determine the equilibrium phase diagrams in terms of the ratios of the interfacial tensions σ_{ac}/σ_{ab} and σ_{bc}/σ_{ab}. For convenience, we assume that $\sigma_{ab} \leq \sigma_{bc}$. If the opposite is true, we may always re-label the blocks such that $\sigma_{ab} \leq \sigma_{bc}$. We define $\gamma_1 = \sigma_{bc}/\sigma_{ab}$ and $\gamma_2 = \sigma_{ac}/\sigma_{ab}$. The $a-b-c$ triblock copolymer systems can be classified into six classes according to the relative strength of the interfacial tensions γ_1, γ_2, as shown in Table I

Table I

(1) $\gamma_1 = 1$, $\gamma_2 < 1$	(2) $\gamma_1 = 1$, $\gamma_2 = 1$	(3) $\gamma_1 = 1$, $\gamma_2 > 1$
(4) $\gamma_1 > 1$, $\gamma_2 < 1$	(5) $\gamma_1 > \gamma_2 > 1$	(6) $\gamma_2 > \gamma_1 > 1$

Once the relative strength of the interaction parameters are specified, the morphology is uniquely determined by the composition of the system.

2.3.1 Variation of Morphologies With Composition

In this section, we focus on the variation of morphologies with composition. To this end, we set $\gamma_1 = \gamma_2 = 1$. The three-component triangle phase diagram is shown in Figure 2.3(a). The increment of the volume fractions f_a, f_b, and f_c in the phase diagram is 0.1. At each grid point of the phase diagram, the free energies of all the morphologies listed in Figure 2.2 are calculated and the equilibrium state is determined by the morphology with the lowest free energy. From Figure 2.3(a), it is evident that with an increasing value of f_b, the equilibrium morphology of the system changes from the lamellar structure to the cylindrical domains in the square lattice structure, and finally to the spherical domains in the $CsCl$-type structure. Their schematic representations are shown in Figure 2.2(a), 2(f), and 2(g), respectively. When $f_a = f_c$, the free energies of spherical, cylindrical, and lamellar phases are as shown in Figure 2.3(b), a result consistent with that of Nakazawa and Ohta [21].

Near the edge of the triangle phase diagram, where at least one of the three components f_a, f_b, and f_c is less then 0.1, other morphologies are possible, although these are not shown in Figure 2.3(a). At the the edge ac of the triangle phase diagram where $f_b \leq 0.1$, we find several other phases competing for stability in addition to the stable lamellar phase. For $f_b = 0.1$ and $f_a \simeq f_c$, the free energies of the lamella-cylinder and lamella-sphere phases are very close to that of the lamellar phase. Their schematic representations are shown in Figure 2.2(c) and 2(d). The free energies of the lamellar, lamella-cylinder, and lamella-sphere phases, for $f_a = f_c$, are shown in Figure 2.3(c). The free energy of the lamella-cylinder phase is lowest for $0.025 < f_b < 0.1$, and that of the lamella-sphere phase is lowest for $f_b < 0.025$. In the lamella-cylinder or lamella-sphere phases, the minority species b blocks form cylindrical or spherical domains along the a/c lamellar interface, rather than flat layers in the lamellar phase. By reducing the interfacial area of a/b and b/c interfaces, the interfacial energy is reduced so that the total free energy is lowered. Although f_b must be quite small to form the lamella-cylinder and lamella-sphere phases in this case, we will show later that when the value of γ_2, the interfacial tension between the two outer blocks a and

c, is reduced in comparison to the interfacial tension between the center block and the outer blocks, these phases can form at much larger values of f_b.

At the other two edges of the triangle phase diagram, i.e. ab (or bc), where the volume fraction of one of the two end-blocks f_c (or f_a) is very small and $f_a \sim f_b$ (or$f_c \sim f_b$), two other morphologies compete for stability with the lamellar phase. One of these phases is demonstrated in Figure 2.2(h); we call this phase the lamella-cylinder-II phase. In this phase, the minority species, say a, forms cylindrical domains located regularly inside the b domains of the b/c lamellar stacking. Another morphology is shown in Figure 2.2(i); we call this phase the lamella-sphere-II phase. In this case , the minority species a forms spheres located hexagonally inside of b domains, with blocks b and c forming a lamellar structure. Although these two morphologies have a similar appearance to the previously studied lamella-cylinder and lamella-sphere phases respectively, they are different structures. The cylindrical or spherical domains in the lamella-cylinder-II or lamella-sphere-II phases respectively are formed by one of the outer blocks and are located inside the domains formed by the center blocks while the cylindrical domains and spherical domains in the lamella-cylinder and the lamella-sphere phases respectively are formed by the center blocks and located at the interface of the two outer blocks. The lamella-cylinder-II phase becomes stable when $f_a < 0.016$ at $f_b = f_c = 0.492$, whereas the lamella-sphere-II phase is alway near stable even when $f_a < 10^{-6}$. The stability of both morphologies can be enhanced when the surface tension γ_1 is decreased. We are not yet aware of any experiments which show these new phases.

At the a or c corner of the phase diagram, where f_b and f_c, or f_b and f_a, respectively are very small, our calculations show that the co-axial cylinder and cylinder-sphere phases are nearly stable. In the co-axial cylinder phase, the minority species, say c, form inner cylinders, blocks b form the shells around these cylinders, and blocks a form the matrix. In the cylinder-sphere phase, blocks c form spheres which are embedded in the cylindrical domains formed by blocks b, and and blocks a form the matrix. Schematic representations of these phases are shown in Figure 2.2(b) and 2(j). At $f_c, f_b = 0.1,\ 0.1$ (or $f_c,\ f_b = 0.1, 0.1$), the free energy ratios $F_{co-axial\ cylinder}/F_{lamellar} = 1.026$ and $F_{cylinder-sphere}/F_{lamellar} = 1.060$. However, the co-axial cylinder phase becomes the dominant phase at $f_b \leq 0.05$ and $f_c \leq 0.05$, while the cylinder-sphere phase is always nearly stable when $\gamma_1 = 1.0$ and $\gamma_2 = 1.0$. As we

will show later, the cylinder-sphere phase is stable only in the region of $f_c/f_b \ll 1.0$ when γ_1 is increased to a large value.

It should be pointed out that near the edges of the phase diagram of Figure 2.3(a) where at least one of the volume fraction of the blocks is very small, the the size of domains formed by the minority species is also very small. As the size of the domains becomes smaller, an increasing number of wave vectors are needed to obtain a given accuracy in the free energy calculation.

A more serious problem arises when one of the volume fraction f_α ($\alpha = a, b, c$) becomes very small. The three edges of the triangle phase diagram are the phase diagrams of $a-b$, $b-c$, and $c-a$ diblock copolymers where one of the three volume fractions f_c, f_a and f_b is zero. It is well-known that diblock copolymers, in the strong segregation limit, undergo the following sequence of morphology changes as the asymmetry in the lengths increases: lamellar $\rightarrow$ hexagonal cylinders $\rightarrow$ b.c.c spheres. (Different theories give slightly different values of f at the transitions [6], [7].) Our calculated phase diagrams do not seem to approach the corresponding diblock phase diagrams as one of the volume fractions vanishes. There are two reasons for this discrepancy. The first reason is that we have used a rather coarse grid (f_α changes by increment of 0.1). The second, and more fundamental, reason is the assumption of strong segregation. The theory that we employ assumes strong segregation between all pairs in the triblock; no intermixing is allowed. This assumption clearly becomes invalid as the volume fraction of one of the blocks becomes small. Rather than forming three distinct domains containing a, b, and c components respectively, the tiny block will become soluble in the matrix of the other two blocks. If strong segregation is insisted upon, then one does not in general expect the triblock phase behavior to approach the diblock phase behavior in the limit of vanishing fraction of one of the blocks. This is because in a true diblock copolymer system, the two ends of the diblock chain are unconstrained. However, in an $a-b-c$ triblock, the two ends of the b block are connected with the a and c blocks on either end, and consequently, when one insists on three distinct domains consisting of the three blocks, the ends of the b blocks are always tethered, even when one of the end blocks (a or c) becomes vanishingly small. This argument leads us to conclude that the diblock phase behavior is approached only in the limit of $f_b \rightarrow 0$, but not in the limit of $f_a$or $f_c \rightarrow 0$.

We have performed a separate calculation on the lamellar to cylinder (the core-shell structure as shown in Figure 2.2(b)) transition and studied the shift of the phase boundary as one of the volume fractions become vanishingly small. Results of this calculation are consistent with the conclusion given above [34]. We have also used the Ohta-Kawasaki-Nakazawa approach to study the behavior of the phase diagram for decreasing f_b (below 0.1). Our results show that very close to the ac edge, the phase behavior indeed becomes qualitatively similar to the $a-c$ diblock. Quantitative recovery of the $a-c$ diblock behavior is not expected because of the approximate nature of the theory.

2.3.2 Effects of Interfacial Tensions

The region of morphologies which appear near the edges and corners of triangle phase diagram in Figure 2.3(a) can be greatly enlarged when we change the relative strength of interaction parameters γ_1 and γ_2. To focus on the influence of γ_2, we set $\gamma_1 = 1$. A system can be classified into one of the three groups shown in the first row of Table I according to the relative strength of γ_2. In the first group, $\gamma_2 < 1$, and the contact between the two outer blocks is more favorable than that between the center block and the two outer blocks. Consequently there is a greater tendency to form morphologies such as the lamella-cylinder, lamella-sphere and cylinder-ring phases, in which some parts of a/b and b/c interfaces are replaced by a/c interfaces. In the second group, the interaction between the two outer blocks is comparable to the interaction between the outer blocks and the center blocks, and morphologies with a/c interfaces can only exist in a small portion of the phase diagram as discussed in section III.A and shown in Figure 2.3(c). In the third group, $\gamma_2 > 1$, the interaction between the two outer blocks is less favorable than the interaction between the center block and the two outer blocks, hence morphologies with a/c interfaces are greatly suppressed.

Figure 2.4(a) shows the phase diagram of a system for which $\gamma_1 = 1$ and $\gamma_2 = 0.2$. In particular, for a symmetric triblock copolymer, where $f_a = f_c$ and $\gamma_1 = 1$, the phase diagram shows that the transition from the lamellar to the lamella-cylinder phase occurs at $f_b = 0.35$ and that the transition from the lamella-cylinder to the lamella-sphere occurs at $f_b = 0.17$. These results qualitatively agree with those in a recent paper by Stadler et al. [24] who studied the morphologies of *symmetric*

triblock copolymers by using the Meier/Alexander/de Gennes/Semenov approach. However, their calculation also shows a stable cylinder-ring phase when γ_2 is reduced to 0.1. This result is puzzling in view of the architectural symmetry of the triblock copolymer and the obvious microstructural asymmetry of the cylinder-ring phase.

We show in Figure 2.4(b) a phase diagram of symmetric triblock copolmers in terms of f_b and γ_2 for transitions from the lamellar, to the lamella-cylinder, and then to lamella-sphere phases. It is clear that the regions for the lamella-cylinder and lamella-sphere phases are greatly enlarged when γ_2 is reduced.

To study the influence of γ_1 on the morphology of triblock copolymers, we fix γ_2 at some large value. Under the assumption that $\sigma_{ab} \leq \sigma_{bc}$, the system can be classified into two types: $\gamma_1 = \sigma_{bc}/\sigma_{ab} = 1$ or $\gamma_1 = \sigma_{bc}/\sigma_{ab} > 1$. For $\gamma_1 = 1$, the morphology of the system remains unchanged when the volume fraction of blocks a and c are exchanged. It is a common feature of systems with $\gamma_1 = 1$ that the three-component triangle phase diagrams have a reflection symmetry with respect to the vertical line $f_a = f_c$. The reflection symmetry disappears when $\gamma_1 \neq 1$. When $\gamma_1 > 1$, i.e. the interfacial tension $\sigma_{bc} > \sigma_{ab}$, near the edge ab, the system can achieve a low interfacial energy by forming a co-axial cylinder phase with c blocks forming the inner cylinder, b blocks forming the shell, and a being the matrix. In Figure 2.5(a), the phase diagram of a system with $\gamma_1 = 2.0$ and $\gamma_2 = 5.0$ is presented, and the region of the co-axial cylinder phase near the edge ab of the phase diagram is greatly enlarged in comparison with that in Figure 2.3(a). Figure 2.5(b) shows the free energies of the lamellar, co-axial cylinder, and cylinder-sphere phases as γ_1 varies, with $f_a = 0.8$, $f_c = 0.1$ and $\gamma_2 = 5.0$. When $\gamma_1 > 1.55$, the co-axial cylinder phase becomes the stable state. However, the cylinder-sphere phase remains near stable in Figure 2.5(b). The cylinder-sphere phase become stable only when an additional condition $f_c/f_b \ll 1.0$ is satisfied. Figure 2.5(c) shows the free energies of the lamellar, co-axial cylinder and cylinder-sphere phases as a function of f_c at $\gamma_1 = 2.0$, $\gamma_2 = 5.0$, and $f_a = 0.8$. The cylinder-sphere phase is the stable phase when $f_c < 0.046$, i.e. $f_c/f_b < 0.3$. Therefore, the relative stability of the co-axial cylinder phase and cylinder-sphere phase is enhanced when γ_1 increases.

2.4 Discussion

A theoretical understanding of the effect of volume fractions and the various interfacial tensions on the morphology of triblock copolymers enables us to predict and explain a variety of structures that can be formed by these system. We now discuss several interesting experimental results in light of our calculated phase diagrams.

In a series of experiments by Auschra et al. [28], [29], the lamella-cylinder, lamella-sphere and cylinder-ring phases were discovered for the first time. Using poly(styrene-b-ethylene-co-1-butene-b-methacrylate)(P(S-b-EB-b-MMA)) triblock copolymers, they demonstrated that the lamellar phase was formed at the composition 0.24/0.38/0.38, the lamella-cylinder phase was formed at 0.48/0.17/0.35, and the cylinder-ring phase was formed at 0.45/0.06/0.49. The literature data for the interfacial tensions between the components of P(S-b-EB-b-MMA) is given in Table II [35] .

Table II

	PS/PMMA	PS/PEB	PEB/PMMA
σ (150°C)/$(dyn\ cm^{-1})$	1.5	5.0	9.5

If we denote "A"as PS, "B" as PEB, and "C" as PMMA, their relative interfacial tensions are $\gamma_2 = \sigma_{AC}/\sigma_{AB} = 0.3$ and $\gamma_1 = \sigma_{BC}/\sigma_{AB} = 1.9$. The system consisting of P(S-b-EB-b-MMA) belongs to the first type in the second row of Table I. Figure 2.6(a) is our calculated phase diagram of such $A - B - C$ copolymers. The phase diagram indicates that the system is in the lamellar phase at the composition 0.24/0.38/0.38, and in the lamella-cylinder phase at 0.48/0.17/0.35; both are consistent with the experimental results of Auschra et al. [28]. However, there is a notable discrepancy at 0.45/0.06/0.49. Our calculation predicts that the system should be in the lamella-sphere phase, while a cylinder-ring phase was observed experimentally by Auschra et al. From Figure 2.6(a), it is clear that the cylinder-ring phase with C blocks forming the cylinder can appear only at the corner of a where $f_b < 0.3$ and $f_c < 0.2$. Although our free energy calculation is approximate, we do not believe that the error due to the approximation can be large enough to lead to this discrepancy. It should also be noted that our calculations predict that cylinder-ring domains on a hexagonal lattice always have a lower energy than on a square lattice.

Figures 6(b) and 6(c) show the phase diagrams of P(S-b-MMA-b-EB) and P(EB-

b-S-b-MMA), simply designated as $A-C-B$ and $B-C-A$ respectively. Using the definition of γ_2 and γ_1, the system consisting of $A-C-B$ has the relative interfacial tensions $\gamma_2 = 3.33$ and $\gamma_1 = 6.33$, and $B-A-C$ has the relative interfacial tensions $\gamma_2 = 6.33$ and $\gamma_1 = 3.33$, which belong to the second and the third in the second row of Table I. It is obvious that switching the sequences of the three blocks leads to very different structures of the phase diagrams.

Another interesting experimental observation can also be explained and the relative interfacial tension of the system can be estimated by the understanding of the effect of γ_2 and γ_1 on the morphology of triblock copolymers. Mogi et al.[25] observed a lamellar phase in 1:1:1 P(isoprene-b-styrene-b-2-vinypyridine) (ISP) triblock copolymers whereas a co-axial cylinder phase of P and I in an S matrix was found in P(S-b-I-b-P) by Gido et al. [26]. Our free energy calculation of the lamellar and the co-axial cylinder phases shows that when $\sigma_{bc}/\sigma_{ab} \geq 4.3$, the co-axial cylinder phase, with C forming the inner cylinders is the stable phase. The fact that the lamellar phase was formed at 1:1:1 of P(I-b-S-b-P) indicates that $1/4.3 < \sigma_{IS}/\sigma_{SP} < 4.3$. On the other hand, the fact that the co-axial cylinders was formed t 1:1:1 of SIP indicated that $\sigma_{IP}/\sigma_{IS} > 4.3$. These results enable us to bracket the range of the relative interfacial tensions for I, S and P.

2.5 Conclusion

In this paper, we have presented a systematic study of the rich and fascinating morphologies that can form in ABC triblock copolymers in the strong segregation limit. Our results demonstrate the crucial dependence of the phase behavior of an ABC triblock copolymer system on the sequencing of the three blocks. The effects of the interaction parameters have also been investigated. In contrast to the AB diblock copolymers where, in the strong segregation limit, the morphology is determined uniquely by the composition, the relative strengths of the interaction parameters in a triblock copolymer system affect the morphology phase diagrams in a significant way.

Our calculation has made use of an approximation proposed by Ohta and Kawasaki in which the chain conformation free energy is approximated by a Coulomb-like interaction. Because of this approximation our phase diagrams can only be considered as qualitatively correct. However, the quantitative accuracy of this approximation

may not be as poor as it appears to be. Since the calculation of the phase diagrams involves taking the difference between the free energies of the different ordered phases, it is possible that the errors caused by this approximation may cancel to some extent.

Another (technical) approximation involves our representation of the ordered structures, in that we only considered domains with uniform curvature. In reality, the cylinders and spheres are deformed due to the lattice structures in which they are embedded. Allowing this deformation will lead to lower free energies for structures involving curved domains relative to the lamellar structure, hence increasing the stability of these phases.

In spite of these approximation, our calculation does seem to have captured many of the essential features of the ABC triblock copolymer systems in the strong segregation limit. Our results compare favorably with experimental observations. In addition, we have predicted the existence of some new structures: the lamella-cylinder-II phase, the lamella-sphere-II phase, and the cylinder-sphere phase; it will be of interest to observe these new phases experimentally. It is hoped that this study provides a systematic (although crude) guide for future experiments and more refined theories of the morphology of ABC triblock copolymers.

Acknowledgement

We thank Julia A. Kornfield for helpful discussions. This research is supported in part by donors of the Petroleum Research Fund, administrated by the American Chemical Society, and by the National Science Foundation (grant number ASC-9217368).

2.6 Appendix

In this Appendix, we present the details of the free energy calculation for the lamella-cylinder phase to illustrate the method that has been used. The calculation of other morphologies which are considered in determining the lowest free energy in the phase diagrams are carried out in a similar way. Instead of presenting the detailed calculations of their free energy, we only provide their schematic representations in Figure 2.2.

The lamella-cylinder phase was first discovered by Auschra et al. [28]. A schematic representation of this structure is given in Figure 2.2(c).

We choose our coordinate system such that the cylinder axis in the lamella-cylinder structure is oriented in the $\hat{z}$ direction. In the xy plane, the primitive translation vectors are $l_x\hat{x}$ and $l_y\hat{y}$. The thickness of the a and c domains are l_a and l_c respectively, and r is the radius of the cylinders containing the b blocks, as shown in Figure 2.7. For simplicity, we have assumed that the two half circles containing blocks b in a domains and c domains have the same curvature. The reciprocal lattice vectors are given by

$$\vec{Q} = \frac{2\pi}{l_x} m_1 \vec{e_x} + \frac{2\pi}{l_y} m_2 \vec{e_y} \tag{2.12}$$

with m_1 and m_2 being integers. The unit cell has been chosen as shown in Figure 2.7 with unit cell volume V_{cell} equal to $l_x l_y L$.

The form factor of a domain and c are given by

$$\Psi_a(Q) = exp\{iQ_x l_a/2\}\Psi_A^{'}(Q) \tag{2.13}$$

$$\Psi_c(Q) = exp\{-iQ_x l_c/2\}\Psi_C^{'}(Q) \tag{2.14}$$

where $\Psi_a^{'}(Q)$ and $\Psi_c^{'}(Q)$ are given by

$$\Psi_\alpha^{'}(Q) = \frac{4L}{V_{cell}} \int_0^{l_\alpha/2} dx \int_{Y_\alpha(x)}^{l_y/2} dy\, cos(Q_x x) cos(Q_y y) \tag{2.15}$$

with

$$Y_\alpha(x) = \begin{cases} 0 & (0 \le x \le l_\alpha/2 - r) \\ [r^2 - (x - l_\alpha/2)^2]^{1/2} & (l_\alpha/2 - r \le x \le l_\alpha) \end{cases} \tag{2.16}$$

and $\alpha = a, c$.

The form factors can be evaluated numerically. We choose l_x as the characteristic length scale l and scale Q, l_a, l_c, l_y and r in equation A(2)-A(5) by l_x. The scaled variables $\hat{l}_a$, $\hat{l}_c$, $\hat{l}_y$ and $\hat{r}$ are not independent of each other, but are related by the equations:

$$\hat{l}_a + \hat{l}_c = 1 \tag{2.17}$$

$$\hat{l}_a - \pi\hat{r}^2/\hat{l}_y = f_a \tag{2.18}$$

$$2\pi\hat{r}^2/\hat{l_y} = 1 - f_a - f_c \tag{2.19}$$

Equation A(7) and A(8) arise from the constraint that the volume fraction of a and c in a unit cell is f_a and f_c, respectively. Thus we have

$$\hat{l_a} = f_a + \frac{1}{2}(1 - f_a - f_c) \tag{2.20}$$

$$\hat{l_c} = \frac{1}{2}(1 - f_a - f_c) \tag{2.21}$$

$$\hat{r} = \sqrt{\hat{l_y}\,(1 - f_a - f_c)/2\pi} \tag{2.22}$$

Substituting equation A(9)-A(11) to Equation (2.1), we have the long range part of the free energy F_L

$$F_L = \frac{l^2}{2N}\Phi(f_a, f_c; \hat{l}_y) \tag{2.23}$$

where

$$\begin{aligned}\Phi(f_a, f_c; \hat{l}_y) \;=\; & \sum_{\hat{Q}} \frac{1}{\hat{Q}^2}(A_L^{aa}(f_a, f_c)\;\Psi_a^{'}(\hat{Q})^2 + A_L^{cc}(f_a, f_c)\;\Psi_c^{'}(\hat{Q})^2 \\ & + 2\;cos(\hat{Q}_x/2) A_L^{ac}(f_a, f_c)\;\Psi_a^{'}(\hat{Q})\;\Psi_c^{'}(\hat{Q}))\end{aligned}$$

with $\hat{Q}_x = Q_x\, l$.

The short range part of the free energy is given by

$$F_S = \frac{\sigma_{av} v_o N}{l} \tag{2.24}$$

where

$$\sigma_{av} = [(\sigma_{ab} + \sigma_{bc})2\pi\hat{r} + 2\sigma_{ac}(\hat{l_y} - 2\hat{r})]/\hat{l_y} \tag{2.25}$$

Substituting $\Phi(f_a, f_c; \hat{l}_y)$ and σ_{av} in Equation (2.10), we can obtain F^*. Since $\Phi(f_a, f_c; \hat{y})$ and σ_{av} are both functions of $\hat{l}_y$, which is the ratio of the two characteristic length scales l_x and l_y, the minimum free energy of the lamella-cylinder-1 phase can be obtained by numerically minimizing F^* with respect of $\hat{l}_y$.

2.7 Figures

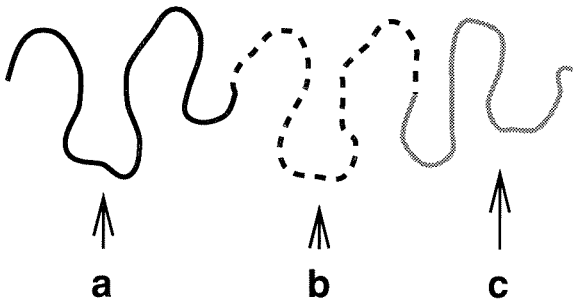

Figure 2.1: Schematic representation of an ABC triblock copolymer. For a given sequence, we use "a" and "c" to denote the end blocks and "b" to denote the center block.

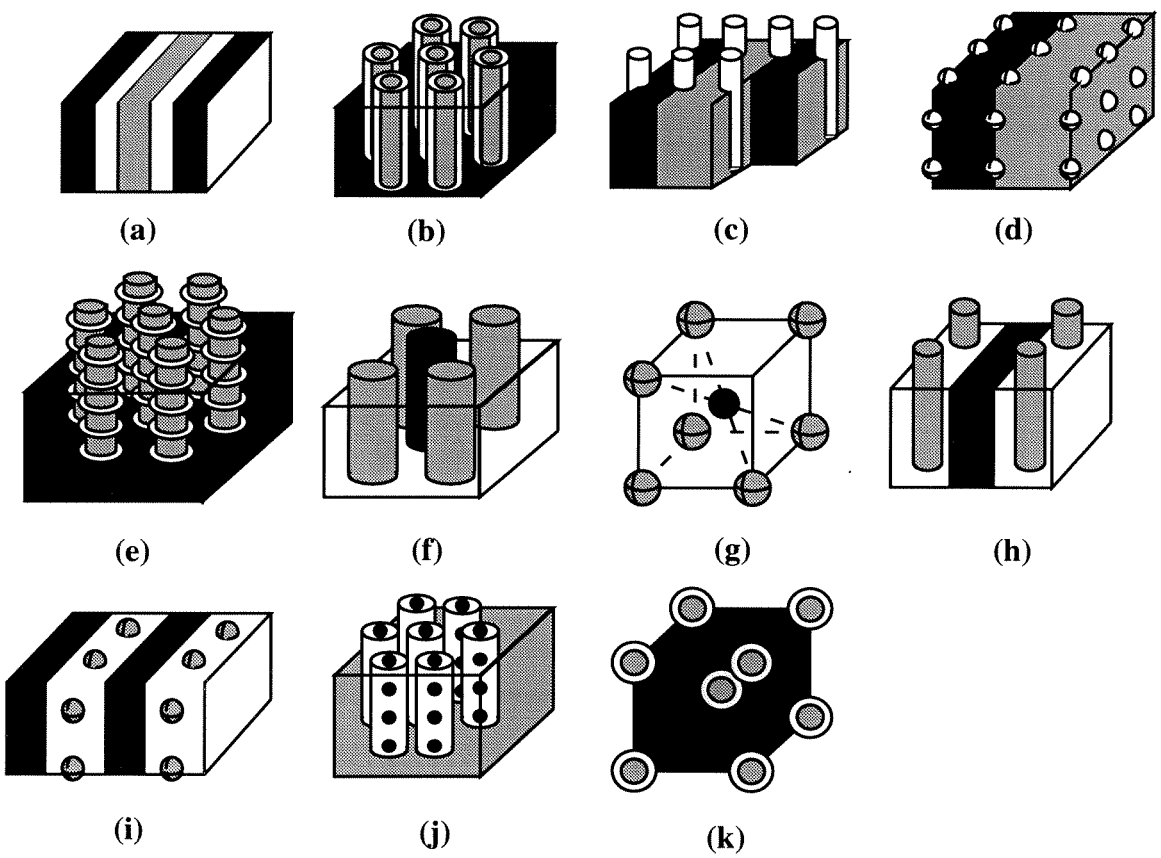

Figure 2.2: Schematic representation of all the phases considered. Dark: a, white: b, and gray: c. : (a) lamellar phase; (b) co-axial cylinder phase; (c) lamella-cylinder phase; (d) lamella-sphere phase; (e) cylinder-ring phase; (f) cylindrical domains in a square lattice structure; (g) spherical domains in the CsCl-type structure; (h) lamella-cylinder-II; (i) lamella-sphere-II; (j) cylinder-sphere; (k) co-centric spherical domain in the bcc structure.

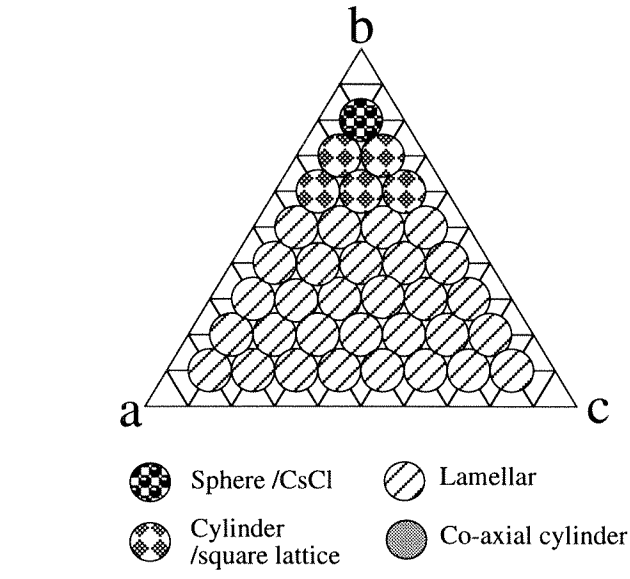

(a)

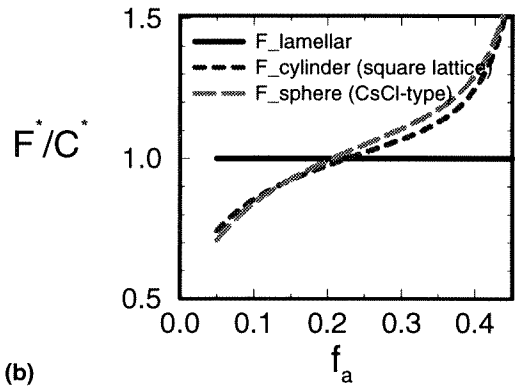

(b)

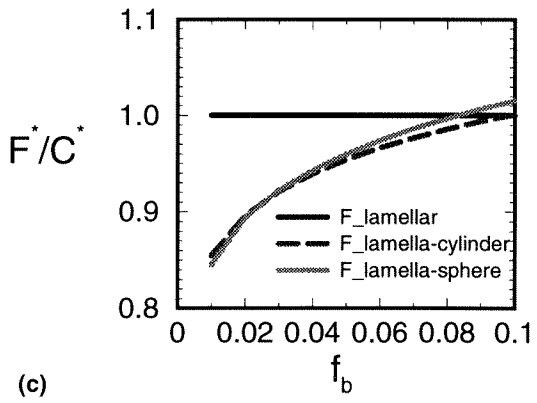

(c)

Figure 2.3: Figure 2.3(a) Phase diagram for $\gamma_1 = 1.0$ and $\gamma_2 = 1.0$. Figure 2.3(b) Equilibrium free energy F^*/C^* for lamellar, cylindrical, and spherical structures for $f_a = f_c$ and $\gamma_1 = 1.0$ and $\gamma_2 = 1.0$. Figure 2.3(c) Equilibrium free energy F^*/C^* for the lamellar, lamella-cylinder, lamella-sphere phases for $\gamma_1 = 1.0$ and $\gamma_2 = 1.0$.

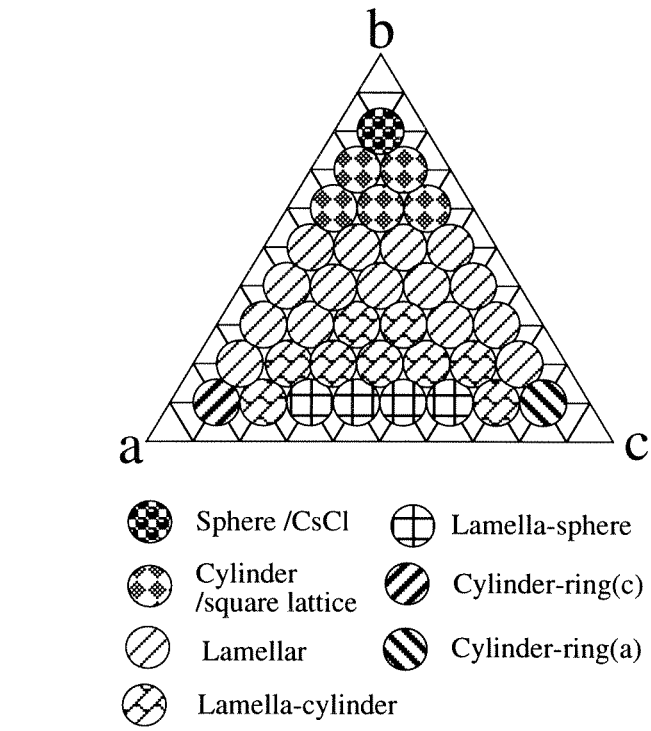

(a)

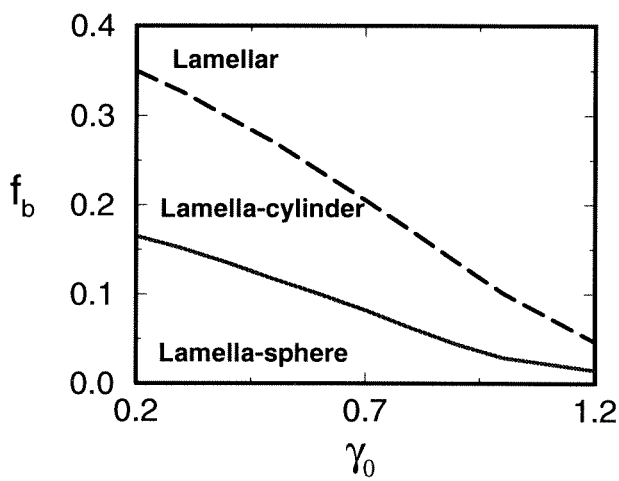

(b)

Figure 2.4: Figure 2.4(a) Phase diagram for $\gamma_1 = 1.0$ and $\gamma_2 = 0.2$. Figure 2.4(b) Phase diagram in terms of f_b versus γ_2 for a system with $f_a = f_c$ and $\gamma_1 = 1.0$.

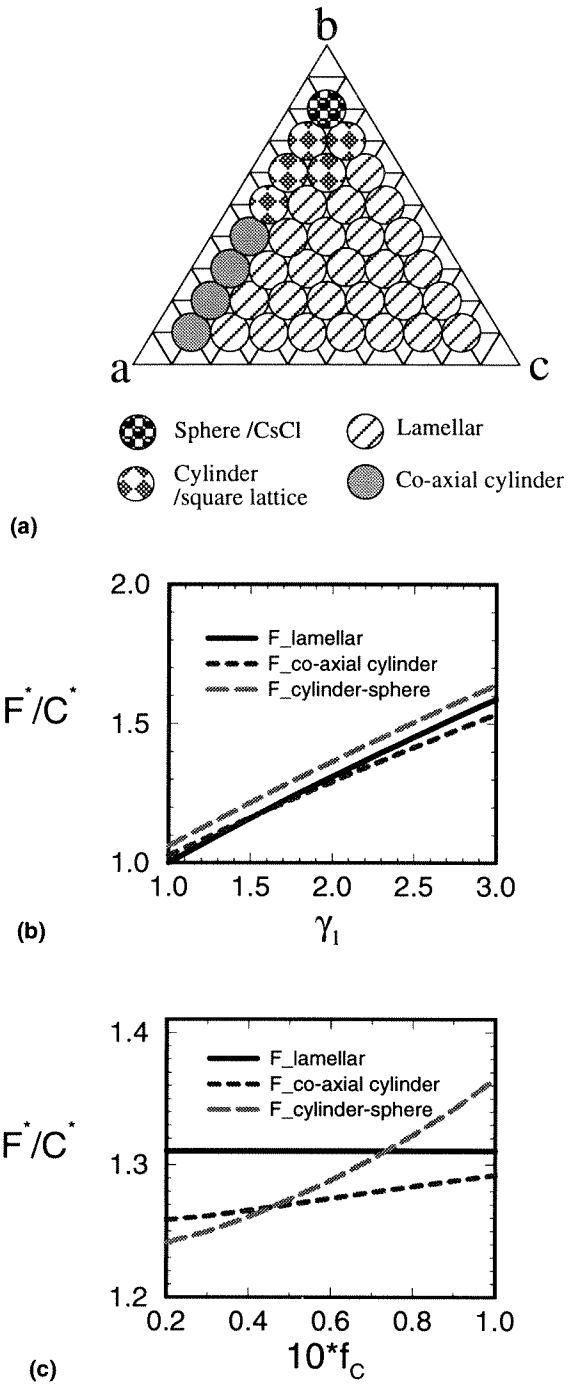

Figure 2.5: Figure 2.5(a) Phase diagram for $\gamma_1 = 2.0$ and $\gamma_2 = 5.0$. Figure 2.5(b) Equilibrium free energy F^*/C^* for the lamellar, co-axial cylinder, and cylinder-sphere phases as a function of γ_1 at volume fractions $f_a = 0.8$ and $f_c = 0.1$ and $\gamma_2 = 5.0$. Figure 2.5(c) Equilibrium free energy F^*/C^* for the lamellar, co-axial cylinder, and cylinder-sphere phases as a function of fc at fixed $f_a = 0.8$ and $\gamma_1 = 2.0$, $\gamma_2 = 5.0$.

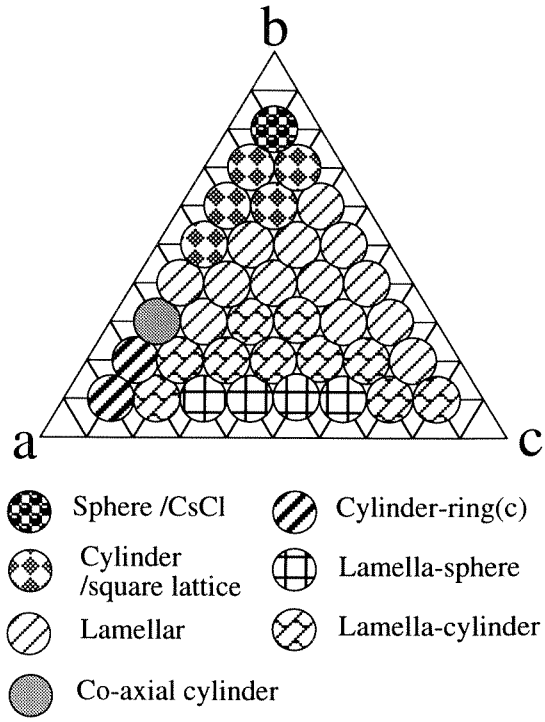

Figure 2.6: Figure 2.6(a) Phase diagram of P(S-b-EB-b-MMA) system of which $\gamma_1 = 1.9$ and $\gamma_2 = 0.3$.

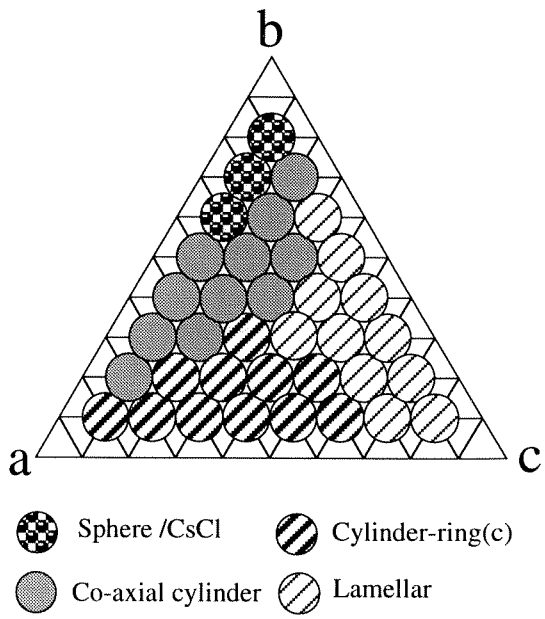

Figure 2.7: Figure 2.6(b) Phase digram of P(S-b-MMA-b-EB) system of which $\gamma_1 = 6.33$ and $\gamma_2 = 3.33$.

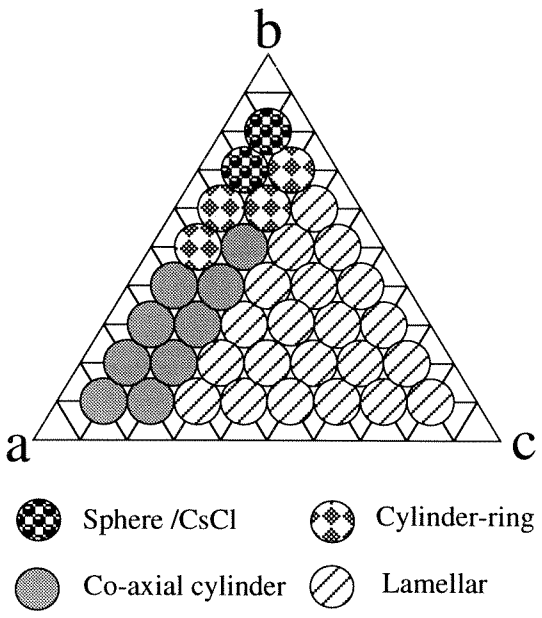

Figure 2.8: Figure 2.6(c) Phase digram of P(MMA-b-S-b-EB) system of which $\gamma_1 = 3.33$ and $\gamma_2 = 6.33$

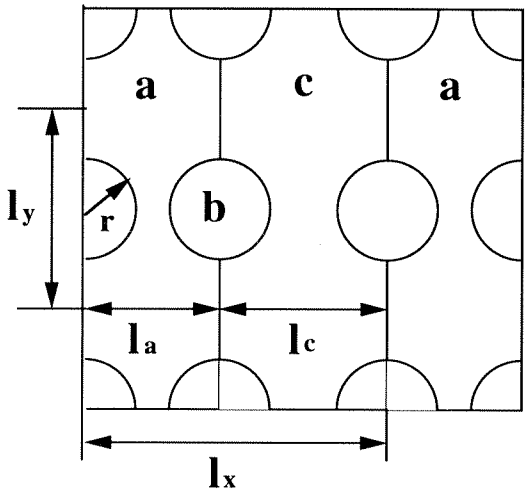

Figure 2.9: Cross-sectional view of lamella-cylinder phase (see also Figure 2.2(c)). l_x and l_y are the primitive translation vectors in the xy plane, l_a and l_c are the thickness of the a and c domains respectively, and r is the radius of the cylinder containing the b blocks.

Bibliography

[1] Morkved, T. L. Wiltzius, P. Jaege, H. M., Grier, D. C., and Witten, T. A., *Appl. Phys. Lett.* **64**, 422 (1994)

[2] Kirk, W. P., and Reed, M. A., eds. *Nanostructures and Mesoscopic Systems* (Academic, New York, 1992)

[3] Archibald, D. D., and Mann, S., *Nature* **364**, 430(1993)

[4] Krege, C. K., Leonowitcz, M. E., Roth, W. L., Vartuli, J. C., and Beck, J. S., *Nature* **359**, 710 (1992)

[5] Helfand, E.; Wasserman, Z.R. *Macromolecules* **1980**, *13*, 994 and the earlier refeerences cited therein.

[6] Semenov, A. N. *Sov. Phys. JETP* **1985**, *61*, 733.

[7] Ohta, T., Kawasaki, K. *Macromolecules* **1986**, *19*, 2621

[8] Ohta, T., Kawasaki, K. *Macromolecules* **1990**, *23*, 2413

[9] Leibler, L. *Macromolecules* **1980**, *13*, 1602

[10] Fredrickson, G.H. and Helfand, E. *J. Chem. Phys* **1987**, *87*, 697

[11] Brazovskii, A. *Sov. Phys. JETP* **1975**, *41*, 85

[12] Hong, K. M. and Noolandi, J. *Macromolecules* **1981**, *14*, 727; ibid **1981**, *14*, 736; Hong, K. M. and Noolandi, J., ibid **1982**, *15*, 482; ibid **1984**, *17*, 1531; Whitmore, M. D., and Noolandi, J., ibid **1988**, *21*, 2972.

[13] Muthukumar, M., Melenkevitz, J., *Macromolecules* **1991**, *24*, 4199

[14] Muthukumar, M., *Macromolecules* **1993**, *26*, 5259

[15] Schick, M., Matsen, M. W., *Macromolecules* **1994**, *27*, 7157

[16] Olmsted , P. D., Milner, S. T., *Phys. Rev. L* **1994**, *72*, 936; ibid **1995**, *74*, 829

[17] Bates, F. S. Fredrickson, G. H. *Annu. Rev. Phys. Chem*, **1990**, *41*, 525

[18] Semonov, A. N., *Macromolecules* **1994**, *27*, 3103.

[19] Anderson, D. M.; Thomas, E. L. *Macromolecules* **1988**, *21*, 3221.

[20] Hadjuk, D. A., Harper, P. E., Gruner, S. M., Honeker, Kim, C., and Thomas, E. L., *Macromolecules* **1994**, *27*, 4063.

[21] Nakazawa, H., Ohta, T. *Macromolecules* **1993**, *26*, 5503

[22] Riess, G. In *Thermoplastic Elastomers. A Comprehensive Review*; Ledge, N. R., Holden, G., Schroeder, H. E., Eds.; Hanser: Munich, 1987; Chapter 12.2, p325.

[23] Riess, G., Schlienger, M., Marti, S. *J. Macromol. Sci. Phys.* **1989**, *B17* (2), 355.

[24] Stadler, R., Auschra, C., Beckmann, J., Krappe, U., Voigt-Martin, I., Leibler, L., *Macromolecules* **1995**, *28*, 3080-3097. This paper appeared after we submitted our manuscript.

[25] Mogi, Y., Kotsuji, H., Kaneko, Y., Mori, K., Matsushita, Y., Noda, I., *Macromolecules* **1992**, *25*, 5408 ; and Mogi, Y., Mori, K., Matsushita, Y., Noda, I. *Macromolecules* **1992**, *25*, 5412; and Mogi, Y., Mori, K., Kotsuji, H., Matsushita, Y., Noda, I., *Macromolecules* **1993**, *26*, 5169

[26] Gido, S.P., Schwark, D. W., Thomas, E. L., do Carmo G. M., *Macromolecules* **1993**, *26*, 2636

[27] Matsushita, Y., Tamura, M., and Noda, I., *Macromolecules* **1994**, *27*, 3680

[28] Auschra, C., Stadler, R., *Macromolecules* **1993**, *26*, 2171

[29] Auschra, C., Stadler, R., *Macromolecules Rapid Communication* **1994**, *15*, 67

[30] Stillinger, F. H., *J. Chem. Phys* **1982**, *78*, 4654

[31] Wu, D., Chandler, D., and Smit, B., *J. Phys. Chem* **1992**, *96*, 4077; Deem, M. W., and Chandler, D., *Phys. Rev. E* **1994**, *49*, 4276 and 4268

[32] Kane, L., Spontak, R. J., *Macromolecules* **1994**, *27*, 1267.

[33] Helfand, E., Tagami, Y. *J. Polym. Sci.***1971**, *B9*, 741; *J. Chem. Phys* **1971** *56*, 3592; ibid **1972**, 1812.

[34] Zheng, W., Wang, Z-G., unpublished results.

[35] *Polymer Handbook*, 3rd ed.; Brandrup., Immergut, E. H., Eds.; J. Wiley & Sons: New York, 1989.

Chapter 3 Microphase Separation of Weakly Charged Diblock Copolymers

3.1 Introduction

Diblock copolymers are macromolecules composed of two sequences of chemically distinct repeat units A and B joined together by covalent bonds. They are fascinating materials with unique mechanical, optical, and structural properties [1], [2]. Due to the incompatibility between monomers A and B and the very low value of mixing entropy for macromolecules, diblock copolymers undergo a microphase separation and assemble into various ordered structures [3]-[6]. It is now well recognized that the phase behavior of AB diblock copolymers is determined by three factors: the overall degree of polymerization, $N = N_A + N_B$; the composition of the copolymer characterized by $f = N_A/N$; and the temperature expressed in terms of the Flory-Huggins interaction parameter χ. For symmetric diblocks (f=0.5), an order-disorder transition takes place at $\chi N \sim 10$ [9]. Depending on the composition and/or temperature, alternating lamellar domains (L), hexagonal packed cylinders (H), body-centered-cubic packed spheres (B), and bicontinuous gyroid structure (G) have been obtained below the order-disorder transition temperature [5], [6].

The distinction between uncharged molecules and electrolytes composed of ions has its counterpart in the field of macromolecules. Recently, considerable attention has been paid to various polyelectrolyte and copolyelectrolyte systems in which a small fraction of charge is incorporated into one or both of the components [7]- [15]. It has been found that the attachment of ionized groups to the backbone of a molecular chain produces striking modifications of the polymer characteristics. For instance, it is well known that a binary mixture of two neutral polymers has a strong tendency toward macroscopic phase separation due to the low values of the mixing entropy [16],[17]. However, even a small amount of charge on one of the polymers can lead to an substantial increase of compatibility and, more surprisingly, alter the character of the transition from macro- to micro-phase separation under certain conditions [8],

[9]. This result is explained by the fact that in the polyelectrolyte system, there are additional contributions to the free energy: the translational entropy of free ions (counterions and salt ions) and the electrostatic interaction among all charged species. The former leads to enhanced compatibility, while the later results in microphase separation due to the new length scale, the Debye screening length.

Charged-neutral diblock copolymers, composed of a charged block A joined to a neutral block B, combine the celebrated microphase separation properties of uncharged diblocks with certain characteristics of charged polymers. In charged-neutral diblock copolymer systems, the long-range electrostatic interactions and the increased mixing entropy due to free ions are influential in determining the microphase separation transition (MST), where the system changes from a disordered state to a periodic structure. Studies of the spinodal instability in charged-neutral diblock copolymers by Marko and Rabin [10], [11], and Mozuelos and de la Cruz [13] show that charged-neutral blocks have greatly enhanced the compatibility between A and B in comparison with the corresponding neutral system. The degree of incompatibility χ and/or the degree of polymerization N at which the microphase separation transition occurs are much larger than in the case of uncharged block copolymers. The most probable wavelength of fluctuation is only weakly affected.

The few limited studies focus on the spinodal limit of the charge-neutral diblock copolymers. The influence of the charge on the relative stability of various ordered structures, the equilibrium properties of charged-neutral diblock copolyemrs remain open questions. In this paper, we theoretically develop a framework which combines the Random Phase Approximation and the Poisson-Boltzmann equation to consistently treat the electrostatic interactions between all charge species as well as the copolymeric contributions to the free energy. Within this framework we then study the microphase separation and the equilibrium properties of charged-neutral block copolymers with an arbitrary amount of added salt in the weak segregation limit.

There are five parameters in the formulation of this system: the Flory-Huggins interaction parameter χ, the monomer charge density α, the molecular weight N, the volume fraction of charged blocks f, and the salt concentration c_s. The different relative strengths of the five parameters give rise to the particular phase behavior of the system. Our analysis of the spinodal instability demonstrates not only the

considerable enhancement of compatibility between A and B, but also the inhibition of the microphase separation under certain conditions.

In order to determine the phase behavior of charged-neutral diblock copolymers, we study the stability of various ordered phases (e.g. lamellae, cylinder, sphere, and gyroid phase) and map out the phase diagrams with various parameter combinations. Due to the breaking of the interchange symmetry between A and B, some new features appear in the phase diagrams that are absent in the neutral case. The mean field critical point, where a direct transition from the disordered to the lamellar phase occurs, is no longer fixed, but rather depends on α, N, and c_s. It is expected that an understanding of the relationship between the relative magnitudes of the five parameters and the phase behavior will provide an important guide for future experimental and theoretical studies.

Since the effective Hamiltonian for charged-neutral block copolymers falls in the same universality class as the Brazovski Hamiltonian [18], concentration fluctuations are important near the mean field critical point. We extend the method of Fredrickson and Helfand [4] to charged-neutral block copolymers by including the fluctuation corrections in the order-disorder transition. The breaking of the interchange symmetry leads to new scaling of fluctuation corrections at a fixed value of monomer charge density α.

The organization of this chapter is as follows: In section 3.2, we derive the effective free energy functional for charged-neutral diblock copolymers by using the Random Phase Approximation. In section 3.3, we discuss the spinodal limit of the system predicted by our model. Some of the results in [10] are reproduced. In section 3.4, we present phase diagrams of charged-neutral diblock copolymers under various conditions. The new features in the phase diagrams are discussed. In section 3.5, fluctuation corrections to the order-disorder transition are discussed. Section 3.6 is the conclusion. In the Appendix, we present the formulas of the self-consistent approach for charged-neutral diblock copolymers.

3.2 Model and Effective Free Energy

We consider a system consisting of charged-neutral diblock copolymers chains. Each chain is made of polyelectrolyte block A of length fNa and neutral block B of length

$(1-f)Na$ joined together by a chemical bond, where N is the overall degree of polymerization, f is the fraction of monomers of block A in a block copolymer, and a is the Kuhn segment length. For convenience, monomers A and B are assumed to have the same monomeric volume v_o and dielectric constant ϵ. Without loss of generality, we assume that block A is positively charged and contains $\alpha f N$ charged ion. There are $\alpha f N$ counterions dissociated from each of the block copolymers, so that the system remains macroscopically neutral. For simplicity we assume that the valency of the charged groups in A blocks and counterion is unity.

In experimental situations, salt is usually added to control the phase behavior of the system. In order to achieve the dissociation of ions (counterions and ions from salt), the average Coulombic energy between two ions has to be much smaller than the thermal kinetic energy ($\sim k_B T$). This requirement leads to the condition: $c_T l_B^3 \ll 1$, where c_T is the total number density of the counterions and salt ions, and l_B is the Bjerrum length $l_B = e^2/\epsilon k_B T$. This inequality is often referred to as the condition for the validity of the Debye-Hückel approximation [19]. The condition can be satisfied by having a low charge density and using polymers with fairly large dielectric constants ($\epsilon \simeq 20$), such as polynitriles or polymers with side-chain alcohols whose backbones will dissolve the ions [10]. An alternative is to add a polar solvent, such as water, to the system to ensure the high polarity of the media. In this paper, we assume that block copolymers have high dielectric constant and the system does not contain solvent, we assume further that the ions are mobile and do not form pairs.

Furthermore, we assume that the counterions are the same species as the negative ions from salt, and hence are not distinguishable. The volume fraction of free ions is negligible. Therefore, the volume fractions of A and B components add to unity and the block copolymers are incompressible.

In a system consisting of charged-neutral diblock copolymer melts and free salt ions, charged species (charged links on block A and free ions) interact by Coulombic interaction, while monomer units A and B interact via a Flory-Huggins interaction. The model Hamiltonian for the system is:

$$H = \sum_i^{n_p} \frac{3}{2Na^2} \int_0^1 ds (\frac{dr_i(s)}{ds})^2 + \chi k_B T \rho_o \int d^3r \hat{\phi}_A(\vec{r}) \hat{\phi}_B(\vec{r}) + \frac{1}{2} \int d^3r \int d^3r' \frac{\hat{\rho}_e(\vec{r}) \hat{\rho}_e(\vec{r'})}{|\vec{r} - \vec{r'}|} \tag{3.1}$$

where the first two terms are the Hamiltonian for neutral block copolymers, χ is the Flory-Huggins interaction parameter for blocks A and B, and $\hat{\phi_A}(\vec{r})$ and $\hat{\phi_B}(\vec{r})$ are the dimensionless monomer-density operators of A and B. They are given by

$$\hat{\phi_A}(\vec{r}) = \frac{N}{\rho_o} \sum_{i=1}^{n_p} \int_0^f ds \delta(\vec{r} - \vec{r}_i(s)) \tag{3.2}$$

$$\hat{\phi_B}(\vec{r}) = \frac{N}{\rho_o} \sum_{i=1}^{n_p} \int_f^1 ds \delta(\vec{r} - \vec{r}_i(s)) \tag{3.3}$$

where $\rho_o = 1/v_o$ is the monomer density per unit volume. The third term in Eq. (3.1) accounts for the electrostatic interaction among all charged species. In the system that we are considering, the charge density of polyelectrolyte A is $e\alpha\rho_o\hat{\phi_A}(\vec{r})$, and the charge density of the positive/negative free ions are $e\hat{c}^+(\vec{r})$ and $-e\hat{c}^-(\vec{r})$, respectively, given by

$$\hat{c^+}(\vec{r}) = \sum_{i=1}^{n_+} \delta(\vec{r} - \vec{r_i^+}) \tag{3.4}$$

$$\hat{c^-}(\vec{r}) = \sum_{i=1}^{n_-} \delta(\vec{r} - \vec{r_i^-}) \tag{3.5}$$

The overall charge density $\rho_e(\vec{r})$ at the point $\vec{r}$ is:

$$\hat{\rho}_e(\vec{r}) = e\alpha\rho_o\hat{\phi_A}(\vec{r}) + e\hat{c}^+(\vec{r}) - e\hat{c}^-(\vec{r}) \tag{3.6}$$

In order for the system to have overall electroneutrality, the space avarage $< \hat{\rho}_e(\vec{r}) >$ must vanish.

In real physical systems, certain amounts of salt are added. For convenience, we choose to use the grand canonical essemble in which the charged-neutral diblock copolymers are in contact with a salt reservoir. The grand canonical partition function of the system is:

$$\begin{aligned} \Xi = & \sum_{i=1}^{n_+} \sum_{j=1}^{n_-} \frac{1}{n_p! n_+! n_-!} \int \prod_i^{n_p} d^3 r_i^p \prod_j^{n_+} d^3 r_j^+ \prod_k^{n_-} d^3 r_k^- \delta(\hat{\phi_A}(\vec{r}) + \hat{\phi_B}(\vec{r}) - 1) \\ & exp\{-\beta H_o - \frac{\beta}{2} \int d^3 r \frac{\hat{\rho}_e(\vec{r})\hat{\rho}_e(\vec{r'})}{|\vec{r} - \vec{r'}|} + \beta\mu_+ n_+ + \beta\mu_- n_-\} \end{aligned} \tag{3.7}$$

where n_p, n_+, n_- are the number of block copolymers, positive free ions and negative free ions, respectively. The number of charged-neutral diblock copolymers n_p is fixed, and the numbers of free ions n_+ and n_- are summed from 0 to ∞ since the system is in contact with a salt reservoir. μ_+ and μ_- are the respective chemical potentials of the positive and negative ions. The delta function selects out only those configurations satisfying the incompressible condition.

Applying the $Kac - Hubbard - Stratnovich$ (KHS) transformation to the electrostatic energy in Eq.(3.7), we obtain:

$$\begin{aligned}\Xi &= \sum_{i=1}^{n_+}\sum_{j=1}^{n_-}\frac{1}{n_p!n_+!n_-!}\int\prod_i^{n_p}d^3r_i^p\prod_j^{n_+}d^3r_j^+\prod_k^{n_-}d^3r_k^-\delta(\hat{\phi_A}(\vec{r})+\hat{\phi_B}(\vec{r})-1)\\ &\int D\xi exp\{-\beta H_o+\frac{1}{8\pi\beta e^2}\int d^3r\xi\nabla^2\xi - i\frac{1}{e}\int d^3r\xi(\vec{r})\hat{\rho}_e(\vec{r})\\ &+\mu_+n_+ + \mu_-n_-\}\end{aligned} \tag{3.8}$$

The field $i\xi(\vec{r})$ is shown below to be the dimensionless potential of the electrostatic field of the system. The KHS transformation introduces the electric potential and decouples the electrostatic interactions between the charged species. The partition function Ξ can be written as a product of the partition functions of charged-neutral block copolymers, and the positive and negative free ions in the electric potential $i\xi(\vec{r})$, i.e.,

$$\Xi = \int D\xi exp\{\frac{1}{8\pi\beta e^2}\int d^3r\xi\nabla^2\xi\}Q_p[\xi]\Xi_+[\xi]\Xi_-[\xi] \tag{3.9}$$

where

$$\Xi_+[\xi] = \sum_{n_+=0}^{\infty}\frac{1}{n_+!}\int\prod_{i=1}^{n_+}d^3r_i^+exp\{-i\int d^3r\xi(\vec{r})\hat{c^+}(\vec{r})+\beta\mu_+n_+\} \tag{3.10}$$

$$\Xi_-[\xi] = \sum_{n_-=0}^{\infty}\frac{1}{n_-!}\int\prod_{i=1}^{n_-}d^3r_i^-exp\{i\int d^3r\xi(\vec{r})\hat{c^-}(\vec{r})+\beta\mu_-n_-\} \tag{3.11}$$

$$\begin{aligned}Q_p[\xi] &= \frac{1}{n_p!}\int\prod_{i=1}^{n_p}d^3r_i^p exp\{-\beta H_o - i\alpha\rho_o\int d^3r\xi(\vec{r})\hat{\phi_A}(\vec{r})\}\\ &\delta(\hat{\phi_A}(\vec{r})+\hat{\phi_B}(\vec{r})-1)\end{aligned} \tag{3.12}$$

Since the electrostatic interactions between charged species are decoupled, the partition functions of the free ions Ξ_+ and Ξ_- are simply those of an ideal gas in an

external field ξ, and thus can be simplified as $\Xi_+ = exp[Q_+]$ and $\Xi_- = exp[Q_-]$, where

$$Q_+ = \int d^3r exp\{-i\xi(\vec{r}) + \beta\mu_+\} \tag{3.13}$$

$$Q_- = \int d^3r exp\{i\xi(\vec{r}) + \beta\mu_-\} \tag{3.14}$$

The configurational partition of block copolymers Q_p, on the other hand, cannot be obtained in closed form. However, we can proceed by using the Random Phase Approximation (RPA). The Random Phase Approximation casts the resultant effective free energy into a Ginzburg-Landau form by performing an order parameter expansion. Here we are going to adopt the RPA approach. The derivation of the effective free energy within the RPA is straightforward extension of that presented by Ohta and Kawasaki [20]. The effective free energy thus obtained is most useful for studying the microphase separation transition in the weak segregation limit. An alternative approach is to use the self-consistent method which involves solving the equations obtained within the Saddle Point Approximation numerically in configuration space. The formulas of self-consistent approach is presented in Appendix.

Within the RPA, the partition function Q_p can be written as

$$Q_p = \int D\psi exp\{-F_o[\psi] - i\alpha\rho_o \int d^3r[\psi(\vec{r}) + f]\xi(\vec{r})\} \tag{3.15}$$

where the order parameter $\psi(\vec{r})$ represents the deviation of the volume fraction of block A from its average value f

$$\psi(\vec{r}) = \phi_A(\vec{r}) - f \tag{3.16}$$

and $F_o[\psi]$ is the effective free energy for the neutral diblock copolymers expanded in terms of the order parameter $\psi(\vec{r})$.

$$\begin{aligned} F_0[\psi] = & \frac{1}{2!}\int_q \Gamma_2(q,-q)\psi(q)\psi(-q) \\ & + \frac{1}{3!}\int_{q_1}\int_{q_2} \Gamma_3(q_1,q_2,-q_1-q_2)\psi(q_1)\psi(q_2)\psi(-q_1-q_2) \\ & + \frac{1}{4!}\int_{q_1}\int_{q_2}\int_{q_3} \Gamma_4(q_1,q_2,q_3,-q_1-q_2-q_3) \end{aligned}$$

$$\psi(q_1)\psi(q_2)\psi(q_3)\psi(-q_1-q_2-q_3)+\cdots \tag{3.17}$$

The first four terms of $F_o[\psi]$ have been derived by Leibler [3], and Ohta and Kawasaki [20]. The coefficients $\Gamma_n(q_1,...,q_n)$, are related to the nth order correlation functions of non-interacting Gaussian copolymer chains $G_{i_1,\cdots,i_n}$, $n=2,3,4,\cdots$, and are given in ref [3] and ref [20]. In particular,

$$\Gamma_2=\frac{g(1,x)}{N(g(f,x)g(1-f,x)-[g(1,x)-g(f,x)-g(1-f,x)]^2/4)}-2\chi \tag{3.18}$$

where $g(f,x)=2(fx+e^{-fx}-1)/x^2$ is the Debye function. The variable $x=q^2R^2$ with $R=(Na^2/6)^{1/2}$ denoting the radius of gyration of an ideal chain of N monomers. Substitution of Eq.(3.15) into Eq.(3.9) yields:

$$\begin{aligned}\Xi &= \int D\xi D\psi exp\{\frac{1}{8\pi\beta e^2}\int d^3r\xi\nabla^2\xi - F_o[\psi] \\ &\quad -i\alpha\rho_o\int d^3r[\psi(\vec{r})+f]\xi(\vec{r})+Q_+[\xi]+Q_+[\xi]\}\end{aligned} \tag{3.19}$$

In order to obtain the effective free energy $F[\psi]$, we need to evaluate the functional integral $\int D\xi$ in the above equation. However, this cannot be done exactly. Instead we apply the Saddle Point Approximation (SPA) to ξ in Eq.(3.19), i.e., approximate the integral $\int D\xi$ by the extremum of the integrand. The Saddle Point Approximation will enable us to solve for the electric field ξ, which can be expanded in term of order parameter ψ.

Within the Saddle Point Approximation, the function ξ must satisfy

$$\frac{1}{4\pi\beta e^2}\nabla^2 i\xi(\vec{r})=-\alpha\rho_o\phi_A(\vec{r})-c^+(\vec{r})+c^-(\vec{r}) \tag{3.20}$$

where $\alpha\rho\phi_A(\vec{r})$, $c^+(\vec{r})$, and $c^-(\vec{r})$ are the respective local number densities of charged blocks, positive, and negative free ions. It is evident that $i\xi$ obey a dimensionless Poisson-Boltzmann equation, and hence is the dimensionless electric potential due to all charge species. For notational convenience, we simply replace $i\xi$ by ξ in the following discussion.

The free ion distributions are derived by taking the derivative of $\Xi_+[\xi]$ and $\Xi_-[\xi]$ with respect to ξ and making use of the relations between $\Xi_+[\xi]$, $\Xi_-[\xi]$ and $Q_+[\xi]$,

$Q_-[\xi]$. The result is

$$c^+(\vec{r}) = exp\{-\xi(\vec{r}) + \beta\mu_+\} \tag{3.21}$$

$$c^-(\vec{r}) = exp\{\xi(\vec{r}) + \beta\mu_+\} \tag{3.22}$$

However, there is no equivalent simple relation between the density distribution $\phi_A(\vec{r})$ and the electric potential ξ.

Since the free ion distributions are related to the electric potential ξ according to Eq.(3.21) and Eq.(3.22), the electric potential field is uniquely determined once the monomer distribution $\phi_A(\vec{r})$ is given. One can solve $\xi(\vec{r})$ and express it as expansion of $\psi(\vec{r})$ using the Poisson-Boltzmann equation. For the convenience of future discussions, we will define some notation from two special cases where the Poisson-Boltzmann equation has simple solutions.

(A) Neutral diblock copolymers The diblock copolymers are neutral when $\alpha = 0$, and there are no counterions in the system. The free ions are all from the salt reservoir and distributed uniformly in space. The electric potential is constant, which can be set to zero. The Poisson equation simply yields $c^+ = c^-$, i.e., the reservoir contains the same amount of positive and negative ions. Let us define c_∞ to be the free ion (positive or negative) density of reservoir. From Eq.(3.21) and (3.22), one obtains

$$\mu_+ = \mu_- = k_B T \log c_\infty \tag{3.23}$$

(B) Homogeneous Phase In a homogeneous phase, all species are distributed uniformly in space and the electric potential ξ is a constant. Let us denote the electric potential in the homogeneous phase as ξ_o. According to Eq.(3.21), (3.22), and (3.23), the free ion density distributions are $c^+ = c_\infty exp(-\xi_o)$ for positive ions and $c^- = c_\infty exp(\xi_o)$ for negative ions. Substituting these expressions into the Poisson equation, we obtain

$$\xi_o = \ln\left[\frac{\alpha\rho_o f + \sqrt{(\alpha\rho_o f)^2 + 4c_\infty^2}}{2c_\infty}\right] \tag{3.24}$$

We define the number density of positive free ions in the homogeneous phase as c_s,

which will be referred to as the salt concentration of the system. c_s is given by

$$c_s = \left[\frac{-\alpha\rho_o f + \sqrt{(\alpha\rho_o f)^2 + 4c_\infty^2}}{2}\right] \tag{3.25}$$

The negative free ion density can be expressed as: $c_- = c_s + \alpha\rho_o f$. The positive free ions are from the salt resevior, while the negative free ions consist of contributions both from counterions and from the salt reservoir. In the homogeneous phase, the density of free ions (postive or negative) from the reservoir is uniquely determined once the monomer charge density α, volume fraction of charged blocks f, and the free ion density of the reservoir, c_∞, are given.

When the system is in an ordered mesophase with a specific symmetry, the electric potential has the same symmetry as the density distribution. In the weak segregation limit, the deviation of the electric potential $\delta\xi(\vec{r})$ from its uniform value ξ_o is small. This deviation can be determined by expanding the quantities in the Poisson equation about their value in uniform phase and the result is

$$\delta\xi(\vec{q}) = \sum_{n=1} \int_{\vec{q}_1} \cdots \int_{\vec{q}_n} h_n(\vec{q}_1, \ldots, \vec{q}_n)\psi(\vec{q}_1)\cdots\psi(\vec{q}_n)\delta(\vec{q} - \vec{q}_1 - \cdots - \vec{q}_n) \tag{3.26}$$

The first three coefficients of $h_n(\vec{q}_1, \cdots, \vec{q}_n)$ are

$$h_1(\vec{q}_1) = G(q) \tag{3.27}$$

$$h_2(\vec{q}_1, \vec{q}_2) = \frac{f}{2} G(\vec{q}_1 + \vec{q}_2) G(\vec{q}_1) G(\vec{q}_2) \tag{3.28}$$

$$\begin{aligned} h_3(\vec{q}_1, \vec{q}_2, \vec{q}_3) = {} & \frac{1}{6} G(\vec{q}_1 + \vec{q}_2 + \vec{q}_3) G(\vec{q}_1) G(\vec{q}_2) G(\vec{q}_3) \\ & \{f^2[G(\vec{q}_1 + \vec{q}_2) + G(\vec{q}_2 + \vec{q}_3) + G(\vec{q}_1 + \vec{q}_3)] - \frac{\alpha N f + 2n_s}{\alpha N}\} \end{aligned} \tag{3.29}$$

where $G(q) = u\alpha N/(x + u(\alpha N f + 2n_s))$ and the symbol n_s denotes the free ions per copolymer volume Nv_o in the corresponding homogeneous phase, i.e.,

$$n_s = c_s N v_o \tag{3.30}$$

Once the expression of the electric field ξ in term of the order parameter ψ is obtained, we can use Eq.(3.19) to obtain the effective free energy $F[\psi]$. Substituting

the expansion of $\delta\xi$ in Eq.(3.19) and expanding Q_p, Q_+ and Q_- in term of the order parameter ψ, we obtain the effective free energy

$$\begin{aligned} NF[\psi] &= \frac{1}{2!}\int_q \gamma_2(q,-q)\psi(q)\psi(-q) \\ &+\frac{1}{3!}\int_{q_1}\int_{q_2}\gamma_3(q_1,q_2,-q_1-q_2)\psi(q_1)\psi(q_2)\psi(-q_1-q_2) \\ &+\frac{1}{4!}\int_{q_1}\int_{q_2}\int_{q_3}\gamma_4(q_1,q_2,q_3,-q_1-q_2-q_3) \\ &\psi(q_1)\psi(q_2)\psi(q_3)\psi(-q_1-q_2-q_3) \\ &+\cdots \end{aligned} \tag{3.31}$$

where $\gamma_n(q_1,...,q_n) = N\Gamma_n(q_1,...,q_n)+N\delta\Gamma_n(q_1,...,q_n)$, $n=2,3,4,\cdots$ The corrections $\delta\Gamma_n$ are the result of the presence of the charges in diblock copolymers and the free ions. Their expressions are:

$$\delta\Gamma_2(q,-q) = \frac{u(\alpha N)^2}{x+u(\alpha Nf+2n_s)} \tag{3.32}$$

$$\delta\Gamma_3(q_1,q_2,-q_1-q_2) = -\frac{u^3(\alpha N)^4 f}{[x+u(\alpha Nf+2n_s)]^3} \tag{3.33}$$

$$\begin{aligned} \delta\Gamma_4(q_1,q_2,q_3,-q_1-q_2-q_3) &= \frac{u^4(\alpha N)^4}{\prod_{i=1}^4[x_i+u(\alpha Nf+2n_s)]} \\ &\{\frac{u(\alpha Nf)^2}{R^2(q_1+q_2)^2+u(\alpha Nf+2n_s)} \\ &+\frac{u(\alpha Nf)^2}{R^2(q_2+q_3)^2+u(\alpha Nf+2n_s)} \\ &+\frac{u(\alpha Nf)^2}{R^2(q_3+q_1)^2+u(\alpha Nf+2n_s)} \\ &-(\alpha Nf+2n_s)\} \end{aligned} \tag{3.34}$$

where the constant $u = (4\pi e^2/6\epsilon a k_B T)a^3/v_o$ is essentially the ratio of the Bjerrum length $l_B = e^2/\epsilon k_B T$ to the monomer size a, renormalized by the factor a^3/v_o. For water at 300K with $\epsilon \approx 80$, the Bjerrum length is about $7\mathring{A}$. The dielectric constant ϵ of a polymer is usually smaller than that of water. However, if it is too small, the assumption of mobile counterions is not valid. We assume that the block copolymers have a high dielectric constant $\epsilon \simeq 20$ with Kuhn length $a = 7\mathring{A}$ and monomer volume $v_o = 100\mathring{A}^3$, thus the constant $u = 28$. The quantity $n_s = c_s N v_o$ is uniquely

determined by c_∞, α and f as shown in Eq.(3.25) and (3.30).

Equations (3.31)-(3.34) completely define the free energy of the system in the weak segregation limit. Minimizing the free energy with respect to the order parameter $\psi(\vec{r})$ determines the equilibrium structure of the system. Once the order parameter $\psi(\vec{r})$ is solved, the electric potential and density distribution of free ions are also determined. We would like to emphasize that the average values of densities of free ions (positive or negative) in an ordered phase are different from their values in the corresponding homogeneous phase. For a particular ordered strucutre, the average density of positive free ions is

$$c_{ord} = c_s \frac{1}{V} \int d^3 r exp[\delta\tilde{\xi}(\vec{r})] \tag{3.35}$$

Since, in general, $\frac{1}{V}\int d^3 r exp[\delta\tilde{\xi}(\vec{r})] \neq 1$, the average values of densities of positive free ions in an ordered phase $c_{ord} \neq c_s$, although their difference is rather small. Similarly, the average density of negative free ions in an ordered phase does not equal the negative free ion density in the corresponding homogeneous phase.

For neutral diblock copolymer melts without including the fluctuation effect, the MST and the phase behavior are completely determined by two parameters: f and χN. In charged-neutral diblock copolymer system, the free energy contains five parameters:

$$\alpha, \chi, N, f, c_\infty \tag{3.36}$$

or, equivalently,

$$\alpha, \chi, N, f, c_s \tag{3.37}$$

These parameters control the behavior of the system. Our goal is to find the region of stability of the microscopically structured phase in the phase diagram of the system and to understand how the parameters Eq.(3.36) or (3.37) control the properties of the phase. Notice that under the simultaneous scaling

$$\alpha \to \lambda\alpha, \chi \to \lambda\chi, N \to \frac{1}{\lambda}N, c_\infty \to \lambda c_\infty, D \to \frac{1}{\lambda}D \tag{3.38}$$

where D is the period of ordered structure, the free energy remains unchanged. So the property of the system after such scaling remains similar to that before the scaling.

3.3 Spinodal Limit of the Homogeneous Phase

In order to investigate the stability of the homogeneous phase and microphase separation transition (MST) in charged-neutral diblock copolymer systems, we study the concentration fluctuation of the system. The fluctuation may be characterized by the density-density correlation function

$$S(\vec{r}-\vec{r'}) =< \psi(\vec{r})\psi(\vec{r'}) > \tag{3.39}$$

The Fourier transform of the correlation function $S(\vec{q})$, also called the structure function in scattering experiments, can be studied by elastic scattering experiments, such as X-ray or neutron scattering ($\vec{q}$ denotes the scattering vector with length $4\pi[sin(\theta/2)]/\lambda$, where λ is the wavelength and θ the scattering angle). Its inverse $S^{-1}(\vec{q})$ is given by $\gamma_2(q,-q)$

$$\begin{aligned} NS^{-1}(\vec{q}) &= \frac{g(1,x)}{(g(f,x)g(1-f,x)-[g(1,x)-g(f,x)-g(1-f,x)]^2/4)} - 2\chi N \\ &+ \frac{u(\alpha N)^2}{x+u(\alpha N f+2n_s)} \end{aligned} \tag{3.40}$$

where the first two terms come from the structure function of neutral diblock copolymers, χ is the Flory-Huggins interaction parameter, and the third term is the contribution from the electrostaic interaction between charged blocks and free ions. The third term has the form of a screened Coulomb interaction with the Debye-Hückel screening length $l_D = Ru^{-1/2}(\alpha N f + 2n_s)^{-1/2}$. The screening is due to the presence of free ions and the rearrangement of them at a given block copolymer density distribution $\psi(\vec{r})$.

For neutral diblock copolymers, it has been shown that only certain fluctuations become anomalously large when the interaction parameter χ approaches the transition point χ_t: $S(\vec{q})$ has a very narrow maximum for a certain value of $|\vec{q}| = q^* \neq 0$. As χN becomes greater than $\chi_t N$ and is equal to a certain value $\chi^* N$, fluctuations with a wavevector $|\vec{q}| = q^*$ diverge: $S(q^*) \to \infty$. This is the spinodal point. The spinodal point determines the limit of metastability of the homogeneous states.

The spinodal wavevector q^* is determined by minimizing

$$F(x) = \frac{g(1,x)}{(g(f,x)g(1-f,x) - [g(1,x) - g(f,x) - g(1-f,x)]^2/4)} \tag{3.41}$$

with respect to x, where $x^* = (q^*R)^2$. An interesting property of neutral diblock copolymers is that q^* only depends on f, while q^* of charged-neutral diblock copolymers depends on the volume fraction f, the molecular weight N, the monomer charge density α, and the free ion concentration of the reservoir c_∞. The spinodal value of χ^*N for neutral diblock copolymers is given by $\chi^*N = 0.5F(x^*)$. Thus, in neutral diblock copolymer systems, the MST can be reached either by reducing the temperature (increasing χ) or by increasing the molecular weight N so that $\chi N \geq \chi^* N$.

In charged-neutral diblock copolymer systems, the MST depends on the five parameters in Eq.(3.36) or (3.37). Their relative magnitude plays an important role in determining the MST. For a system with a given N, α, f, and c_∞, the system can reach the MST by reducing the temperature (increasing χ). However, for a system with a fixed temperature, the system cannot always reach the MST with increasing N; certain relations among c_∞, α, χ and f must be satisfied in order to achieve MST. We will discuss each of the possible situations in detail.

MST by reducing temperature In charged-neutral block copolymer systems, if we allow a change in temperature, the spinodal wavevector can be obtained using a similar method that used for neutral chain system, i.e., by minimizing

$$F(x) + \frac{u(\alpha N)^2}{x + u(\alpha N f + 2n_s)} \tag{3.42}$$

with respect to x. The spinodal value of χ^* is given by

$$\frac{0.5}{N}\{F(x^*) + \frac{u(\alpha N)^2}{x^* + u(\alpha N f + 2n_s)}\} \tag{3.43}$$

Both the spinodal value χ^* and the corresponding wavevector q^*R depend on the parameters f, α, N and n_s.

Figure 3.1 shows the dependence of χ^*N on number of charges αN on a block copolymer for two salt concentrations $n_s = 0, 10$ with f equals to 0.5. It is shown that a small amount of charge in a polyelectrolyte can greatly enhance the compatibility

of monomers A and B. The interaction χ^*N increases far above the corresponding neutral diblock copolymers value. and a microphase separation takes place at a lower temperature. On the other hand, as αN increases the critical wavevector q^*R is weakly affected and the MST occurs at a slightly shorter length scale.

When $\alpha Nf \gg n_s$, the electrostatic energy dominates the free energy. For the salt free case, a linear dependence of χ^*N on αN was first observed by Marko and Rabin [10]. For an arbitrary value of the volume fraction, f, and a small amount of salt, it can easily be shown that $\chi^*N \sim \alpha N/(2f) - n_s/f^2$.

Figure 3.2(a) and (b) show the dependence of spinodal value χ^*N and the corresponding wavevector as functions of charges αN with the volume fractions $f = 0.2$, 0.5, and 0.8 in a salt free system. These figures demonstrate that adding charge to block A breaks the $A-B$ interchange symmetry. Thus, the dependence of the critical parameters on αN differs for the two cases. For the same monomer charge density α, the system with $f = 0.2$ has a much higher spinodal point of χ^* than that of the system with $f = 0.8$. Thus, for a system with a given monomer charge density α, the smaller the volume fraction of charged block the more stable the system in the homogeneous phase.

Figure 3.3(a) shows the dependence of χ^*N on the salt concentration n_s with $f = 0.5$ and $\alpha N = 10, 20$, and 50 respectively. Addition of salt reduces the electrostatic interactions due to screening. The spinodal value of χ^*N approaches the neutral chain limit as $n_s \to \infty$. The corresponding wavevector q^*R also decays toward its neutral limit as the salt concentration n_s increases (Figure 3.3(b)). Notice that q^*R decays toward its neutral limit much faster than the spinodal value χ^*N does.

MST with fixed value of Flory-Huggins parameter χ For a given diblock copolymer $A-B$, the Flory-Huggins parameter χ (of order $10^{-3} - 10^{-1}$) is the net interaction (van der Waals interaction) between segements A and B, divided by k_BT. Due to the chemical and physical nature of a particular diblock copolymer, the temperature can be varied only within a certain range (e.g. temperature should not be smaller than glass transition temperature), thus the interaction parameter χ can vary only within a certain range as well. For a given value of χ, the system is not always able to reach the MST with increasing molecular weight N. In this situation, certain relations among the monomer charge density α, salt concentration c_s and volume

fraction f has to be satisfied in order to achieve MST. To investigate the MST condition at a fixed temperature, we rewrite the inverse of structure function $NS^{-1}(q)$ as follows:

$$\begin{aligned} NS^{-}(q) &= F(x,f) - 2\chi N + \frac{u\beta^2(\chi N)^2}{x + \beta\chi N u(f + 2n_s/\alpha N)} \\ &\propto (\chi N)^2\{u\beta^2 - 2u\beta(f + 2n_s/\alpha N)\} \\ &\quad +\chi N\{F(x)u\beta(f + 2n_s/\alpha N) - 2x\} + F(x)x \end{aligned} \tag{3.44}$$

where $\beta = \alpha/\chi$. The solution of spinodal instability exists only when $u\beta^2 - 2u\beta(f + 2n_s/\alpha N) < 0$, i.e.,

$$4c_s v_o/\alpha > (\beta - 2f) \tag{3.45}$$

This inequality is a criterion for the MST at fixed temperature. It shows that:

(a) For a system with given values of monomer charge density α, temperature χ, and volume fraction f, if $\beta \leq 2f$, the MST is possible even without additional salt from the reservoir, however, if $\beta > 2f$, the compatibility of A and B is enhanced to the extent that without a sufficient amount of additional salt from reservoir the homogeneous phase is always stable.

(b) For a system with given value of salt concentration c_s, temperature χ, and volume fraction f, the MST is possible only if $\alpha < \alpha_{max} = f\chi + \sqrt{(f\chi)^2 + 4c_s v_o \chi}$.

(c) For a system with given value of salt concentration c_s, monomer charge density α, and temperature χ, MST is possible only if $f > 0.5(\beta - 4c_s v_o)$. Thus for a system with $\beta < 4c_s v_o$, MST is possible at any value of f, while for a system with $\beta \geq 4c_s v_o$, MST is possible only when the volume fraction of the charged block A is sufficiently large.

When the condition stated in Eq.(3.45) is satisfied, the minimum value of N at which the spinodal occurs is

$$N^* = (-b - \sqrt{b^2 - 4ac})/(2a\chi) \tag{3.46}$$

where $a = u\beta^2 - 2u\beta(f + 2c_s v_o/\alpha)$, $b = F(x^*)u\beta(f + 2c_s v_o/\alpha) - 2x^*$, and $c = F(x^*)x^*$. For a system with a given Flory-Huggins parameter χ, only when the condition in

Eq.(3.45) is satisfied can the MST be achieved by increasing $N \geq N^*$.

In Figure 3.4, we have plotted the solutuions expressed in Eq.(3.46). The molecular weight N dependence on α for given values of χ, f, and c_s is clearly illustrated in the figure. When $\alpha = 0$, the system is a neutral diblock copolymer and N^* equals its neutral limit. The critical value N^* of charged-neutral block copolymers is always larger than that of neutral block copolymers, and increases as α increases. At a sufficiently large value of α, the minimum value of molecular weight N^* for spinodal instability approaches infinity, i.e., microphase separation is inhibited. In a salt free system, the minimum molecular weight N^* increases drastically even for a small increase of charge, while in a system with salt concentration $c_s v_o = 0.01$, the minimum molecular weight N^* increases slowly as α increases from zero and N^* approaches infinity only when α approaches its maximum value α_{max}. In a system with a fixed value of Flory-Huggins parameter, the MST cannot always be reached by increasing molecular weight alone, but can always be reached by increasing salt concentration and molecular weight so that the criterion in Eq.(3.45) is satisfied.

3.4 Transition between Different Ordered Phases

In this section, we study the stability of various microdomain patterns including the lammellar, cylinder, bcc, and gyroid phases, and determine how molecular weight, temperature, monomer charge density, and salt concentration affect the equilibria of various morphologies. These calculations allow the constructions of phase diagrams of the charged-neutral diblock copolymers under various conditions.

(A) Free Energy for Lamellar, Cylinder, and BCC phases In order to determine the equilibrium property of charged-neutral diblock copolymers, we want to further simplify the Landau-Ginzburg expansion of the free energy density given in Eq.(3.31)-(3.34). The order parameter can be written as

$$\psi(\vec{r}) = \sum_i \psi_i f_i(\vec{r}) \tag{3.47}$$

where $f_i(\vec{r})$ are basis functions which posses the symmetry of that particular structure. For lamellar, cylinder, and bcc structures, we use a one-mode approximation, i.e., we consider only the first shell of reciprocal space. This approach becomes exact in the

limit that $S(q) = \delta(q - q^*)$, i.e., in the limit that the composition profile is exactly sinusoidal. Although this is not the case, in practice the correlation function has a very pronounced maximum for $|\vec{q}| = q^*$ near the spinodal, i.e., the important fluctuations are those with wavevector $|\vec{q}| = q^*$. As a result the one-mode approximation is a good approximation.

Within the one-mode approximation, the order parameter for lamellar, cylinder, and bcc phases takes the form

$$\psi(\vec{r}) = \frac{1}{\sqrt{n}}\psi_n \sum_{k=1}^{n}\{exp[i\vec{Q}_k + \phi_k] + cc\} \tag{3.48}$$

$$|\vec{Q}_i| = q^*, \qquad i = 1, ...n \tag{3.49}$$

In the above expression, the equilibrium values of the amplitude ψ_n and the phase ϕ_k are determined by minimizing the free energy. There are three simple cases: the case $n = 1$ corresponds to the lamellar phase; the case $n = 3$ with

$$\vec{Q}_1 = q^*[1, 0, 0], \quad \vec{Q}_2 = \frac{1}{2}q^*[-1, \sqrt{3}, 0], \quad \vec{Q}_3 = \frac{1}{2}q^*[-1, -\sqrt{3}, 0] \tag{3.50}$$

corresponds to the hexagonally arranged cylinder phase; and the case $n = 6$ with

$$\begin{aligned} \vec{Q}_1 &= 2^{-1/2}q^*(1, 1, 0) & \vec{Q}_2 &= 2^{-1/2}q^*(-1, 1, 0) \\ \vec{Q}_3 &= 2^{-1/2}q^*(0, 1, 1) & \vec{Q}_4 &= 2^{-1/2}q^*(0, 1, -1) \\ \vec{Q}_5 &= 2^{-1/2}q^*(1, 0, 1) & \vec{Q}_6 &= 2^{-1/2}q^*(1, 0, -1) \end{aligned} \tag{3.51}$$

corresponds to the bcc phase.

The vertex functions γ_n defined in Eq.(3.32)-(3.34) can also be simplified using the one-mode approximation. The coefficient $\gamma_3(\vec{q}_1, \vec{q}_2, \vec{q}_3)$ vanishes unless $\vec{q}_1 + \vec{q}_2 + \vec{q}_3 = 0$. The wavevectors $\vec{q}_1, \vec{q}_2, \vec{q}_3$ form an equilateral triangle with magnitude $|\vec{q}_i| = q^*$. All nonvanishing $\gamma_3(\vec{q}_1, \vec{q}_2, \vec{q}_3)$ are equal and depend on f, α, N, and c_∞, which will be denoted as $\gamma_3(f, \alpha, N, c_\infty)$. The coefficient $\gamma_4(\vec{q}_1, \vec{q}_2, \vec{q}_3, \vec{q}_4) \neq 0$ only if $\sum_{i=1}^{4} \vec{q}_i = 0$, so that γ_4 depends only on two independent angles: that between vectors $\vec{q}_1$ and $\vec{q}_2$ and that between vectors $\vec{q}_1$ and $\vec{q}_4$ (since $|\vec{q}_i| = q^*$) . For convenience, we approximate

$\gamma_4(\vec{q}_1, \vec{q}_2, \vec{q}_3, \vec{q}_4)$ by setting $\vec{q}_1+\vec{q}_2 = 0$ and $\vec{q}_1+\vec{q}_4 = 0$. This approximation has been used by other authors [4] and can be shown to be fairly accurate. The coefficient γ_4 also depends on f, α, N, and c_∞, and is denoted as $\gamma_4(f, \alpha, N, c_\infty)$.

Substituting the order parameter expression in Eq.(3.48) and (3.49) into the Landau-Ginzburg expression for free energy, Eq.(3.31), the free energy of the lamellar, cylinder, and bcc phases within a one-mode approximation can be written as

$$FN/k_BT = 2N(\chi^* - \chi)\psi_n^2 - \alpha_n\psi_n^3 + \beta_n\psi_n^4 \tag{3.52}$$

where the coefficients α_n and β_n for various phases were first given by Leibler [3] and are listed in the following table for convenience:

Table I

	lamellar $n=1$	*cylinder* $n=3$	*bcc* $n=6$
α_n	0	$\alpha_3 = -\frac{2}{3\sqrt{3}}\gamma_3$	$\alpha_6 = -\frac{4}{3\sqrt{6}}\gamma_3$
β_n	$\beta_1 = \frac{\gamma_4}{4}$	$\beta_3 = \frac{5\gamma_4}{12}$	$\beta_6 = \frac{15\gamma_4}{24}$

(B) Free Energy for the Gyroid Phase The gyroid phase is a bicontinuous cubic structure whose symmetry belongs to space group $Ia\bar{3}d$. The structure consists of a channel-forming minority phase embedded in a matrix of the majority component. The minority and majority components are continuous and periodic in all three principle directions. The channels are subdivided into two distinct, interpenetrating networks. The channels join as triads and the two networks are mirror images of one another. Underlying the topology is an infinity triply periodic minimum surface, called a G minimal surface, as mathematically discovered by Schoen [21].

The gyroid phase was first experimentally observed in lipid-water system a few decades ago [22]. In block copolymer systems, it was first observed by Gobran in polystyrene-polyisoprene diblock copolymers consisting of $37wt\%$ styrene [23] and was identified by Gruner, Thomas and co-workers [24] in a weakly segregated melt. The first few basis functions of the gyroid phase are:

$$f_0(\vec{r}) = 1 \tag{3.53}$$

$$f_1(\vec{r}) = \sqrt{8/3}[cos(X)sin(Y)sin(2Z) + cos(Y)sin(Z)sin(2X) + cos(Z)sin(X)sin(2Y)] \tag{3.54}$$

$$
\begin{aligned}
f_2(\vec{r}) &= \sqrt{(4/3)}[cos(2X)cos(2Y) \\
&\quad +cos(2Y)cos(2Z) + cos(2Z)cos(2X)] \qquad (3.55) \\
f_3(\vec{r}) &= \sqrt{(4/3)}\{sin(2X)[cos(3Y)sin(Z) - sin(3Y)cos(Z)] \\
&\quad +sin(2Y)[cos(3Z)sin(X) - sin(3Z)cos(X)] \\
&\quad +sin(2Z)[cos(3X)sin(Y) - sin(3X)cos(Y)]\} \qquad (3.56) \\
f_4(\vec{r}) &= \sqrt{2/3}[cos(4X) + cos(4Y) + cos(4Z)] \qquad (3.57)
\end{aligned}
$$

where $X = 2\pi x/D$ is a dimensionless length, Y and Z are defined similarly, and D is the size of the cubic unit cell. The order parameter of the gyroid phase must contain at least the first three basis functions in order to capture the main features of the struture,i.e.,

$$\psi(\vec{q}) = \psi_1 f_1(\vec{q}) + \psi_2 f_2(\vec{q}) \qquad (3.58)$$

where the coefficient ψ_0 vanishes because the space average of the order parameter $< \psi >$ is zero. The function $f_i(\vec{q})$ is the Fourier transform of the basis function $f_i(\vec{r})$, which can be written explicitly as

$$f_i(\vec{q}) = \sum_{k=1}^{n_i} C_i^{(k)} \delta(\vec{q} - \vec{Q}_i^{(k)}) \qquad (3.59)$$

$$i = 1, 2, \cdots$$

where $n_1 = 24$ and $n_2 = 12$. The vector $\vec{Q}_i^{(k)}$ is the kth wavevector contained in $f_i(\vec{r})$, and the coefficient $C_i^{(k)} = 1/v \int d^3r f_i(\vec{r}) exp(-i\vec{Q}_i^{(k)}\vec{r})$.

Substituting the order parameter of the gyroid phase as expressed in Eq.(3.59) into the Landau-Ginzburg free energy in Eq.(3.31), we obtain the free energy of the gyroid phase:

$$
\begin{aligned}
FN/k_BT &= 0.5\psi_1^2 S^{-1}(q^*) + 0.5\psi_2^2 S^{-1}(\sqrt{4/3}q^*) \\
&\quad +(a_3^{(1)}\ \psi_1^3 + a_3^{(2)}\ \psi_1^2\psi_2^1 + a_3^{(3)}\ \psi_1^3)\ \gamma_3 \\
&\quad +(b_4^{(1)}\ \psi_1^4 + b_4^{(2)}\ \psi_1^2\psi_2^2 + b_4^{(3)}\ \psi_2^4)\ \gamma_4 \qquad (3.60)
\end{aligned}
$$

where $a_3^{(1)} = 0.068041$, $a_3^{(2)} = -0.144338$, $a_3^{(3)} = 0.192450$, $b_4^{(1)} = 0.088542$, $b_4^{(2)} = 0.124998$, $b_4^{(3)} = 0.15625$. In the derivation of the above free energy, all nonvanishing

$\gamma_3(\vec{q}_1, \vec{q}_2, \vec{q}_3)$, and $\gamma_4(\vec{q}_1, \vec{q}_2, \vec{q}_3, \vec{q}_4)$, where $\vec{q}_i \in \vec{Q}_i^{(\alpha_i)}$, $i = 1, 2$, $\alpha_i = 1, 2, ...n_i$, have been approximated as constants $\gamma_3(f, \alpha, N, c_\infty)$ and $\gamma_4(f, \alpha, N, c_\infty)$ respectively. The correction due to this approximation is negligible.

(C) The Third and Fourth Order Vertex Functions Before we start to calculate the phase diagram for charged-neutral diblock copolymers, we study the quantitative relation between the vertex functions γ_3 and γ_4, and the parameters f, αN, and c_∞. The vertex functions γ_3, γ_4 of neutral diblock copolymers have been studied by Leibler. Within the one-mode approximation they depend only on the volume fraction f, and their dependence on f is shown in Figure 3.5(a) and (b) as dotted lines. For neutral diblock copolymers, γ_3 is antisymmetric with respect to $f = 0.5$, which reflects the interchange $A - B$ symmetry. At $f \neq 0.5$, γ_3 of neutral diblock copolymers does not vanishes identically and the MST is, in general, a first order phase transition according to the Landau theory. At $f = 0.5$, the coefficient γ_3 vanishes and the MST is a second order transition.

The influence of monomer charge density α and the reservoir salt concentration c_∞ on the vertex functions γ_3 and γ_4 of charged-neutral diblock copolymers are shown in Figure 3.5. In Figure 3.5(a), we have plotted γ_3 as a function of the volume fraction f at $\alpha N = 40$, $c_\infty v_o N = 0$ and $\alpha N = 40$, $c_\infty v_o N = 20$ respectively. In contrast to γ_3 of neutral diblock copolymers, γ_3 of charged-neutral diblock copolymers does not vanishes at $f = 0.5$. Instead, it vanishes at an f larger than 0.5. Clearly, adding charges to A blocks breaks the $A - B$ interchange symmetry. The amount of shift increases as αN increases and decreases as the salt concentration increases. In Figure 3.5(b), we have plotted the corresponding γ_4 as a function of f for charged-neutral diblock copolymers. The value of γ_4 of charged-neutral diblock copolymers in the salt free case ($c_\infty = 0$) is much larger than its neutral limit. To explicitly demonstrate the influence of monomer charge density α on γ_4, we have plotted γ_4 as a function of αN at a volume fraction of $f = 0.5$ and various reservoir concentrations $n_r = 0, 5, 10$ in Figure 3.6, where n_r denotes the number of positive/negative ions per volume Nv_o in the reservoir. When the system does not have added salt, γ_4 increases linearly as αN increases. In fact, it can be shown that for $n_r \simeq 0$, γ_4 increases as $2\alpha N/f^3$. The addition of salt reduces the electrostatic interaction, thus reducing the value of γ_4 to it neutral limit.

(D) Phase Diagrams The analysis of the microphase separation transition follows from the minimization of the free energy with respect to the amplitudes of order parameters. At a given set of parameters f, χ, N, α, and c_∞, the morphology which has the lowest free energy is the equilibrium state of the system. By varying the five parameters, we can map out the phase diagrams under various conditions.

(1) Dependence of the Morphology on χ and f

The dependence of the morphology of the charged-neutral block copolymers on the Flory parameter χ and the volume fraction f is demonstrated in Figure 3.7. The phase diagram is set at constant monomer charge density α and constant reservoir concentration c_∞ such that $\alpha N = 50$ and $c_\infty v_o N = 30$. In the phase diagram, the molecular weight N is fixed, although its value can be arbitrary so that the phase diagarm presents a class of systems related to each other through the scaling relation in Eq.(3.36).

The difference between the charged-neutral diblock copolymers and neutral diblock copolymers was pronounced. In contrast to the phase diagram for neutral diblock copolymers which shows that the disordered phase always transits to bcc phase and is first order, except at $f = 1/2$ where the transition is second order and to the lamellar phase [3]. For charged-neutral block copolymer, the symmetry of interchange $A - B$ is broken. At $f = 1/2$, the transition is to bcc phase and first order. The second order transition from disorder to lamellar occurs at f_c which depends on the monomer charge density α, the molecular weight N, and the reservoir concentration c_∞. In this particular case $f = 0.561$. In mapping out the phase diagram in Figure 3.7, we have considered the free energies of the lamellar, cylinder, bcc, and gyroid phases. In addition, we also calculated the free energy of structures of simple-cubic packed sphere (sc) and face-centered-cubic packed sphere (fcc) which are not stable in neutral diblock copolymers in the weak segregation limit. We found that the fcc and sc phases are not stable in charged-neutral diblock copolymers either.

Unlike the other phases which extend to the critical point, the gyroid phase ends at the triple points: $f = 0.525$, $\chi N = 30.116816$ and $f = 0.610$, $\chi N = 30.579898$, where it coexists with the lamellar, cylinder phases. For a system with $0 < f < 0.525$ or $0.610 < f < 1$, the system will go from $Dis \rightarrow Bcc \rightarrow Hex \rightarrow Gyroid \rightarrow Lam$ as temperature decreases (χ increases). For a system with $0.525 < f < 0.561$ or

$0.561 < f < 0.610$, the gyroid phase is not stable at any temperature, and the system will go from $Dis \rightarrow Bcc \rightarrow Hex \rightarrow Lam$ as temperature decreases.

At phase boundaries where two different morphologies coexist, the chemical potentials of the free ions of the two phases are the same: they all equal to the chemical potential of the reservoir ($\mu = \log(c_\infty)$). However, the average value of positive free ion concentrations in the two coexisting phases are different. For a given phase, the average value of free ion concentration is related to the reservoir concentration through Eq.(3.25) and (3.35). In the phase diagram shown in Figure 3.7, the differences of the average the free ion concentrations of the coexisting phases are $\sim 2\%$ at $\chi N = 50$, and decrease as χN decreases. The ion concentration difference vanishes at $\chi N = 29.65$, where the phase transition is second order.

(2) Dependence of the Morphology on c_∞ and f

The dependence of the equilibrium state of the charged-neutral block copolymer melts on the volume fraction f and the concentration of the reservoir c_∞ (or equivalently, the chemical potential of the reservoir) is Figure 3.8. The phase diagram is set at a constant Flory parameter χ (equivalently constant temperature) and constant monomer charge density α. We choose $\chi N = 30$ and $\alpha N = 50$. The phase diagram demonstrates that the concentration of the reservoir plays a similar role in controlling the morphology of the system at constant temperature as the Flory parameter χ does at constant free ion density. When $c_\infty v_o N$ is large enough the microphase separation occurs. The system transfers from the disordered phase to the bcc phase through a first order transition except at $f = 0.57$, where the disordered phase transfers directly to lamellar phase through a second order transition. As the reservoir concentration $c_\infty v_o N$ increases further, depending on the value of f, the system transfers to various ordered phases such as lamellar, cylinder, bcc, and gyroid phases. The triple points at which the lamellar, cylinder, and gyroid phases coexist are at $f = 0.528$, $c_\infty v_o N = 19.4$, and $f = 0.589$, $c_\infty v_o N = 18.4$, which are indicated on Figure 3.8. For a system with $0 < f < 0.528$ or $0.589 < f < 1$, the system goes from $Dis \rightarrow Bcc \rightarrow Hex \rightarrow G \rightarrow Lam$ as c_∞ increases; for a system with $0.528 < f < 0.570$ or $0.570 < f < 0.589$, the gyroid phase is always unstable and the system goes from $Dis \rightarrow Bcc \rightarrow Hex \rightarrow Lam$ as c_∞ increases.

(3) Molecular Weight N Dependence of Morphology

The dependence of the equilibrium states of charged-neutral block copolymer melts

on the molecular weight N and the volume fraction f is shown in Figure 3.9. We have set $\alpha/\chi = 2.0$, and $c_\infty v_o/\alpha = 0.86$. As with the previous two phase diagrams, we have not assigned a specific value to χ so that the phase diagram can represent a class of systems that relate to each other by Eq.(3.36). The phase diagram shows that as molecular weight N increases, the system can transfer from the disordered phase to various ordered structures depending on the value of the volume fraction f. The direct transition from the disordered to the lamellar phase occurs at $f = 0.55$, $\chi N = 30.07$. The triple points are at $f = 0.512$, $\chi N = 32.5$, and $f = 0.595$, $\chi N = 31.50$.

For a system with given volume fraction f, monomer charge density α, and the Flory parameter χ, the equilibrium state of the system depends on the molecular weight and the concentration of the reservoir c_∞. Figure 3.10 shows the phase diagrams of charged-neutral block copolymers at volume fraction $f = 0.4$, $\alpha/\chi = 2.0$ (Figure3.10(a)) and $\alpha/\chi = 0.6$ (Figure3.10(b)), respectively. The variable on vertical axis is $c_\infty v_o/\alpha$. At the limit c_∞ approaches infinite, the values of χN at phase transitions approach their neutral limit. In Figure 3.10(a), the MST occurs only when $c_\infty v_o/\alpha$ is largesr than some minimum value. This is due to the fact that $\alpha/\chi = 2.0 > 2f$, and that in order to satisfy the condition in Eq.(3.45), $c_\infty v_o/\alpha$ has to be greater than 0.46. On the other hand, the ratio $\alpha/\chi = 0.6 < 2f$ in Figure 3.10(b), thus the MST can occurs at $c_\infty v_o/\alpha = 0$.

3.5 Fluctuation Effects

Although charged-neutral diblock copolymer melts seems to be a more complicated system than the corresponding neutral diblock copolymers, the effective Hamiltonian for charged-neutral block copolymers is in the same universality class as that of neutral block copolymers, which belongs to a model Hamiltonian first considered by Brazovskii [18]. A Brazovskii Hamiltonian is characterized by having a large field fluctuation in the vicinity of a shell of nonzero wavevector. The fluctuation diverges as the system approaches the order-disorder transition. Using a self-consistent Hartree approximation, Brazovskii has shown how to handle the divergent terms and demonstrated that systems in this universality class exhibit a fluctuation-induced first order phase transition in place of the continuous second order transition predicted by mean field theory. This is a consequence of the increased volume in the reciprocal space of

important field fluctations. Fredrickson and Helfand applied the Brazovskii analysis to the particular case of diblock copolymers [4]. They found: (i) For a symmetric diblock copolymers ($f = 0.5$), the nature of phase transition is changed from second order to weakly first order. The location of the transition is predicted to be at $(\chi N)_t = 10.495 + 41.022N^{-1/3}$. (ii) There are windows in composition, with finite width, through which it is possible to pass from the disordered phase to each of the ordered microphases (lamellar, hexagonal, and body-centered-cubic) by changing temperature.

An interesting feature of diblock copolymer melts that distinguish them from other systems in the Brazovskii universality class is that the fluctuation corrections to the mean field theory can be made arbitrarily small by increasing the molecular weight (polymerization) N of the chains, and that when $N \to \infty$, the mean field theory is recovered. This feature is commom in neutral macromolecule systems. For instance, in homopolymer blends the nonclassical corrections to mean field critical behavior vanish as the length of the chains approaches infinity [25], although homopolymer blends belongs to a different universality class (Ising universality class), which show critical singularity near the onset of phase transition.

Since charged diblock copolymers belongs to the same universality class as neutral diblock copolymers (Brazovskii universality class), we expect that large fluctuations near the order-disorder transition will also change the nature of the phase transition and exhibit true critical behavior in the vicinity of the MST. On the other hand, a charged diblock copolymer system is a more complicated system: it contains more parameters, and the $A-B$ interchange symmmetry is broken due to the added charge in one of the blocks. Hence, the fluctuation effect on charged diblock copolymer systems gives rise to some interesting features in phase diagrams which are absent in neutral block copolymers.

The fact that effects of fluctuations become vanishingly small in the limit of infinite molecular weight is not obviously valid for charged-neutral block copolymers. The vertex functions $N\Gamma_3$, $N\Gamma_4$ of neutral block copolymers depend on N in a simple fashion: $N\Gamma_3$, $N\Gamma_4 \sim O(1)$, while the vertex functions $N\Gamma_3$, $N\Gamma_4$ of charged-neutral block copolymers are more complicated functions of N, and in particular, $N\Gamma_4$ is proportional to N (see Figure 3.6) at large values of αN and small salt concentration. However, as we will show below, the molecular weight N still plays the role of a

Ginzburg parameter in charged diblock copolymer systems and the mean field theory is recovered as N approaches infinite.

In order to study the fluctuation effect on charged diblock copolymers, we apply the Brazovskii and Fredrickson and Helfand theory to the system. The Hamiltonian for charged-neutral diblock copolymers is similar to that for neutral diblock copolymers, and the application is straightforward.

The fluctuation of the order parameter can be characterized by the strucutre function $S^{-1}(q)$. Near the MST, the structure function $S^{-1}(q)$ is very sharply peaked about $q = q^*$ as is shown in Section 3, and the dominant composition fluctuations are those with $q = q^*$. Hence we can expand the structure function about q^*

$$S^{-1}(q) \sim 2(\chi^* - \chi) + c^2(q - q^*)^2 \tag{3.61}$$

where χ^* is given by Eq.(3.43), and

$$c = \left[\frac{1}{2}\frac{d^2S^{-1}(q)}{d^2q^2}\right]^2 \tag{3.62}$$

Since $S^{-1}(q)$, which is given by Eq.(3.40), depends on f, α, N, and c_∞, the coefficient c also depends on these parameter. The effective free energy of the system under consideration can be written in Brazovskii form as:

$$\begin{aligned} F[\phi]/k_BT &= \frac{1}{2!}\int_q [\tilde{\tau} + (q - q^*)^2]\phi(\vec{q})\phi(-\vec{q}) \\ &+ \frac{\tilde{\mu}}{3!}\int_{\vec{q}_1}\int_{\vec{q}_2} \phi(\vec{q}_1)\phi(\vec{q}_2)\phi(-\vec{q}_1 - \vec{q}_2) \\ &+ \frac{\tilde{\lambda}}{4!}\int_{\vec{q}_1}\int_{\vec{q}_2}\int_{\vec{q}_3} \phi(\vec{q}_1)\phi(\vec{q}_2)\phi(\vec{q}_3)\phi(-\vec{q}_1 - \vec{q}_2 - \vec{q}_3) \\ &+ \int_q h(\vec{q})\phi(-\vec{q}) \end{aligned} \tag{3.63}$$

where $\tilde{\tau}$ is a reduced temperature variable that is a measure of the distance from the spinodal, i.e.,

$$\tilde{\tau} = \frac{2[(\chi^* N) - \chi N]}{c^2 N} \tag{3.64}$$

and $\phi(\vec{q}) = c\psi(\vec{q})$, $\tilde{\mu} = \gamma_3/c^3N$, $\tilde{\lambda} = \gamma_4/c^3N$. In eq.(3.63) the external field $h(\vec{q})$ couples to the order parameter and allows us to generate the self-consistent Hartree

equations. At the end of the calculation this field is set equal to zero [26].

The free energy can be recast in terms of the mean value of the order parameter $\bar{\phi}(\vec{q}) =< \phi(\vec{q}) >$, and its fluctuation $\delta\phi(\vec{q}) = \phi(\vec{q}) - \bar{\phi}(\vec{q})$. The resulting free energy has the form

$$F[\phi]/k_BT = F[\bar{\phi}]/k_BT + \tilde{F}[\bar{\phi}, \delta\phi(\vec{q})]/k_BT \tag{3.65}$$

where the first term $F[\bar{\phi}]/k_BT$ is similar to the effective free energy in Eq.(3.63), except that the order parameter $\phi(q)$ is replaced by its mean field average $\bar{\phi}(q)$. The second term depends on the fluctuation

$$\begin{aligned}
\tilde{F}[\bar{\phi}, \delta\phi(\vec{q})] \;=\; & \frac{1}{2!}\int_q [\tilde{\tau} + (q-q^*)^2][\delta\phi(\vec{q})\delta\phi(-\vec{q}) + 2\bar{\phi}(\vec{q})\delta\phi(-\vec{q})] \\
& + \frac{\tilde{\mu}}{3!}\int_{\vec{q}_1}\int_{\vec{q}_2} [\delta\phi(\vec{q}_1)\delta\phi(\vec{q}_2)\delta\phi(-\vec{q}_1-\vec{q}_2) \\
& + 3\delta\phi(\vec{q}_1)\delta\phi(\vec{q}_2)\bar{\phi}(-\vec{q}_1-\vec{q}_2) \\
& + 3\delta\phi(\vec{q}_1)\bar{\phi}(\vec{q}_2)\bar{\phi}(-\vec{q}_1-\vec{q}_2)\bar{\phi}(\vec{q}_1)\bar{\phi}(\vec{q}_2)\bar{\phi}(-\vec{q}_1-\vec{q}_2)] \\
& + \frac{\tilde{\lambda}}{4!}\int_{\vec{q}_1}\int_{\vec{q}_2}\int_{\vec{q}_3} [\delta\phi(\vec{q}_1)\delta\phi(\vec{q}_2)\delta\phi(\vec{q}_3)\delta\phi(-\vec{q}_1-\vec{q}_2-\vec{q}_3) \\
& + 4\delta\phi(\vec{q}_1)\delta\phi(\vec{q}_2)\delta\phi(\vec{q}_3)\bar{\phi}(-\vec{q}_1-\vec{q}_2-\vec{q}_3) \\
& + 6\delta\phi(\vec{q}_1)\delta\phi(\vec{q}_2)\bar{\phi}(\vec{q}_3)\bar{\phi}(-\vec{q}_1-\vec{q}_2-\vec{q}_3) \\
& + 4\delta\phi(\vec{q}_1)\bar{\phi}(\vec{q}_2)\bar{\phi}(\vec{q}_3)\bar{\phi}(-\vec{q}_1-\vec{q}_2-\vec{q}_3)]
\end{aligned} \tag{3.66}$$

The partition function is given by

$$Z = exp\{-F[\bar{\phi}]/k_BT\}\int \mathcal{D}\delta\phi\; exp\{-\tilde{F}[\bar{\phi}, \delta\phi(\vec{q})]\} \tag{3.67}$$

and the free energy is given by $W = -k_BT \ln Z$. From $\delta Z/\delta\delta\phi = 0$, we obtain $< \delta\tilde{F}/\delta\delta\phi >= 0$, which leads to Brazovskii's equation of state

$$\begin{aligned}
\tilde{h}(q) \;=\; & [\tilde{\tau} + (q-q^*)^2]\bar{\phi}(\vec{q}) + \frac{\tilde{\mu}}{2}\int_q \bar{\phi}(\vec{q})\bar{\phi}(\vec{q}) \\
& + \frac{\tilde{\lambda}}{2}\left[\int_{q'} g(q')\right]\bar{\phi}(\vec{q}) + \frac{\tilde{\lambda}}{6}\int_{\vec{q}_1}\int_{\vec{q}_2} \bar{\phi}(\vec{q}_1)\bar{\phi}(\vec{q}_2)\bar{\phi}(-\vec{q}_1-\vec{q}_2)
\end{aligned} \tag{3.68}$$

where $g(q)$ is given by $< \delta\phi(\vec{q})\delta\phi(\vec{q}') >= g(\vec{q})\delta(\vec{q}+\vec{q}')$. The self-consistent equation

for $g(q)$ in the one-loop approximation is

$$g^{-1}(q) = \tilde{\tau} + (q - q^*)^2 + \frac{\tilde{\lambda}}{2}\int_{q'} g(q') + \frac{\tilde{\lambda}}{2}\int_{q'} \bar{\phi}(\vec{q}')\bar{\phi}(-\vec{q}') \tag{3.69}$$

Equations (3.68), (3.69) and the effective free energy $F[\bar{\phi}]/k_BT$ can be simplified to determine the equilibrium structure of the system. Near the MST, the important composition fluctuations in the system will be plane waves or superpositions of plane waves with wave vectors of magnitude $q = q^*$. The mean value of order parameter $\bar{\phi}(\vec{q})$ can be written as

$$\bar{\phi}(\vec{q}) = a_n \sum_{k=1}^{n} [exp(iQ_k \cdot x) + exp(iQ_k \cdot x)] \tag{3.70}$$

The $2n$ wave vectors $\{\pm Q_k\}, k = 1, \ldots, n$ with magnitude $|Q_k| = q^*$ are given in Section 4 for various periodic structures. With the above definitions, the equation of state can be written $[h \equiv h(Q_i)]$

$$h = ra_n - \theta_n a_n^2 + \eta_n a_n^3 \tag{3.71}$$

where the coefficients θ_n and η_n for various phases are listed in Table II. The renormalized inverse susceptibility $r = g^{-1}(q^*)$ satisfies

$$r = \tau + d\lambda/(rN)^{1/2} + n\lambda a_n^2 \tag{3.72}$$

where $d = 3x^*/2$, $\tau = N\tilde{\tau}$, $\mu = N\tilde{\mu}$, $\lambda = N\tilde{\lambda}$.

Table II

	lamellar $n = 1$	*cylinder* $n = 3$	*bcc* $n = 6$
θ_n	0	$\theta_3 = -\mu$	$\theta_6 = -2\mu$
η_n	$\eta_1 = -\lambda/2$	$\eta_3 = -\lambda/2$	$\eta_6 = 3\lambda/3$

The thermodynamic potential can be obtained by using the relation $\partial\Phi[\bar{\phi}]/\partial a_n = 2nh$, thus

$$\Phi[\bar{\phi}] = \int_0^{a_n} da 2nh$$

$$= \frac{1}{2\lambda}(r^2 - r_o^2) + \frac{d}{N^{1/2}}(r^{1/2} - r_o^{1/2}) - \frac{2}{3}n\theta_n a_n^3 + \frac{1}{2}n\eta_n a_n^4 \tag{3.73}$$

with r_o being the inverse susceptibility of the disordered phase given by

$$r_o = \tau + \frac{d\lambda}{r_o\sqrt{N}} \tag{3.74}$$

The potential Φ is minimized by the amplitude a_n which satisfies the equation of state with $h = 0$, i.e.,

$$\eta_n a_n^2 - \theta_n a_n + r = 0 \tag{3.75}$$

The thermodynamic potential $\Phi[\bar{\phi}]$ in Eq.(3.73) together with Eq.(3.72), (3.74), and (3.75) completely determine the equilibrium properties of a charge-neutral diblock copolymer system with given set of parameters f, α, N, χ, and c_∞. The morphology with the lowest value of Φ is the equilibrium state of the system.

The microphase separation transition in the Hartree approximation is given by the solution of

$$\Phi(\bar{\phi}, \chi) = 0 \tag{3.76}$$

For a given set of parameters f, α, N, and c_∞, Eq.(3.76) is solved for each possible order structure (lamellar, cylinder, bcc, and gyroid phase). The lowest χ_t that results corresponds to the MST temperature and the corresponding microstructure is the equilibrium state that first appears at the transition.

Similar to the fluctuation corrections to the phase diagram of neutral block copolymers in the Hartree approximation, the fluctuation corrections to the charged-neutral diblock copolymers gives rise to a first order transition to lamellar phase at $f = f_c$, where μ turns to zero. Unlike neutral block copolymer system where $f_c = 0.5$, the critical value f_c of charged-neutral block copolymers depends on αN and salt concentration n_s, as shown in Figure (3.11). The transition temperature from disorder to lamellar phase is obtained by solving Eq.(3.76)

$$(\chi N)_t = (\chi N)^* + 1.0154 \cdot c^2 \frac{(d\lambda)^{2/3}}{N^{1/3}} \tag{3.77}$$

The first term on the right-hand side of this equation is the Landau mean field value of $(\chi N)^*$ at volume fraction f_c and the second term is the correction obtained

by including fluctuations in the Hartree approximation. The sign of λ is positive, indicating that fluctuations always decrease the stability of the ordered phases.

In neutral diblock copolymers, the critical point of the MST is $(\chi N)^* = 10.495$, λ is independent of N ($\tilde{\lambda} \sim 1/N$, $\lambda = N\tilde{\lambda} \sim O(1)$), d is a constant. The molecular weight dependence of the Hartree correction is $N^{-1/3}$. (It has been proved that this molecular weight dependence of fluctuation correction is universal in neutral block copolymers regardless of their architecture [27].) In the limit $N \to \infty$, the transition temperature $(\chi N)_t \to (\chi N)^*$, hence the mean field theory result is recovered.

In charged-neutral diblock copolymers, λ is a function of f, αN, and n_s. There are two different situations which result in two different molecular weight dependencies of the fluctuation corrections. (1) For a system with given αN and salt concentration n_s, λ is a constant, thus, $(\chi N)_t \to (\chi N)^*$ in the limit $N \to \infty$. (2) For a system with given α and salt concentration, increasing molecular weight N results in increasing λ. As a consequence the Hartree correction, which is proportional to $\lambda^{2/3}/N^{1/3}$, inceases according to N^{δ} $(0 < \delta < 1)$, as N approaches infinity as shown in Figure 3.13. Eq.(3.77) can be written

$$(\chi N)_t = N\left[\chi^* + 1.0154 \cdot c^2 \frac{(d\lambda)^{2/3}}{N^{4/3}}\right] \tag{3.78}$$

The second term inside of bracket $\sim \lambda^{2/3}/N^{4/3}$ vanishes in the limit $N \to \infty$, thus $\chi \to \chi^*$.

At the transition to the lamellar phase, the amplitude a_1 jumps from zero in the disordered phase to a nonzero value at the transition:

$$a_1 = 1.4554(d^2/\lambda N)^{1/6} \tag{3.79}$$

For a system with a given α, λ increases as N increases ($\lambda \sim N^{(3\delta+1)/2}$). Hence, the amplitude a_1 has molecular weight dependence $\sim N^{-(\delta+1)/4}$, approaching its mean value slower than $N^{-1/6}$.

Figure 3.14(a) and 3.14(b) show the phase diagrams of charged-neutral diblock copolymer systems with $\alpha N = 40$, and salt concentration $n_s = 0$ using the mean field theory and the Hartree approximation, respectively. Figure 3.14(a) demonstrates that the transition is to bcc phase except at $f_c = 0.77$, where transition is second order

and is to the lamellar phase. Figure 3.14(b) is the phase diagram with the fluctuation correction from the Hartree approximaition with $N = 10^9$. The asymmetric features of charged block copolymers noted from the mean field theory are even more striking here. The phase diagram indicates that direct first order transition between the disordered and hexagonal phases is possible in the volume fraction range $f < 0.767$, and that direct first order transition between the disordered and the lamellar phase are possible in the volume fraction range $f > 0.767$. However, we find that the bcc phase is never more stable than the hexagonal phase or the lamellar phase at the MST for $N = 10^9$. Whether this feature is physical in the charged-neutral block copolymers or an artifact due to the break down of the Hartree approximation is not clear.

For neutral diblock copolymers, the validity of the Hartree approximation is examed by Fredrickson and Helfand by considering the value of those diagrams not included in the approximation. Although, their calculation indicated that the Hartree approximation is only rigorously accurate for N of order 10^{10} or larger, they pointed out that such approximations are often accurate well beyond their range of rigorous validity. They demonstrated that the Hartree approximation gave reasonable results for molecular weight $N = 10^9$, while breaking down at $N = 10^4$. We can apply the requirements of accuracy of the Hartree approximation to the charged-neutral block copolymer system with $\alpha N = 40$, and $n_s = 0$, and find that the approximation is valid when $N > 10^{10}$. Since the requirement is very stingent, we have reason to believe that the approximation should be valid here.

3.6 Conclusion

A charged-neutral diblock copolymer system is studied in a theoretical framework which combines the Random Phase Approximation and the Poisson-Boltzmann equation for consistently treating the electrostatic interactions between all charged species and the neutral diblock copolymer contributions to the free energy. Within this framework, we have studied the microphase separation and the equilibrium properties of charged-neutral block copolymers with an arbitrary amount of added salt in the weak segregation limit. Our spinodal instability analysis demonstrates not only the considerable enhancement of compatibility between A and B, but also the inhibition

of the microphase separation under certain conditions. A criterion for microphase separation in the system is derived.

In order to determine the phase behavior of charged-neutral diblock copolymer system, we have studied the stability of various ordered phases (e.g. lamellae, cylinder, sphere, and gyroid phase) and mapped out the phase diagrams under various parameter variations. We find out that gyroid phase is stable between the lamellar and cylinder phases, and it terminates at a triple point, with a lamellar to hexagonal transition occuring in the weak segregation limit. Due to the breaking of the interchange symmetry between A and B, some new features appear in the phase diagrams. The critical point, where a direct transition from the disordered to the lamellar phase occurs, is no longer fixed but rather depends on α, N, and c_s.

The concentration fluctuation near the order-disorder transition is also studied by extending the method of Fredrickson and Helfand method to the charged-neutral diblock copolymer system. We find out that the breaking of the interchange symmetry leads to new scaling of fluctuation corrections at a fixed value of α.

Acknowledgement

We thank Julia A. Kornfield for helpful discussions. This research is supported in part by donors of the Petroleum Research Fund, administrated by the American Chemical Society, and by the National Science Foundation (grant number ASC-9217368).

3.7 Appendix

Self-Consistent Approach to Charged-Neutral Diblock Copolymers

The grand canonical partition function of charged-neutral diblock copolymers is given in Eq.(3.9) with the partition functions of free ions Ξ_+, Ξ_- and diblock copolymer Q_p given in Eq.(3.10)-(3.12). To make the functional Q_p more tractable, we insert functional integral, $1 = \int D\phi_K \delta[\phi_K - \hat{\phi_K}]$, $K = A, B$, and present the delta functionals by standard integral representations, thus we have:

$$Q_p = \int D\phi_A D\phi_B DW_A DW_B D\eta exp\{-F/k_BT\} \tag{3.80}$$

where

$$F_p/k_BT = -\log Q - \int d^3r[\sum_{\alpha=A,B} iW_\alpha\phi_\alpha + i\eta(1-\phi_A-\phi_B) - \chi\rho_o\phi_A\phi_B - \alpha\rho_o\xi\phi_A] \tag{3.81}$$

with

$$Q = \frac{1}{n_p!}\int \prod_{i=1}^{n_p} d^3r_i \; exp\{-\frac{3\beta}{2Na^2}\int_0^1 ds(\frac{dr_i(s)}{ds})^2 - \sum_{\alpha=A,B}\int d^3r i W_\alpha(\vec{r})\hat{\phi}_\alpha(\vec{r})\} \tag{3.82}$$

The partition function Q of n_p noninteracting Gaussian chains is a functional of the effective fields W_A and W_B, i.e., $Q = Q[W_A.W_B]$. It can be written as a product of partition functions of a single chain:

$$Q = \frac{1}{n_p}Q_1^{n_p} \tag{3.83}$$

where

$$Q_1 = \int d^3r \; exp\left[-\frac{3\beta}{2Na^2}\int_0^1 ds(\frac{dr(s)}{ds})^2 - i\frac{N}{\rho_o}\int_0^f ds W_A(r(s)) - i\frac{N}{\rho_o}\int_f^1 ds W_B(r(s))\right] \tag{3.84}$$

Substitution of Eq.(3.81) and (3.82) to Eq.(3.9), we have

$$\Xi = \int D\phi_A \int D\phi_B \int DW_A \int DW_B \int D\eta \int D\xi exp\{-F/k_BT\} \tag{3.85}$$

where

$$F/k_BT = -\int d^3r[\sum_{\alpha=A,B} iW_\alpha\phi_\alpha + i\eta(1-\phi_A-\phi_B) - \chi\rho_o\phi_A\phi_B - \alpha\rho_o\xi\phi_A]$$
$$-\log Q - \ln\Xi_+[\xi] - \ln\Xi_-[\xi] - \frac{1}{8\pi\beta e^2}\int d^3r\xi\nabla^2\xi \tag{3.86}$$

In the self-consistent theory, one approximate the functional integral in Eq(3.83) by the extremum of the integrand, thus the free energy, $-k_BT\ln\Xi$, is given by $F[\phi_A,\phi_B,W_A,W_B,\xi,\eta]$, where ϕ_A,ϕ_B,W_A,W_B, ξ, and η are the functions for which F attains its minimum. Taking functional derivatives of F with respect to these functions, we obtain the self-consistent equations

$$W_A(\vec{r}) = \chi N\phi_B(\vec{r}) + \alpha N\xi(\vec{r}) + \eta(\vec{r}) \tag{3.87}$$

$$W_B(\vec{r}) = \chi N\phi_A(\vec{r}) + \eta(\vec{r}) \tag{3.88}$$

$$\phi_A(\vec{r}) = -\frac{Nn_p}{\rho_o}\frac{\partial Q_1}{\partial W_A} \tag{3.89}$$

$$\phi_B(\vec{r}) = -\frac{Nn_p}{\rho_o}\frac{\partial Q_1}{\partial W_B} \tag{3.90}$$

$$\phi_A + \phi_B = 1 \tag{3.91}$$

$$\frac{1}{4\pi\beta e^2}\nabla^2 i\xi(\vec{r}) = -\alpha\rho_o\phi_A(\vec{r}) - c^+(\vec{r}) + c^-(\vec{r}) \tag{3.92}$$

In deriving the above equations, we have scaled W_A, W_B, and η by a factor iN/ρ_o. The density distribution ϕ_A and ϕ_B in Eq.(3.91) and (3.92) can be written explicitly as

$$\phi_A(\vec{r}) = \frac{V}{Q_1}\int_0^f dsq(\vec{r},s)q^+(\vec{r},s) \tag{3.93}$$

$$\phi_B(\vec{r}) = \frac{V}{Q_1}\int_f^1 dsq(\vec{r},s)q^+(\vec{r},s) \tag{3.94}$$

where $q(\vec{r},s)$ and $q^+(\vec{r},s)$ are the two end-segment distribution functions,

$$q(\vec{r},s) = \int Dr_\alpha exp\{-\frac{3\beta}{2Na^2}\int_0^1 ds(\frac{dr(s)}{ds})^2 - \int_0^s dt$$
$$[\gamma(t)W_A(\vec{r}_\alpha) + (1-\gamma(t))W_B(\vec{r}_\alpha)]\} \tag{3.95}$$

The distribution function $q^+(\vec{r}, s)$ is defined similarly except that integration over $\vec{r}_\alpha(t)$ is done for t=f to 1. The distribution function satisfies the modified diffusion equation,

$$\frac{\partial q(\vec{r}, s)}{\partial s} = \begin{cases} \frac{1}{6}Na^2\nabla^2 q - W_A(\vec{r})q & \text{if } 0 < s \leq f \\ \frac{1}{6}Na^2\nabla^2 q - W_B(\vec{r})q & \text{if } f < s < 1 \end{cases} \tag{3.96}$$

with the initial condition, $q(\vec{r}, 0) = 1$. A similar diffusion equation can be derived for $q^+(\vec{r}, s)$ with initial condition $q^+(\vec{r}, 1) = 1$

Eq.(3.89), (3.90), (3.93)-(3.96), (3.98) together with Eq.(3.21) and (3.22) are a complete set of self-consistent equations for determining the thermodynamic property of the system. Solutions of the equations can be obtained numerically and the free energy can be determined.

3.8 Figures

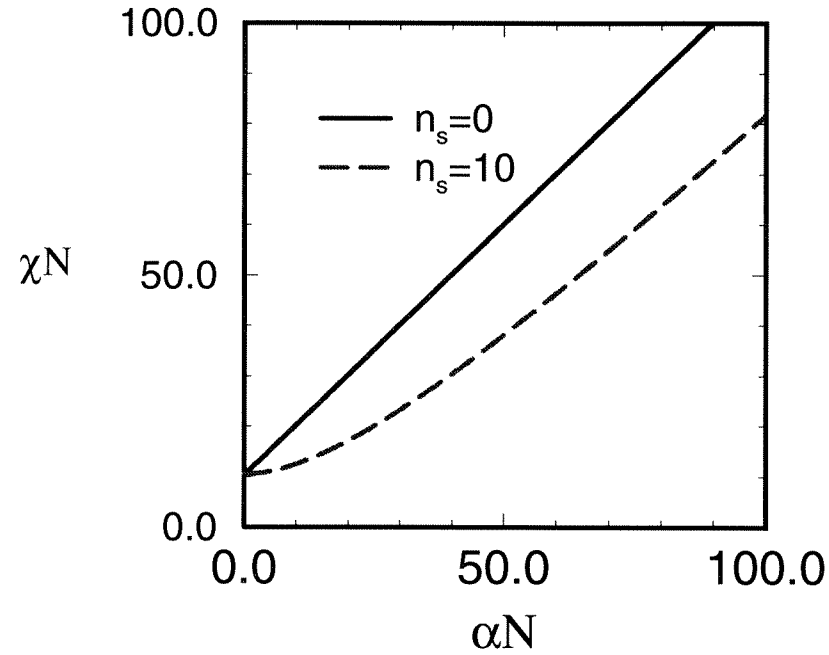

(a)

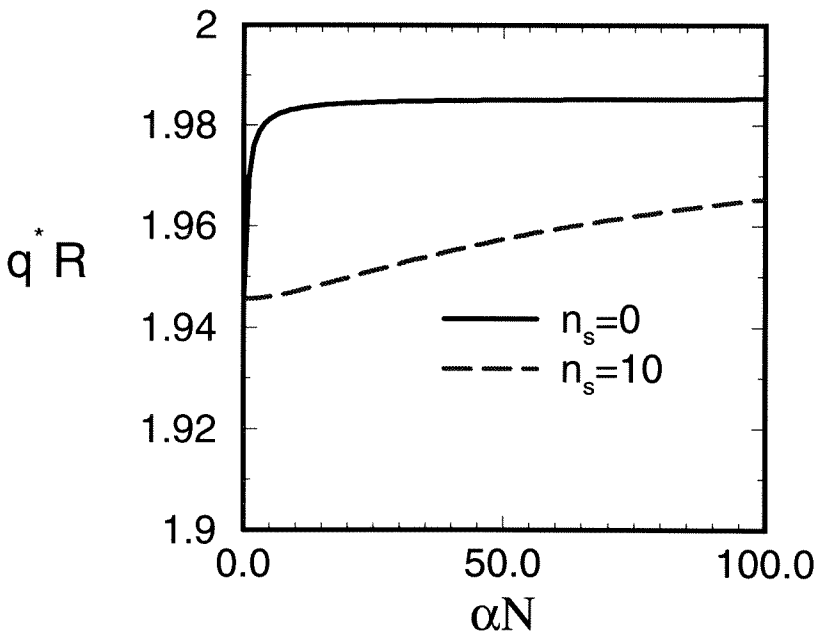

(b)

Figure 3.1: (a) The spinodal value χN as a function of charges αN for systems with volume fraction $f = 0.5$ for two different salt concentrations per chain: $n_s = 0.0$ (solid line), $n_s = 10$ (long dashed line); (b) the corresponding critical wavevector q^*R as functions of αN.

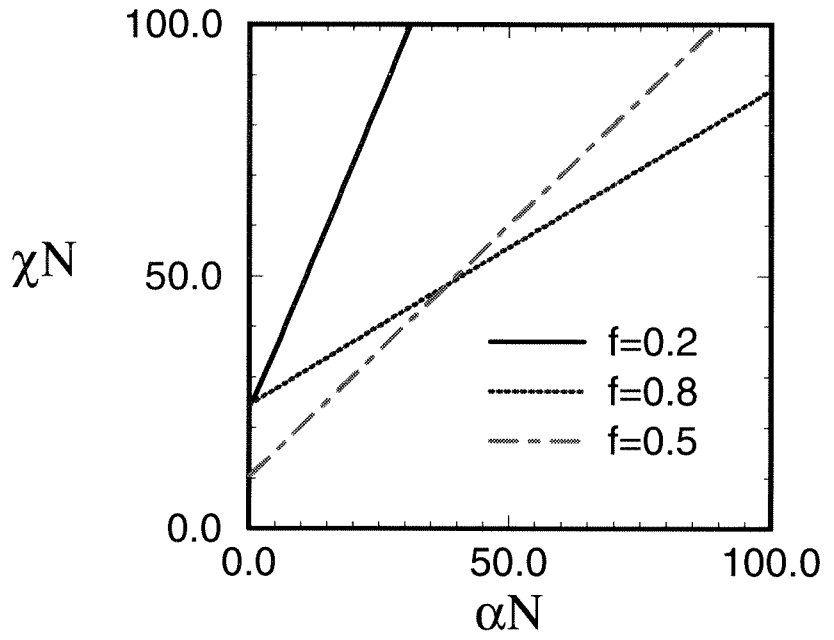

(a)

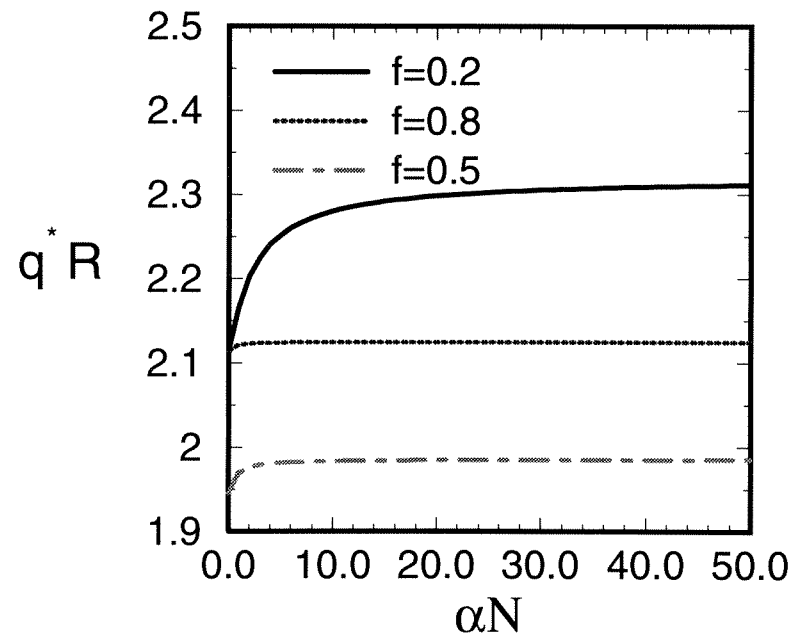

(b)

Figure 3.2: (a) The spinodal value χN as a function of charges αN for systems with salt concentration per chain $n_s = 0$ and three different volume fractions $f = 0.2$ (solid line), $f = 0.5$ (dot-dashed line), and $f = 0.8$ (dotted line); (b) the corresponding critical value wavevector as a function of αN.

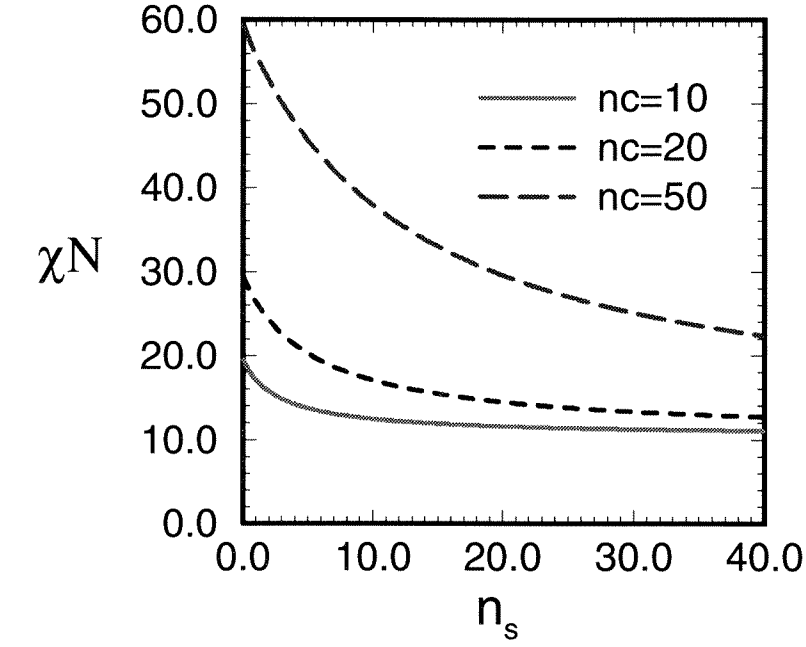

(a)

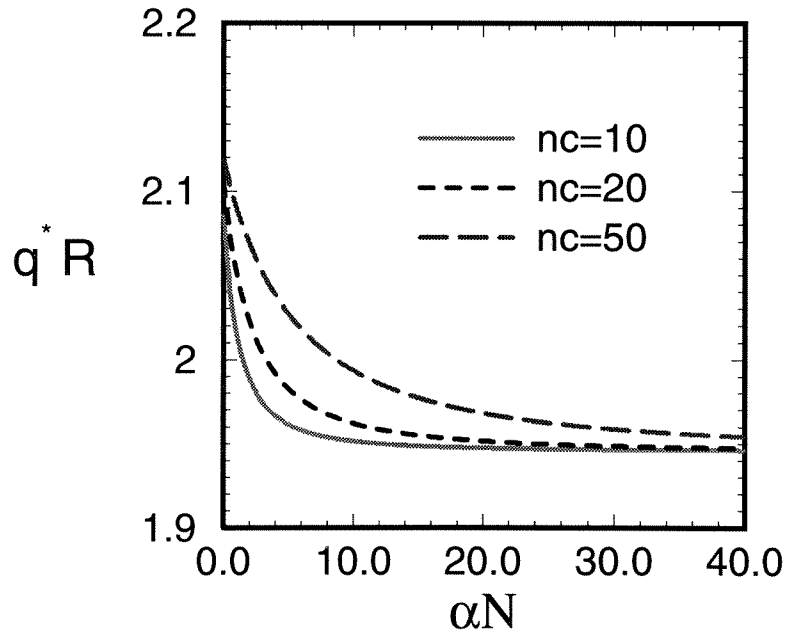

(b)

Figure 3.3: (a) The spinodal value χN as a function of salt concentration per chain n_s for systems with volume fraction $f = 0.5$ and different charges $\alpha N = 10$ (solid line), $\alpha N = 20$ (dashed line), $\alpha N = 50$ (long dashed line); (b) the corresponding critical wavevectors

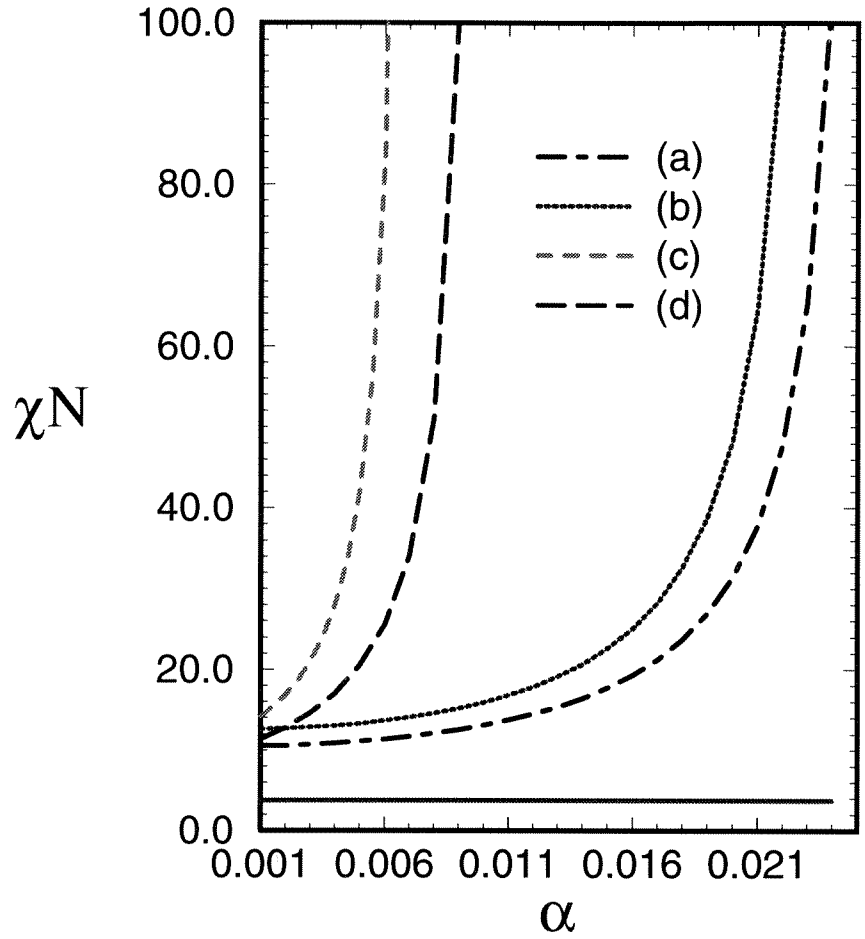

Figure 3.4: The spinodal value χN as a function of monomer charge density α for systems with (a) volume fraction $f = 0.5$, and salt concentration per monomer volume $c_s v_o = 0.01$; (b) $f = 0.35$, and $c_s v_o = 0.01$; (c) $f = 0.35$, and $c_s v_o = 0.0$; (d) $f = 0.50$, and $c_s v_o = 0.0$.

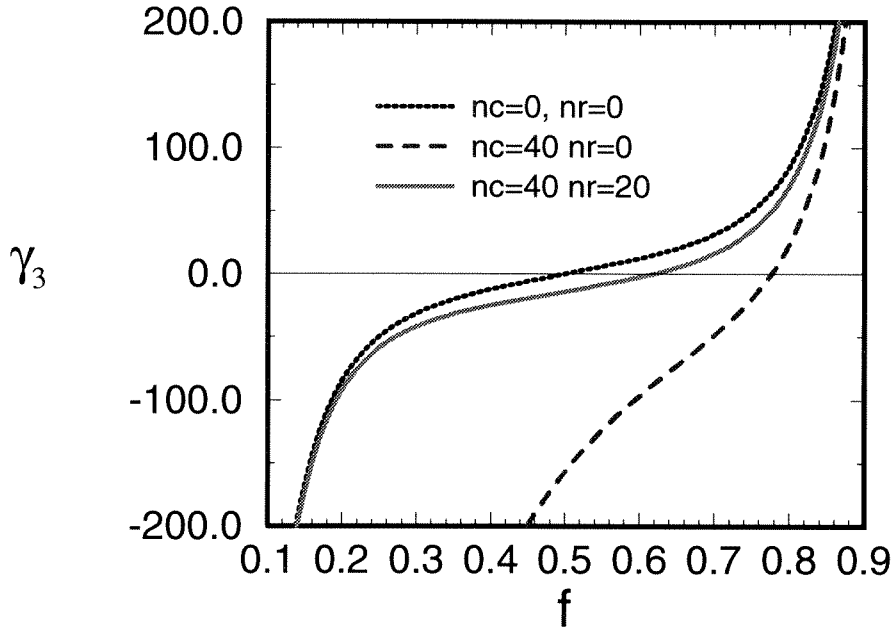

(a)

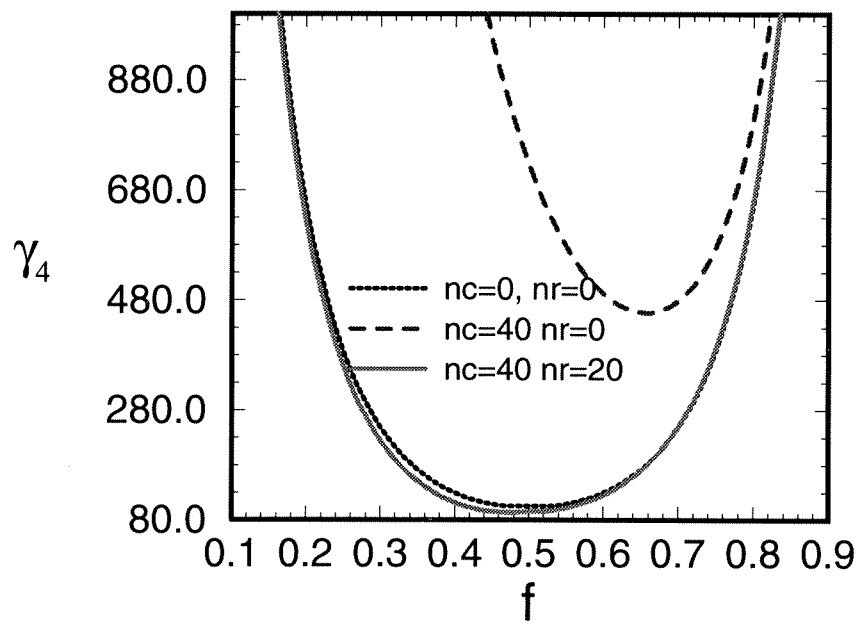

(b)

Figure 3.5: The vertex functions (a) γ_3 (b) γ_4 as a function of volume fraction f at charges $n_c = 0$, and dimensionless reservoir concentration $n_r = 0$ (dotted line); $n_c = 40$, and $n_r = 0$ (dashed line); $n_c = 40$, and $n_r = 40$ (solid line), where $n_c = \alpha N$ and the dimensionless reservoir concentration $n_r = c_\infty v_o N$

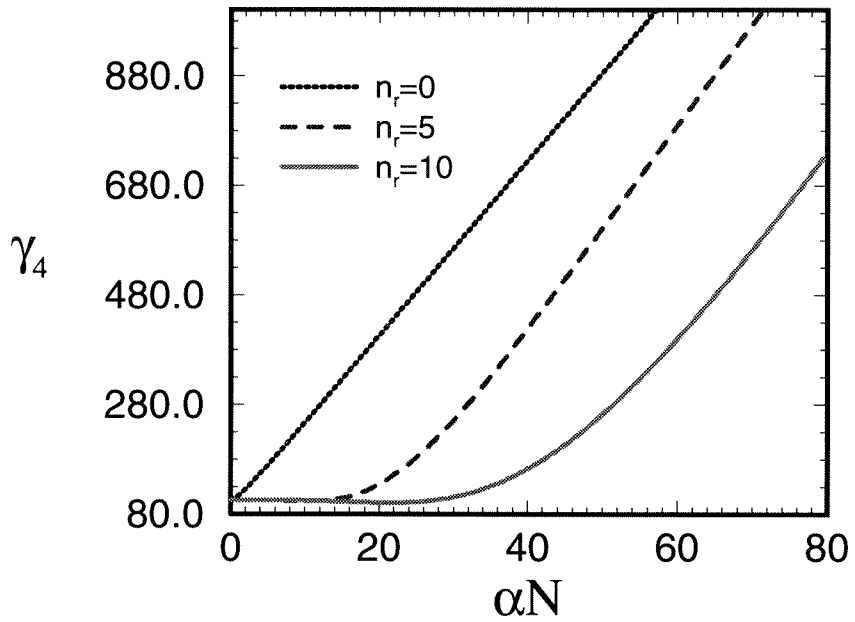

Figure 3.6: (a) The vertex function γ_4 as a function of charges αN at: dimensionless reservoir salt concentration $n_r = 0$ (dotted line); $n_r = 5$ (dashed line); and $n_r = 10$ (solid line), where $n_r = c_\infty N v_o$

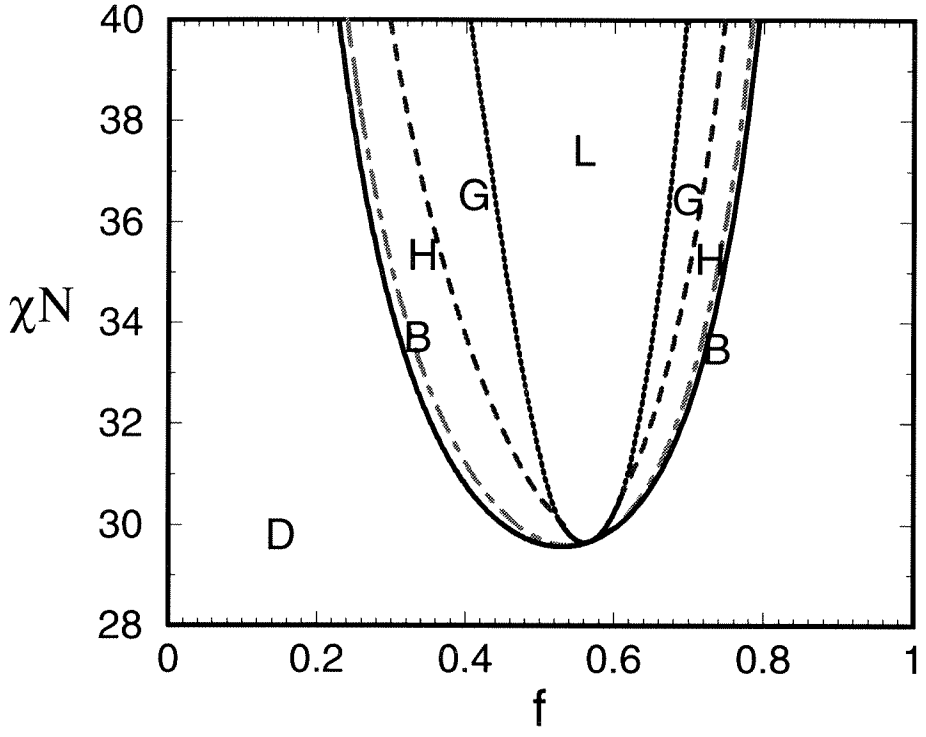

Figure 3.7: Phase diagram at $\alpha N = 50$, and constant dimensionless reservoir salt concentration $c_\infty v_o N = 30$

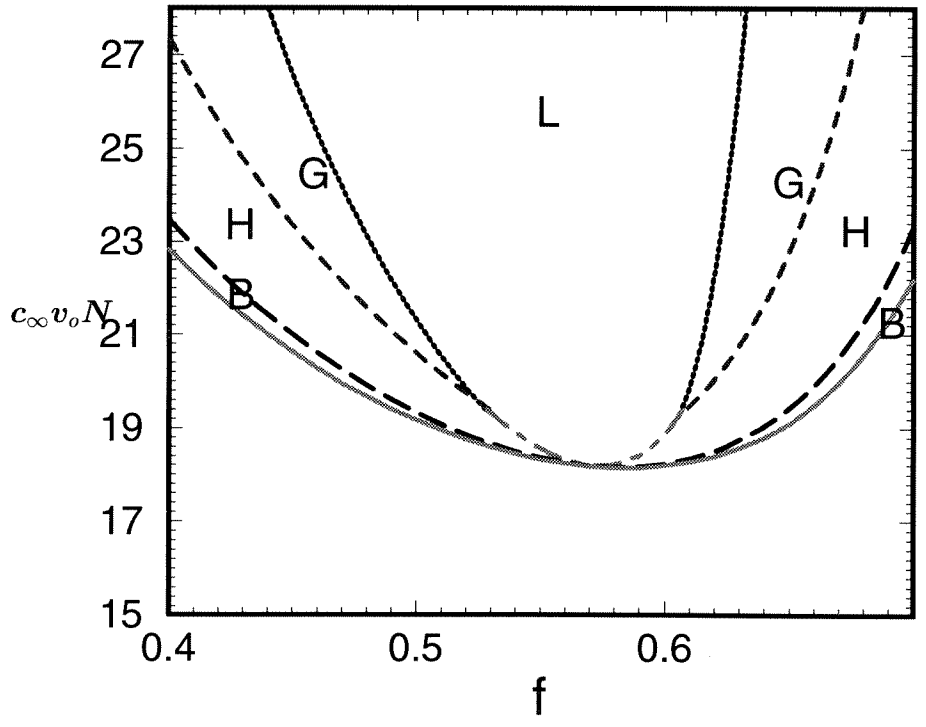

Figure 3.8: Phase diagram at $\alpha N = 50$, and constant interaction parameter $\chi N = 30$

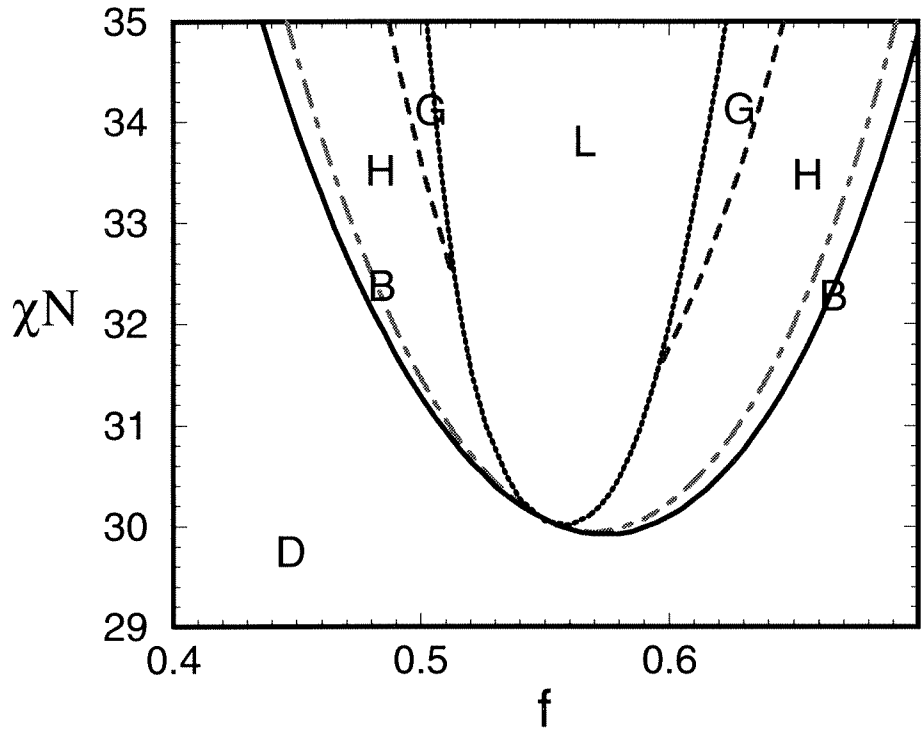

Figure 3.9: Phase diagram at constant value of monomer charge density α, Flory parameter χ, and reservoir salt oncentration c_∞, where $\alpha/\chi = 2.0$, and $c_\infty v_o/\alpha = 0.86$

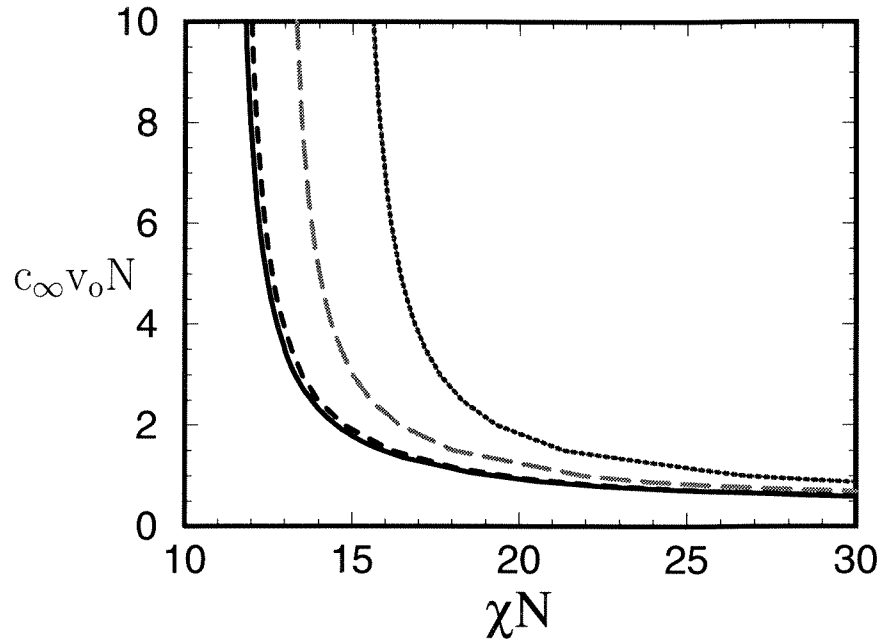

(a)

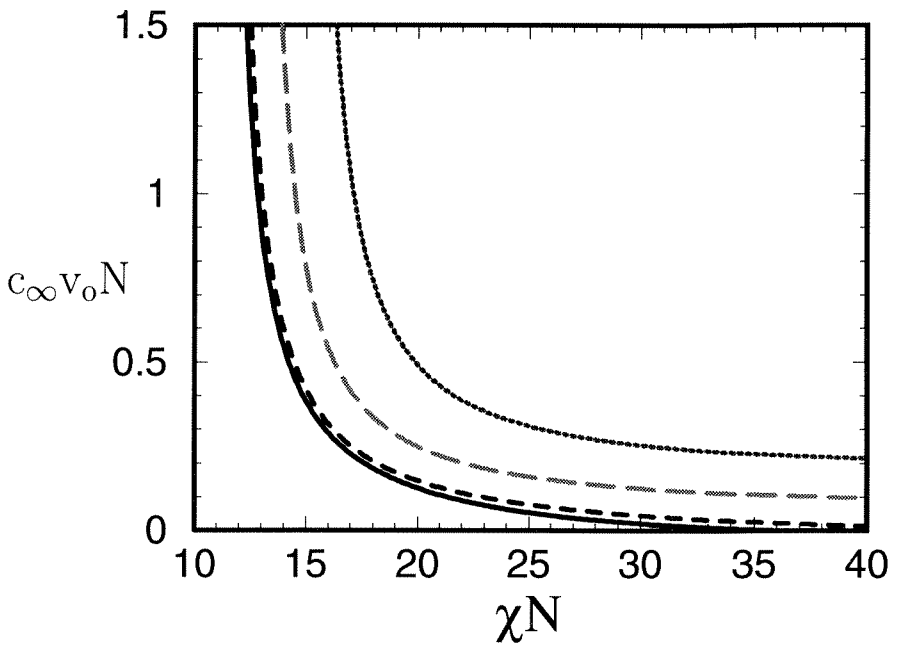

(b)

Figure 3.10: Phase diagram for a system with constant monomer charge density α, Flory parameter χ, and volume fraction f, where (a) $\alpha/\chi = 2.0$ and $f = 0.4$; (b) $\alpha/\chi = 0.6$ and $f = 0.4$.

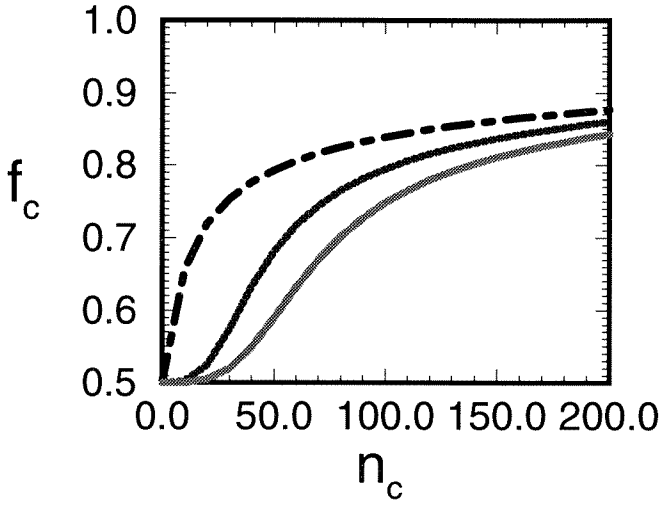

Figure 3.11: Dependent of volume fraction f_c where disordered to lamellar transition occurs on αN.

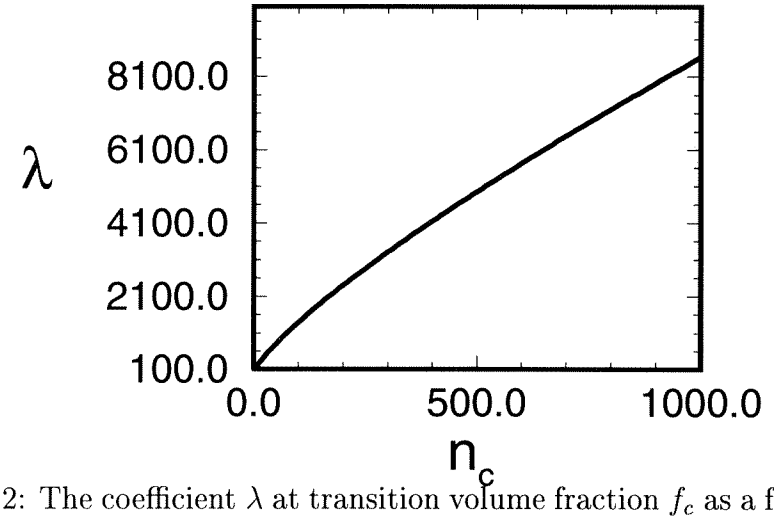

Figure 3.12: The coefficient λ at transition volume fraction f_c as a function of charges αN

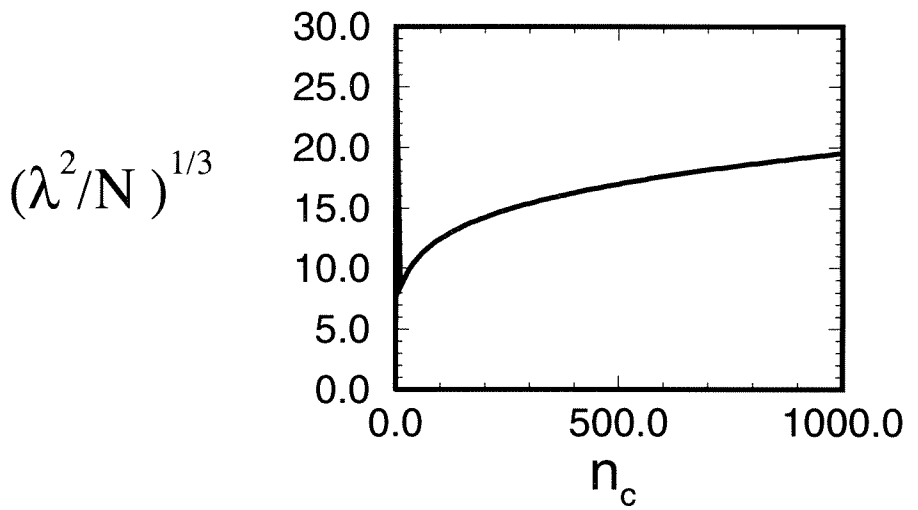

Figure 3.13: The scaling variable $\lambda^{2/3}/N^{1/3}$ as a function of charges αN

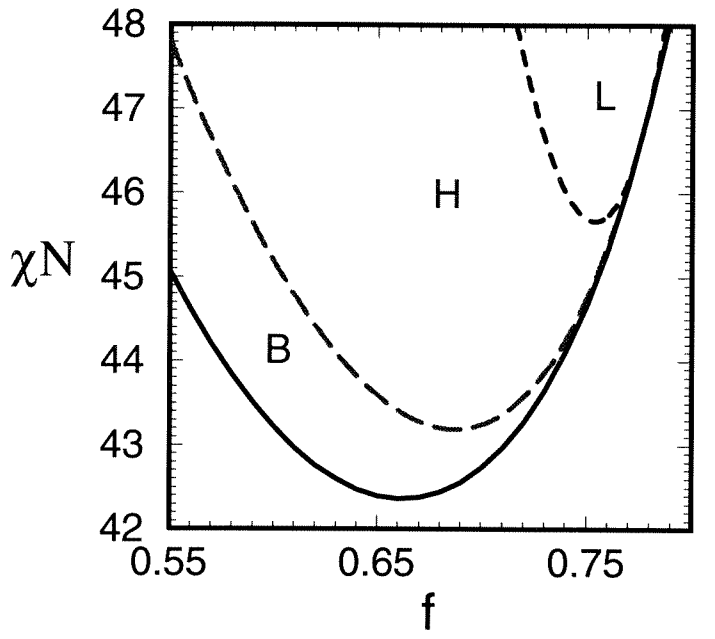

(a)

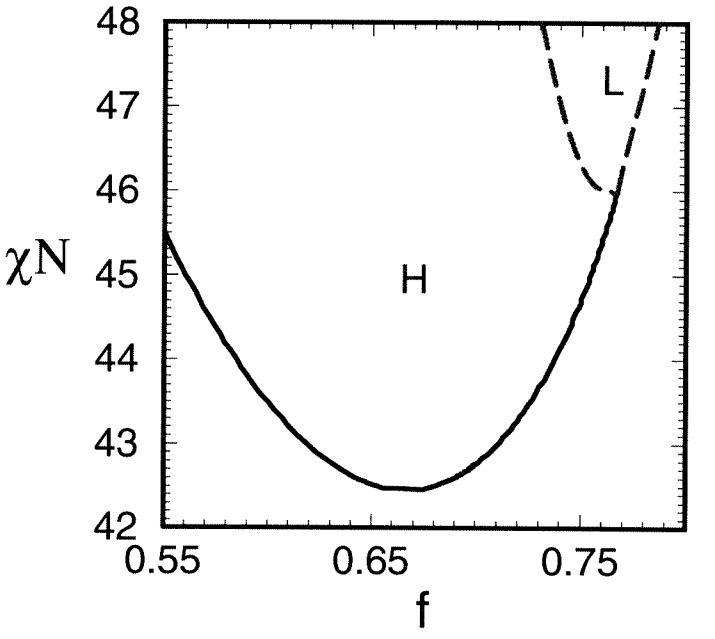

(b)

Figure 3.14: Phase diagram for a system with charges $\alpha N = 40$, dimensionless reservoir salt concentration $n_r = 0$, where $n_r = c_\infty v_o N$. (a) the mean fiels theory result; (b) the Hartree approximation.

Bibliography

[1] *Processing Strucure, and Properties of Block Copolymers*, edited by M. J. Folkes (Elsevier, New York, 1985)

[2] *Developments in Block Copolymers -1*, edited by I. Goodman (Applied Science, New York, 1982)

[3] L. Leibler, *Macromolecules 13.* 1602 (1980)

[4] G. H. Fredrickson and E. Helfand, *J. Chem. Phys 87.* 697 (1987)

[5] F. S. Bates, G. Fredrickson, *Ann. Rev. Phys. Chem. 41.* 525 (1990)

[6] M. W. Matsen and F. S. Bates, *Macromolecules 29.* 1092 (1996), and refrence within.

[7] J. F. Joanny and L. Leibler, *J. Phys. France 51.* 545 (1990)

[8] I. A. Nyrkova and A. R. Khokhlov, *Macromolecules 25.* 1493 (1992)

[9] I. A. Nyrkova and A. R. Khokhlov, *Macromolecules 27.* 4220 (1994)

[10] J. F. Marko and Y. Rabin, *Macromolecules 25.* 1503 (1992)

[11] J. F. Marko and Y. Rabin, *Macromolecules 24.* 2134 (1991)

[12] M. Benmouna and Y. Bouayed, *Macromolecules 25.* 5318 (1992)

[13] P. González-Mozuelos and M. O. de la Cruz, *J. Chem. Phys 100.* 507 (1994)

[14] J. Wittmer and J. F. Joanny *Macromolecules, 26.* 2691 (1993)

[15] N. P. Shusharina, I. A. Nyrkova, and A. R. Khokhlov, *Macromolecules 29.* 3167 (1996)

[16] P. G. de Gennes, *Scaling Concepts in Polymer Physics*; Cornell University Press; Ithaca, NY, 1979

[17] P. Flory, *Principles of Polymer Chemistry*; Cornell University Press; Ithaca, NY, 1953

[18] A. Brazovskii, *Sov. Phys. JETP, 41*, 85 (1975)

[19] L. D. Landau, E. M. Lifshitz, *Statistical Physics* Pergamon Press, 1980

[20] T. Ohta and K. Kawasaki, *Macromolecules 19.* 2621 (1986)

[21] A. H. Schoen, *NASA Technical Report* No. *05541.* 697 (1970)

[22] V. Luzzati, A. Tardieu, T. Gulik-Krzywicki, E. Rivas, F. Reiss-Husson, *Nature 220.* 485 (1968)

[23] D. Gobran Ph.D. Thesis, University of Massachusetts, Amherst, MA, 1990

[24] D. A. Hajduk, P. E. Harper, S. M. Gruner, C.C. Honeker, G. Kim, E. L. Thomas, *Macromolecules 27.* 4063 (1994)

[25] P. G. de Gennes, *Scaling Concepts in Polymer Physice* Cornell University Press; Ithaca, NY, 1993

[26] D. J. Amit, *Field Theory, the Renormalization Group, and Critical Phenomena* World Scientific, New York, 1984

[27] A. M. Mayers and M. Olvera. de la Cruz, *J. Chem. Phys 95.* 4670 (1991)

Chapter 4 Morphology of Diblock Copolymer Melts in Confined Geometries

4.1 Introduction

Most prior research on block copolymer melts has focused on the bulk properties of the material. Block copolymers with mutually incompatible components have the remarkable feature that they form microphase-separated structures. Extensive experimental and theoretical studies have been conducted on the microphase separation transition (MST) of diblock copolymers (AB) in bulk [1]- [16]. It is well known that for temperatures below the order-disorder temperature, T_{ODT}, depending on the composition and/or temperature, diblock copolymers self-assemble in the melt to form lamellae, hexagonally packed cylinders, body-centered-cubic spheres, or bicontinuous structures (gyroid phase). This microphase separation is the key to many valuable properties which make block copolymers of great technological interest.

Recently block copolymers are finding increasing applications as thin-film adhesives and surfactants. As a result, surface effects on the microphase separation of diblock copolymers have attracted widespread attention. Most studies have focused on the influence of external surfaces on the behavior of symmetric diblock copolymers. Recent experimental and theoretical studies show that the presence of surface interactions, in otherwise homogeneous diblock copolymer melt, yields several interesting surface induced ordering phenomena. Experimental studies of symmetric block copolymer thin films demonstrate that the interactions of the blocks with the surfaces induce a nearly perfect orientation of lamellar microdomains parallel to the film surface, thus producing a multilayered structure. As consequence, the film thickness in the ordered state is quantized. When the film thickness is not commensurate with the bulk lamellar thickness, the films are geometrically frustrated. "Islands" or "holes" are observed in the upper-most layer [17] - [24]. The thermal equilibrium state consists of regions of two discrete thickness correponding to neighboring free energy minima.

Theoretical studies of surface effects on the microphase separation of diblock copolymers were first undertaken by Fredrickson who extended Leibler's mean field theory to study nearly-symmetric diblock melts in the vicinity of a solid wall or free surface having preferential affinity for A (or B) repeat units [25]. He found that a composition oscillation exists near the surface even when the bulk copolymer is disordered. The oscillations are characterized by a decay length which diverges at the critical point. Shull applied a quantitative mean-field theory to diblock copolymer melts, as well as surfaces and thin films of these melts [19]. For thick films and small values of the order parameter, his results reduce to the analytical results of Fredrickson. For thin films, he found that the free energy is an oscillatory function of the film thickness due to the interference between the composition oscillations originating from the two surfaces. The thickness between different thickness minima is equal to the bulk repeat period, which is consistent with experimental results [19], [23], [24].

Microphase separation of diblock copolymer melts in confined geometries is a interesting system that combines both the surface interactions and confinement effects. Since the film cannot relax by creating islands on top of an ideal structure, the equilibrium morphology has to ajust to achieve overall minimum free energy. Turner has studied the equilibrium behavior of the lamellar phase of $A-B$ diblock copolymers in the strong segragation limit [30]. Assuming that each lamellar layer is an $A-B, B-A$ structure parallel to two identical flat plates (Figure 4.1), he calculated the phase diagrams of both integer number, n, and half-odd-integer number, $(2n+1)/2$, layers in terms of the distance between two plates L and the interfacial parameter δ, $\delta = (\gamma_{BS} - \gamma_{AS})/\gamma_{AB}$, where γ_{AB} is the $A-B$ interfacial tension, γ_{AS} and γ_{BS} are surface tensions between the A, B blocks and the plates, respectively. He found that the configurations with a half-odd-integer number of layers occur when the difference between the two polymer-plate surface tensions is small and L is below some critical plate separation.

The above mentioned studies on diblock copolymer films or diblock copolymers in confined geometries have focusd on symmetric or nearly symmetric diblock copolymers. Furthermore, only the lamellar structure parallel to the surface of the plates, or the variation of the density profile in the direction perpendicular to the surface are considered. Therefore, potential structures in the xy plane have not been addressed.

In general, depending on the strength of surface tensions and the plate separation, the microdomains can align either parallel or perpendicular to the plates even for symmetric diblock copolymers. On the one hand, a lamellar structure parallel to the plates is favored because of the surface interactions; on the other hand, if the distance between the two plates L is not commensurate to the lamellar period in bulk, the diblock copolymer chains are either stretched or compressed, which gives rise to a higher energy than lamellae perpendicular to the plates. Hence, the orientation of lamellar structure for symmetric or nearly symmetric diblock copolymers is the result of competition between the surface interactions and the confinement effects. This has been demonstrated by Kikuchi and Binder [27] and Brown and Chakrabati [28].

Kikuchi and Binder used Monte Carlo simulation of a lattice model to study the microphase separation of symmetric diblock copolymer melts between two rigid walls. They found tilted or deformed lamellar structure, as well as coexistence of lamellae in different orientations when the distance between the two plates is strongly incompatible with the bulk equilibrium lamellar period L^* [27]. Brown and Chakrabati studied the morphology of symmetric diblock copolymers confined between two plates by simulating a coarse-grain model without presupposing the basic shape. In the case where the two plates are identical, they observed horizontally and vertically oriented integer number lamellae. However, they did not observe any horizontally oriented half-odd-integer number lamellar phase, which has been shown to be stable at some range of δ and L by Turner [30].

In this paper, we study the morphology of symmetric and asymmetric diblock copolymer melts confined between two rigid plates in the strong segregation limit by extending the method developed by Ohta and Kawasaki [7] and [8]. Instead of restricting the diblock copolymers to be nearly symmetric, we allow the volume fraction f to vary and explore possible changes in morphology as the asymmetry in the volume fraction increases. It is well known that bulk diblock copolymers undergo the following sequence of morphology changes as the asymmetry in the volume fraction increases: lamellar $\rightarrow$ hexagonal cylinders $\rightarrow$ b.c.c spheres. In the strong segregation limit, the morphology is determined by the volume fraction f except for very weak dependence on χN (Figure 1.3a). Diblock copolymers confined between the two plates can also form cylindrical and spherical structures as the asymmetry in the volume fraction increases. However, the existence of the two plates introduces interactions

between the surfaces of the plates and repeat units of diblock copolymers as well as a new length scale L (the distance between the two plates), in addition, it breaks the rotational and translational symmetry present in the isotropic bulk system. Thus, we expect modifications to the phase diagrams from that observed in bulk. The competition between the confinement and the surface interactions has a profound effect on the formation of the equilibrium phase.

In order to focus on the effects of confinement and the surface interactions on the morphology of diblock copolymers, we restrict the distance between the two plates L to be of the same order of magnitude as the period L^* of the lamellar structure in the bulk sample. Thus, only a monolayer or bilayers can be formed between the two plates. When the plate distance is much larger than L^*, the surface interactions only affect the layers near the surfaces. In the middle of the two plates where the surface effect can be ignored, the stable phase is the same as that in bulk. As demonstrated by Turner, Rubinstein, and Marques, lamellar ordering is induced in a hexagonal phase of diblock copolymers in the presence of a single flat surfaces [31]. A similar situation is expected for a block copolymer melt confined between two plates, i.e., when L is large enough the morphology can contain a gradual transition between the surface-induced ordering and the bulklike order. Once L is restricted to be an order of L^*, morphologies that form between the two plates are purely due to effects of surface interaction and confinement.

We have sketched the possible morphologies that can form between the two plates in Figure 4.2. We calculate the free energy of each morphology by extending Ohta and Kawasaki's method for diblock copolymers in the strong segregation limit [7], [8] and calculate various phase diagrams in a parameter space consisting of volume fraction f, distance between the two plate L, and $\delta_i = (\gamma^i_{BS} - \gamma^i_{AS})/\gamma_{AB}$ $(i = 1, 2)$, where $\gamma^i_{AS}, \gamma^i_{BS}$ are the surface tensions between the plates i and blocks A and B, respectively.

The organization of the paper is as follows: In section 4.2, we present the general formulation of the free energy of diblock copolymers confined between two rigid walls by extending the theory of Ohta-Kawasaki to include the surface effect. In section 4.3, we discuss the equilibrium property of diblock copolymers between two *identical* plates. Subsection 4.3.1 focuses on the symmetric and nearly symmetric diblock copolymers and Subsection 4.3.2 explores the possible morphologies which include

cylindrical or spherical domains as the asymmetry of diblock copolymers increases. In section 4.4, we discuss the equilibrium property of diblock copolymers confined between two distinct plates. Section 4.5 is the conclusion.

4.2 Free Energy of Diblock Copolymers Confined between Two Plates

The system that we consider is a diblock copolymer melt confined between two solid walls as depicted in Figure 4.3. We choose the coordinates such that the surfaces of walls are parallel to the xy plate and the surface normal is in the z direction. Plate 1 is located at $z = 0$ and the plate 2 is located at $z = L$. Each block copolymer chain consists of Nf segements of the A block and $N(1-f)$ segments of the B block. For the sake of simplicity, we assume that both block A and B have the same Kuhn statistical segment length, which we take to be unity, and the same monomeric volume v_o. The interfacial tension between block A and block B is γ_{AB}, and the interfacial tensions between the two plates and blocks A and B are γ^1_{AS}, γ^2_{AS}, γ^1_{BS}, γ^2_{BS}, respectively. In this paper, we study two cases: (1) The two plates are identical, i.e., $\gamma^1_{AS} = \gamma^2_{AS}$ and $\gamma^1_{BS} = \gamma^2_{BS}$; (2) the two plates attract different blocks differently.

To study the equilibrium properties of diblock copolymers confined between two plates in the strong segregation limit, we extend the theory of Ohta and Kawasaki [7], [8] to take into account the surface effects. The free energy per chain of the system can be written as a sum of the bulk and surface contributions:

$$F[\Psi] = F_b[\Psi] + F_s[\Psi] \tag{4.1}$$

where $F_b[\Psi]$ is the bulk free energy, the driving force for microphase separation, and $F_s[\Psi]$ is the surface energy.

In the strong segregation limit, diblock copolymers form microdomains with periodic structures. The interfacial width of the domains is much smaller than the lattice dimensions. The free energy of the bulk system, $F_b[\Psi]$, can therefore be separated into two parts: an entropic chain-conformational free energy, and an interfacial free energy, whose strength is characterized by the Flory-Huggins parameters [33]. The

free energy density of bulk part can be written as:

$$F_b[\Psi] = CL^2\Phi(f) + \frac{\gamma_{AB}A_{AB}}{AL} \tag{4.2}$$

where $C = 3v_o/(8N^2b^2)$ is a constant. A is the contact area of diblock copolymers with one of the plates within a unit cell. A_{AB} is the total interfacial area of blocks A and B within a unit cell. $\Phi(f)$ is a scaling function which depends on the morphology of the system. Using the approximation suggested by Ohta and Kawasaki, in which $\Phi(f)$ is calculated from the asymptotic behavior of the structure factor in the long wave length limit [7], [8], we obtain

$$\Phi(f) = \frac{12}{f^2(1-f)^2}\sum_Q \frac{1}{(QL)^2}\Psi_\alpha(Q)\Psi^*_\beta(Q) \tag{4.3}$$

where $\Psi_\alpha(Q)$ is the Fourier Transform of $\Psi_\alpha(\vec{r})$ which is the local volume fraction deviation of monomers α from its uniform distribution. It can be proved rigorously that the $\Psi_\alpha(Q)$ can be expanded as

$$\Psi_\alpha(Q) = \frac{1}{AL}\int_\Sigma dxdy \int_0^L dzexp(-i(Q_x x + Q_y y))cos(\frac{m\pi z}{L})\Psi_\alpha(x,y,z) \tag{4.4}$$

The normal modes in the z direction are chosen to be $cos(m\pi z/L)$ with $m = 0, 1, 2, \cdots$, which satisfy the reflecting boundary conditions on the surfaces of both plates.

The surface energy density of a diblock copolymer melt confined between two surfaces can be written as

$$F_s[\Psi] = \frac{\gamma^1_{AS}A^1_{AS} + \gamma^2_{AS}A^2_{AS}}{AL} + \frac{\gamma^1_{BS}A^1_{BS} + \gamma^2_{BS}A^2_{BS}}{AL} \tag{4.5}$$

where A^i_{AS} and A^i_{BS} $(i = 1, 2)$ are the contact areas of blocks A and B with plates 1 and 2 in the unit cell, respectively, which satisfy $A^i_{AS} + A^i_{BS} = A$, $i = 1, 2$.

Hence, the total free energy density of diblock copolymer melt confined between two plates is

$$F = CL^2\Phi(f) + \frac{\gamma_{AB}A_{AB}}{AL} + \frac{\gamma^1_{AS}A^1_{AS} + \gamma^2_{AS}A^2_{AS}}{AL} + \frac{\gamma^1_{BS}A^1_{BS} + \gamma^2_{BS}A^2_{BS}}{AL} \tag{4.6}$$

This free energy density F can be used to evaluate the equilibrium free energy of

the bulk sample. In the bulk sample, the surface interactions vanish, i.e., $\gamma^i_{KS} = 0$, where $K = A, B$ and $i = 1, 2$. Thus, the free energy of bulk lamellar phase is:

$$F_b[\Psi] = CL^2 + \frac{2\gamma_{AB}}{L} \tag{4.7}$$

Minimization of the free energy in Eq.(4.6) with respect to L gives the equilibrium layer thickness

$$L^* = [\gamma_{AB}/C]^{1/3} \tag{4.8}$$

which correctly predicts the experimentally observed scaling of the lamellar period with diblock copolymer molecular weight, $L^* \sim N^{2/3}$. The corresponding bulk free energy is given by

$$F^* = 3[C\gamma^2_{AB}]^{1/3} \tag{4.9}$$

For diblock copolymer melts confined between two plates the free energy can be simplified by normalizing all lengths by L^*, and all energies by F^*. The normalized free energy is

$$F/F^* = \frac{1}{3}[d^2\Phi(f) + \frac{\sigma_{AB}}{d} + \sum_{i=1,2} \frac{\delta_i A^i_{BS}/A}{d} + \frac{(\gamma^1_{AS} + \gamma^2_{AS})/\gamma_{AB}}{d}] \tag{4.10}$$

where $\sigma_{AB} = A_{AB}/A$, $d = L/L^*$, and

$$\delta_i = (\gamma^i_{BS} - \gamma^i_{AS})/\gamma_{AB} \qquad i = 1, 2 \tag{4.11}$$

The interfacial parameter δ_i is a quantitative measure of the difference between the interfacial tension of the blocks A and the surface i and that of the blocks B and the surface i. The last term in Equation (9) is independent of the morphology, and thus does not play a role in the calculation of phase diagrams.

For two identical plates which have the same preferential affinity for, say A blocks, the free energy of diblock copolymers can be further simplified as

$$\hat{F} = \frac{1}{3}\left\{d^2\Phi(f) + \frac{\sigma_{AB}}{d} + \frac{2\delta(\sum_{i=1,2} A^i_{BS})/A}{d} + \frac{2\gamma_{AS}/\gamma_{AB}}{d}\right\} \tag{4.12}$$

where $\delta = (\gamma_{BS} - \gamma_{AS})/\gamma_{AB}$ is the interfacial parameter.

Thus, when the two plates are identical the free energy of confined diblock copolymer melt depends on the three parameters: the normalized distance between the plates, the interfacial parameter δ, and the volume fraction of the diblock copolymers. For two distinct plates, the free energy of confined diblock copolymers depends on four parameters: the interfacial parameters δ_1 and δ_2, the normalized distance between the plates, and the volume fraction of the diblock copolymers.

4.3 Diblock Copolymers Confined between Two Identical Plates

In this section, we study the equilibrium behavior of diblock copolymer melts confined between two identical plates. The free energy of the system is given in Eq.(4.12). We assume that $\gamma_{AS} < \gamma_{BS}$, i.e., the plates attract A blocks.

In the simple diblock copolymer melts in the strong segregation limit, the mophology is mainly determined by the volume fraction f and has very weak dependence on χN. The morphology of diblock copolymer melts confined between two identical plates, however, strongly depends on the three physical parameters: the copolymer volume fraction f, the normalized distance d, and the interfacial parameter δ. The existence of two plates introduces both the surface interactions and a new length scale. In addition, it breaks the rotational and translational symmetry of the bulk copolymer melt. In order to focus on each of the effects, we divide this section to two parts. In section 4.3.1, we study the morphology of symmetric or nearly symmetric diblock copolymers. In this case, the basic structure is lamellar. The competition between the surface interactions and the confinement effects is manifested itself in the change of the orientation of the lamellar structure or leads to the breaking of reflecting symmetry with respect to the midplane of the system. In section 4.3.2, we study the phase behavior of diblock copolymers with an arbitrary volume fraction f. The changes in the volume fraction f primarily affect the shape (lamellar, cylinder, or sphere) and packing symmetry of the ordered structure. Due to the breaking of the rotational and translational symmetry, the transition point f depends not only on the distance between the two plates, but also on the interfacial parameter.

4.3.1 Symmetric or Nearly Symmetric Diblock Copolymers

For symmetric/nearly symmetric diblock copolymers, the basic structures are lamellar. We define one lamellar layer to be an entire $A-B$, $B-A$ repeat unit. The number of lamellar layers n can be either an integer or half-odd-integer, as shown in Figures 4.1(a) and 4.1(b). Configurations consisting of integer number of layers with a horizontal orientation is refered to as the "symmmetric" horizontal lamellar phase ($HL(n)$), those with a half-odd-integer number of layers as the "asymmetric" horizontal lamellar phase ($AHL(n)$), and vertically oriented lamellae as VL (Figure 4.1(c)).

Obviously, the HL structure consisting of an integer numbers of layers with A blocks preferentially segregating to the surfaces can achieve the minimum surface interaction energy. However, when the distance between the two plates is incommensurate to the period of bulk lamellar layers, L^*, the symmetric horizontally oriented lamellar structure posses an large inherent tensile or compressive strain and thus is geometrically frustrated. The vertically oriented lamellar structure (VL) or asymmertic lamellar structure (AHL) can achieve relatively low overall energy when the interfacial parameter δ is small. In certain cases, the entropic penalty associated with the chain deformation is larger than the energetic penalty of having the B blocks adjacent to the surfaces. To be more specific, for a vertical lamellar structure the imposed thickness constraint acts perpendicularly to the lamellar ordering and the bulk lamellar period is realized. For asymmetric lamellar structure, when the distance between the two plates is most incommensurate to the bulk length, i.e., $L \sim L^*(n+1/2)$, the size of each domain is the about the same as that in bulk and the polymer chains are not stretched or compressed. Hence both the VL and AHL morphologies have low entropic energy.

On the other hand, at a sufficiently large value of the interfacial parameter δ, the surface interactions dominate the free energy. Even when the distance between the two plates is most incommensurate with the lamellar period in bulk, both the VL and AHL phases have very high overall free energy due to the contact between the B blocks and the surfaces, and thus are unfavorable. In this case, the large tension can lead to undulations in the horizontal directions. The undulating phase does not have high surface interaction, since A-rich domains are adjacent to the plates, while the

tension due to the stretching of chains can be relieved by forming undulation where the true distance between the two adjacent layers is less than the vertical distance. This undulation instability is well-known for semetic-A liquid crystals [34] and has been shown to exist in a bulk lamellar phase under tension [35].

Small δ — The Stability of HL vs. VL and AHL

We study the stability of the HL, VL, and AHL phases for symmetric/nearly symmetric diblock copolymers confined between two identical plates with small interfacial parameter δ. The free energies of these three morphologies can be calculated according to Eq.(4.12). They are:

$$F_{HL} = \frac{1}{3}\left\{\frac{d^2}{n^2} + \frac{2n}{d} + \frac{2\gamma_{AS}/\gamma_{AB}}{d}\right\} \tag{4.13}$$

$$F_{VL} = \frac{1}{3}\left\{3 + \frac{2(1-f)\delta}{d} + \frac{2\gamma_{AS}/\gamma_{AB}}{d}\right\} \tag{4.14}$$

$$F_{AHL} = \frac{1}{3}\left\{\frac{d^2}{(n+1/2)^2} + \frac{2(n+1/2)}{d} + \frac{\delta}{d} + \frac{2\gamma_{AS}/\gamma_{AB}}{d}\right\} \tag{4.15}$$

where n is the number of $A-B$, $B-A$ repeat units of lamellar layers.

The free energies of these three phases is plotted in Figure 4.4 as a function of the normalized distance between the two plates d with the interfacial paramter $\delta = 0.2$. The volume fractions of the diblock copolymers are $f = 0.4$ (Fig.4.4a), $f = 0.5$ (Fig 4.4b), and $f = 0.6$ (Fig. 4.4c), respectively. From the figures we can see that the vertically oriented lamellar phase is always accessible when the distance between the two plates is incommensurate to the bulk lamellar period. For diblock copolymers with volume fraction $f < 0.5$, the horizontally oriented lamellar phase has the lowest free energy when the distance between the two plates is most incommensurate to the bulk lamellar period, i.e., $d \sim n+0.5$; for the volume fraction $f > 0.5$, the free energy of the AHL phase is always higher than that of the VL phase and, therefore, the AHL phase is not accessible. For $f = 0.5$, the free energy of the AHL is higher than that of the VL phase except at $d = n + 0.5$.

The above observation can be verified by considering the free energy difference

between the AHL and VL phases.

$$F_{AHL} - F_{VL} = \frac{1}{3}\left\{\frac{d^2}{(n+1/2)^2} + \frac{2(n+1/2)}{d} - 3 + \frac{\delta(1-2(1-f))}{d}\right\} \tag{4.16}$$

The free energy difference reaches its minimum value at d_c:

$$d_c = (n+1/2)\left[1 + \frac{\delta(1-2(1-f))}{2n+1}\right]^{1/3} \tag{4.17}$$

with

$$(F_{AHL} - F_{VL})_{min} = \left[1 + \frac{\delta(1-2(1-f))}{2n+1}\right]^{2/3} - 1 \tag{4.18}$$

The minimum is always larger than zero when $f > 0.5$ and equals zero at $f = 0.5$, $d = n + 0.5$. Only when $f < 0.5$, is the minimum of the energy difference negative, which implies that the Eq.(4.15) has two roots and that the AHL phase can be realized between the two roots.

The Maximum δ for the Existence of *AHL* and *VL* Phases

It should be reiterated that the existence of the AHL and VL phases as equlibrium morphologies for symmetric/nearly symmetric diblock copolymer melts is a result of the balance between the surface interactions and entropic energy due to confinement effects. At a sufficiently large interfacial parameter δ, the surface interactions are dominant, and neither the AHL nor the VL phases is favored over the HL phase. The maximum values of δ below which VL and AHL are accessible can be obtained though comparing the free energies of the three phases.

For a system with $f \geq 0.5$, we only need to compare the free energy of the VL and HL phases (AHL is unstable at any value of δ). The maximum δ for the existence of the VL phase is

$$\delta_{max} = d_1(n)\left\{d_1^2(n)/n^2 + 2n/d_1(n) - 3\right\}/(2(1-f)) \tag{4.19}$$

with $d_1 = [2n^2(n+1)^2/(2n+1)]^{1/3}$ where the energies of the $HL(n)$ and $HL(n+1)$ states coincide.

For the system with $f < 0.5$, the maximum value of δ can be obtained by comparing the free energies of the AHL and the $HL(n)$ phases since the free energy of

AHL phase is lower than that of the VL phase when $d \sim n + 0.5$. The result is

$$\delta_{max} = \frac{6n^2 + 6n + 1}{(2n+1)^3} \tag{4.20}$$

Therefore, when $\delta > \delta_{max}$ both the AHL and VL phases are inaccessible. Note that the maximum δ decreases as the number of layers n increases and vanishes as n approaches infinity. This means that for diblock copolymers confined between two plates with large separation, the symmetric horizontal lamellar phase is always stable even when it is deformed. This conclusion is not surprising, since in this case the deformation can be distributed over many layers, thus effectively eliminating the entropic penalty that stablizes the VL and AHL phases.

Large δ — The Undulation Phase

At a sufficiently large value of the interfacial parameter δ, neither the VL nor the AHL phase is stable, even when the distance between the two plates is incommensurate with L^*. The diblock copolymers in the horizontal oriented lamellar structure are stretched. However the tension can released by forming the undulating lamellar phase ($1dUL$, Figure 4.2e). Indeed, the undulating lamellar phase is accessible at $n + \Delta$ when Δ exceeds a critical value. The transition from $HL(n)$ to the undulation lamellar phase is a second order transition.

We study the one dimensional undulation phase at $1 < d < 2$, where $d = L/L^*$. The profile of the two interfaces between the A and B domains can be described by

$$u_1(x,z) = u_o cos(kx) + 0.5d + 0.5(1-f)d \tag{4.21}$$

$$u_2(x,z) = u_o cos(kx) + 0.5d - 0.5(1-f)d \tag{4.22}$$

where u_o and k are the amplitude and the wavevector of the undulation, respectively. The ampliude of undulation $u_o < 0.5fd$.

In the strong segregation limit, the free energy per chain of the undulation phase can be obtained by applying Eq.(4.11) to the undulation morphology. To fourth order in the amplitude, we obtain

$$F_{1dUL} = F_{HL}(1,d) + C_2(d,f,k)u_o^2 + C_4(d,f,k)u_o^4 \tag{4.23}$$

For a system with given f, the undulation instability sets in when the coefficient $C_2(d, f, \lambda)$ first becomes negative at a critical value of d_c and a wave vector k_c which minimizes C_2. In general, the critical value of d_c depends on f. We found that $d_c = 1.31$ for a system with $f = 0.5$, and $d_c = 1.37$ for a system with $f = 0.4$, which corresponds to 31% and 37% strains respectively. The amplitude u_o can be obtained by minimizing the free energy,

$$u_o = \sqrt{\frac{-C_2(d, f, \lambda_c)}{2C_4(d, f, \lambda_c)}} \tag{4.24}$$

and the corresponding free energy is

$$F_{1dUl} = F_{HL}(1, d) - \frac{C_2(d, f, k_c)^2}{4C_4(d, f, k_c)} \tag{4.25}$$

In Figure 4.5, we show the period of the undulation λ, $\lambda = 2\pi/k$, the coefficient $C_2(d, f, k_c)$, and the free energy difference between the lamellar and undulating phases ΔF as functions of the distance between the two plates. The volume fraction is set at $f = 0.5$. The transition from $HL(1)$ to the undulation phase is a second order phase transition, and the transion from the undulation phase to $HL(2)$ is a first order transition.

Phase Diagram for Symmetric/Nearly Symmetric Diblock Copolymers

The phase diagrams for symmetryic/nearly symmetric diblock copolymers with the volume fractions $f = 0.5$ and $f = 0.4$ are shown in Figures 4.6(a) and 4.6(b) respectively. In calculating the phase diagrams, we have considered all the morphologies listed in Figure 4.2. The diagrams explicitly demonstrate the conclusions that we have drawn in the above discussion.

For large δ, the structure of equilibrium phase of the diblock copolymers is essentially horizontal. The system undergo the following morphology changes as the distance between the two plates increases: $HL(1) \rightarrow 1dUL \rightarrow HL(2)$. For small δ, depending on the volume fraction f, the VL and AHL (for $f \leq 0.5$ only) phases are accessible when the distance between the two plates is incommensurate with the lamellar period in bulk. In Figure 4.6a, the stable regions for the AHL phase are represented by long dashed lines. There is a little island between the VL and $HL(1)$ phases where the morphology consisting of B blocks forming half cylinders located on

the surfaces of the plates is stable (TCY, Fig. 4.2g). We suspect that tilted lamellar structure could be stable in that region, since the structure of the TCY phase is very close to a tilted lamellae. In Figure 4.6b we do not show the stable region of the $1dUL$ phase since the width of $1dUL$ phase decreases with decreasing f and is very narrow when $f = 0.4$.

4.3.2 Asymmetric Diblock Copolymers

In this section, we explore the morphological change as the asymmetry of the volume fraction increases when diblock copolymers are confined between two rigid walls. The morphologies considered are shown in Figure 4.2. In Figures 4.7, 4.8, and 4.9, we present the phase diagram of diblock copolymers confined between two plates with $\delta = 0$, $\delta = 0.5$, and $\delta = 1.0$ respectively.

The phase diagram for diblock copolymers confined between two identical walls with $\delta = 0$ is depicted in Figure 4.7. The solid lines are phase boundaries, the horizontal long dashed line and the dot-dashed lines indicate the coexistence of the VL/HL and $VL/\ AHL$ phases, and the dashed lines indicate the coexistence of the $VCY/\ TCY$ phases. Since the surface interaction between the two plates and the A and B blocks are the same, the phase diagram has $A-B$ interchange symmetry. In this case, the confinement effect plays an important role in determining the equilibrium state of the system.

When $f \simeq 0.5$, the VL phase is the most favored for diblock copolymers, since the distance of bilayer can be ajusted to be the same as that in bulk and there is no additional surface interactions penalty. The $HL(n)$ phase has the same energy as that of the VL only when $d = n$. When $d \neq n$, the $HL(n)$ phase is subjected to compressive or tensile stress and thus has a higher energy than the VL phase.

When $f \geq 0.35$ (or $f < 0.65$) , the VL phase transfers to the vertically aligned cylinder phase (VCY, Fig.4.2h) with minority components B (or A) forming the hexagonally packed cylinders in a matrix of A blocks. Since the confinement effect only acts perpendicularly to the lamellar and hexagonal ordering, the VL and VCY phases have the same structure as their corresponding structures in bulk. Therefore, the volume fraction f of the transition from the VL to the VCY is exactly the same as in the bulk. In the phase space where the VL is stable, the TCY phase has the

same energy as the VCY phase at the dashed lines.

When the volume fraction is further reduced (or increased), the minority components B(or A) form spherical domains located on a horizontally oriented hexagonal lattice ($HS(1)$) or even on two such layers ($HS(2)$), depending on the distance between the two plates. The schematic representation of the $HS(1)$ phase is shown in Fig.4.2k. In the $HS(2)$ phase, the spherical domains are located on two sets of horizontal square lattices, which are translated with each other by the vector $e = (a/2, a/2, b)$, where a is the lattice spacing and b is the distance between the two plates that contain the centers of the spherical domains. Both a and b can be determined by minimizing the free energy. The breaking of translational and rotational symmetry due to the confinement effects gives rise to the HS which has a different symmetry as its corresponding phase in bulk (spherical domains located on a $b.c.c$ lattice). Therefore, the value of f where transition from VCY to HS occurs is different from that found in bulk. More importantly, the transition value of f depends on the distance between the two plates.

The phase diagram for interfacial parameter $\delta = 0.5$ is shown in Figure 4.8. Since $\delta > 0$, the two surfaces have a preferential affinity for blocks A, and as a consequence, the phase diagram has some new features in comparison with the phase diagram in Fig.4.7.

The regions of the $HL(1)$, $HL(2)$, and $AHL(0.5)$ are greatly enlarged while the regions of the VL and VCY are reduced. This due to the fact that the VL and VCY phases have the advantage of achieving the minimum of the entropic energy but do not have the advantage of achieving the minimum of the surface interactions. As a result, their stable region in the phase diagram is reduced as δ increases from 0 to 0.5. The $HL(1)$ and $HL(2)$ phases, which have the advantage of minimizing the surface interactions, have an increasingly large stable region as δ is increased from 0 to 0.5.

When the distance between the two plates $d \sim 0.5$, at the left side of phase diagram where the volume fraction of A blocks is small, the A-rich domains form half spheres on tops of the plates (TS phase, Fig.4.2j), while at the right side of the phase diagram where the volume fraction of the B blocks is small, the B-rich domains form spheres located in the midplane between the two blocks ($HS(1)$). This reflects the fact the surface attracts the A blocks but not the B blocks.

When the distance between the two plates $d \sim 1.5$, the minority components (the A blocks at the left side of phase diagram and the B blocks at the right side of the phase diagram) simply form vertically oriented cylindrical domains ($VCY(A)$ and $VCY(B)$.

Figure 4.9 presents the phase diagrams for interfacial parameter $\delta = 1.0$. As the interfacial parameter increases further, the regions of the $HL(1)$ and $HL(2)$ phases are further enlarged and the regions of the VL and VCY phases are further reduced. The AHL phase between the HL and VL and VCY phases disappears in the phase diagram due to the high surface interactions. For the same reason, at left side of phase diagram, the TS and VCY phase also disappear even when the volume fraction of the A blocks is very small, instead the blocks A completely covered the surfaces and the contacts between the$B$ blocks and the surfaces are completely ruled out.

4.4 Diblock Copolymers Confined between Two Distinct Plates

We now study the morphologies that can form between two distinct plates that have different preferential affinity for blocks A and B. The free energy is given by Eq.(4.10), which depends on morphology and four physical parameters: copolymer volume fraction f, the normalized distance between the two plates d, and the two interfacial parameters δ_1 and δ_2. We study two special cases: (1) plate 1 attract blocks A and plate 2 attracts B; (2) plate 1 attract A and plate 2 has the same interaction with blocks A and B.

The analysis of surface effects on the equilibrium properties of diblock copolymer melts confined between two distinct plates can be done in the same way as that on diblock copolymer melts confined between two idenitcal plates. In particular case when the strength of attraction bewteen plate 1 and the A blocks is the same as that of the attraction between the plate 2 and the B blocks, and the diblock copolymers are symmetric/nearly symmetric, the AHL phase always has the minimum surface energy while it can achieve the minimum entropic energy when the distance between the two plates $d = n+0.5$. The HL phase, on the other hand, always has high surface energy while it can achieve minimum entropic energy at $d = n$. Similar to the VL

phase in two identical plates, the VL in the two distinct plates can always achieve the minimum entropic energy at penalty of relatively high surface energy. Thus, the AHL and the HL phase in two distinct plates are similar to the HL and AHL in two identical plates respectively. The quantitative analysis of the surface effect on the morphology can be done similarly as in section 4.3. However, we will simply present the phase diagrams.

The phase diagram of diblock copolymer melt confined between two distinct plates with plate 1 attracts A blocks and plate 2 attracts B blocks is shown in Figure 4.10. The prefrential affinities of the two plates are $\delta_1 = 0.5$ and $\delta_2 = -0.5$ respectively. The phase diagram is symmetric with respect to $f \to 1 - f$. When $d = 0.5$ and $0.045 < f < 0.954$, the diblock copolymer melt forms the AHL phase with blocks A forming a layer on the surface of plate 1 and blocks B forming a layer on the surface of plate 2. In this case, the morphology has both the minimum surface energy and entropic energy. When $f < 0.045$ (or $f > 0.954$), the minority components A blocks form half spheres located on a hexagonal lattice on plate 1 where they are attracted to (AS, Fig.4.2l), while plate 2 are completely covered by B blocks. When reducing L, the system transform from the AHL to the VL and VCY phases depending on the asymmetry in the volume fraction. We include in our analysis the morphology where the minority components form half cylinders layered on the surface to which it is attract to (Fig.4.2i), however, it is not stable and therefore does not appear in the phase diagram.

The phase diagram with one of the plates attracs A blocks and another has the same surface interactions with blocks A and B is depicted in Figure 4.11. We set $\delta_1 = 0.5$ and $\delta_2 = 0.0$. The phase diagram does not have the symmetry with respect to $f \to 1 - f$. When $L \sim 0.5$ and $0.12 < f < 0.72$, the stable state is the AHL phase. When $f < 0.12$ ($f > 0.72$), the system form the TS phase (Fig.4.2j). When reducing L, the system transform to the VL, VCY, and AS phases depending on the value of f.

4.5 Conclusion

The equilibrium property of diblock copolymers confined between two rigid plates in the strong segregation limit is studied by extending Ohta and Kawasaki's theory

to take into account the surface effects. Unlike bulk diblock copolymer melts in the strong segregation limit, where the mophology is determined by the volume fraction f except for a very weak dependence on χN, the morphology of diblock copolymer melts confined between two plates depends on four physical parameters: the copolymer volume fraction f, the normalized distance d, and the two interfacial parameters δ_1 and δ_2 defined in Eq.(4.11).

The existence of two plates introduces the surface interactions and a new length scale. In addition, it also breaks the rotational and translational symmetry that exists for diblock copolymers in bulk. By studying the phase behavior of symmetric/nearly symmetric diblock copolymers, we have demonstrated that for small values of interfacial parameter δ, the competition between the surface interactions and the confinement effects can not only change the orientation of the lamellar structure but also leads to the breaking of reflecting symmetry with respect to the midplane of the system. We find that there are the maximum values of δ for the existence of the VL and AHL phases beyond that the surface interactions dominate, and the VL and AHL phases are unstable. For large values of interfacial parameter δ, we have shown the possibility of one dimensional undulation instability.

We have studied the phase behavior of diblock copolymers with arbitrary volume fraction f to explore the surface effects on the stability of various morphologies (lamellar, cylinder, and sphere). We have shown that the volume fraction f at the transition between the VL and VCY phases is the same as its corresponding value in the bulk copolymer due to the fact that the confinement effects act perpendicularly to the lamellar and hexagonal ordering. On the other hand, the volume fraction f at the transition between the VCY and the HS phases depends on the distance between the two plates, since the HS phase is a three dimensional structure and the presence of two plates changes the symmetry of the structure. The distance dependence of the transition volume fraction is a consequence of the broken translational and rotational symmetry. The phase diagrams under various conditions have been mapped out.

We also studied the equilibrium property of diblock copolymers confined between two distinct plates by studing two special cases. In one of the cases, one of the plates attracts block A and the other attracts block B, in the other case, one of the plates attracts block A, and the other plate has no preferential affinity for either blocks. The phase diagrams in both cases are presented.

4.6 Figures

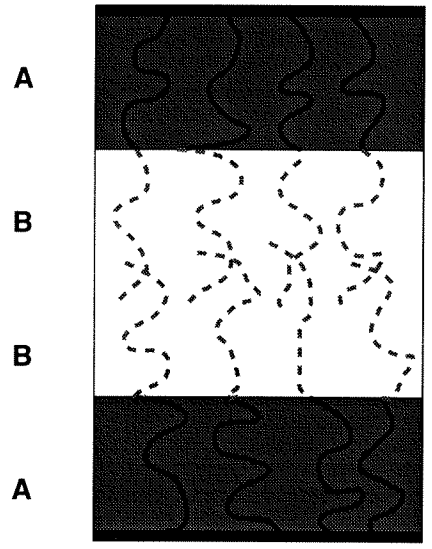

HL(1)

(a)

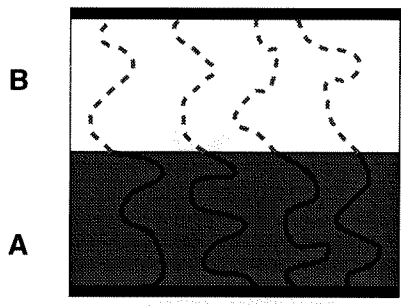

AHL(0.5)

(b)

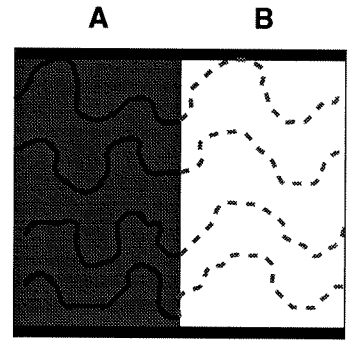

VL

(c)

Figure 4.1: Schematic illustration of horizontally oriented one layer lamellar structure ($HL(1)$), horizontally oriented half layer lamellar structure (AHL), and the vertically oriented lamellar structure (VL).

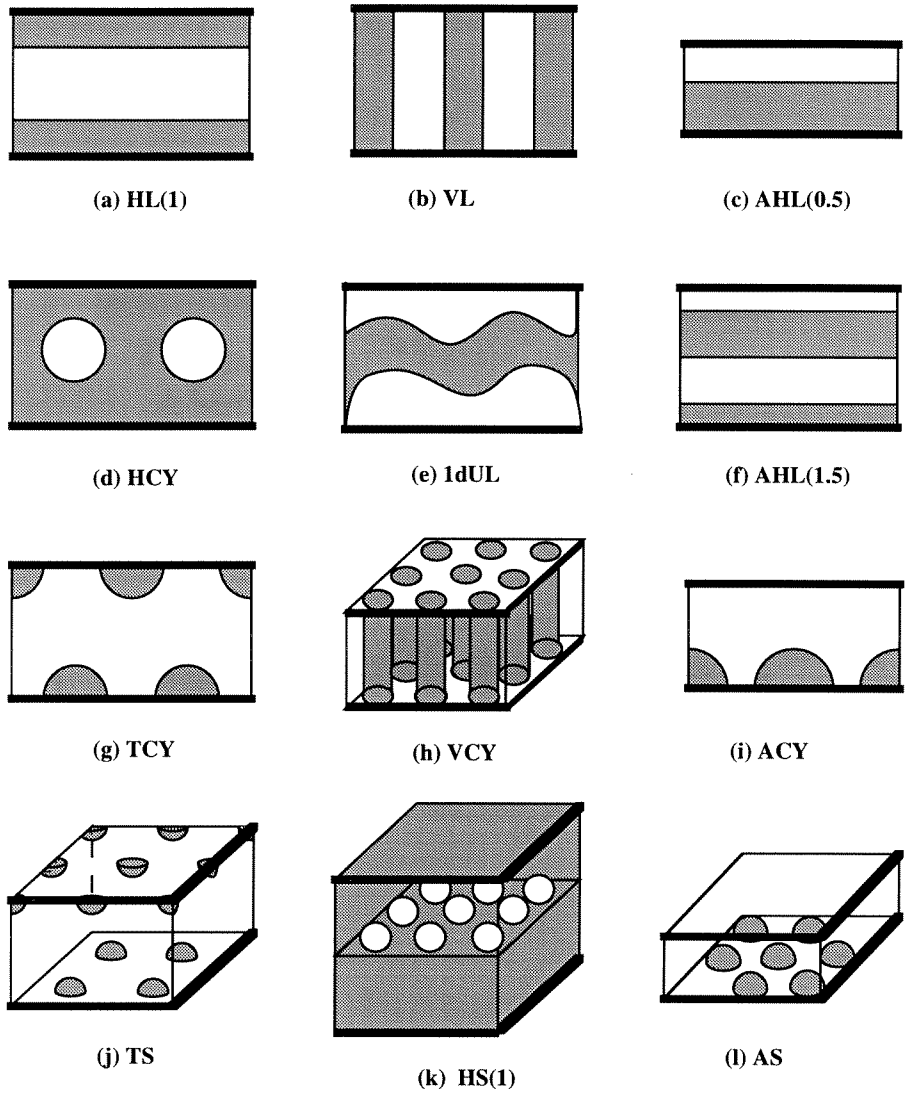

Figure 4.2: Schematic illustration of all the phases considered. (a) Horizontally oriented lamellae (HL); (b) Vertically oriented lamellae (VL); (c) Horizontally oriented asymmetric lamellae ($AHL(0.5)$); (d) Horizontally oriented cylinders (HCY); (e) One dimensional undulation ($1dUL$); (f) Horizontally oriented asymmetric lamellae ($AHL(1.5)$); (g) Horizontally oriented half cylinders on tetragonal lattice (TCY); (h) Vertically oriented cylinders (VCY); (i) Asymmetric, half cylinders on one of the surfaces (ACY); (j) Spheres on tetragonal lattice on the surfaces (TS); (k) Spheres on horizontal plane (HS) (l) Asymmetric, half spheres on hexagonal lattice on one of the surfaces (AS).

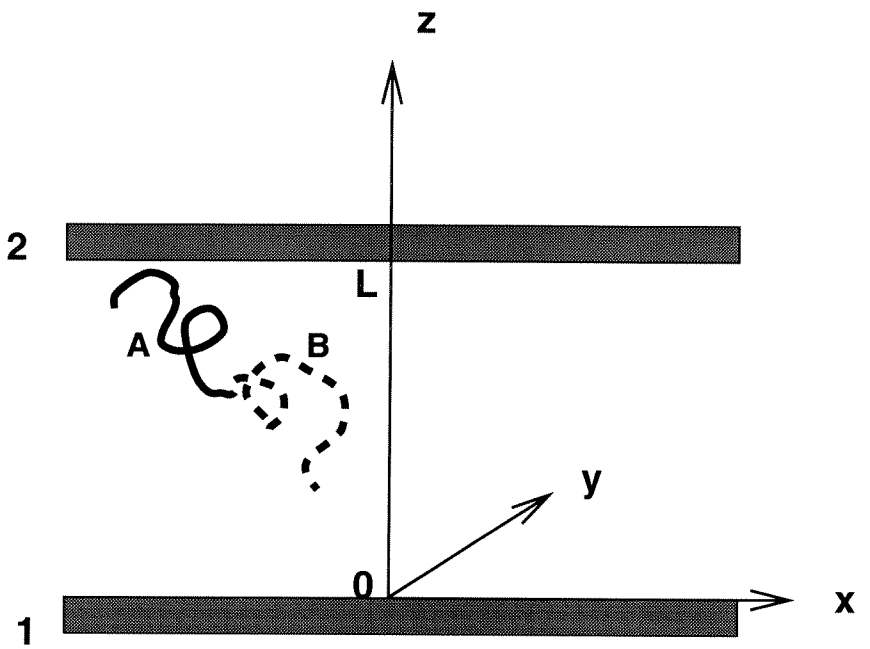

Figure 4.3: Schematic illustration of the system considered in the present chapter. Diblock copolymers are confined between two solid plates 1 and 2. The distance between two plates is L.

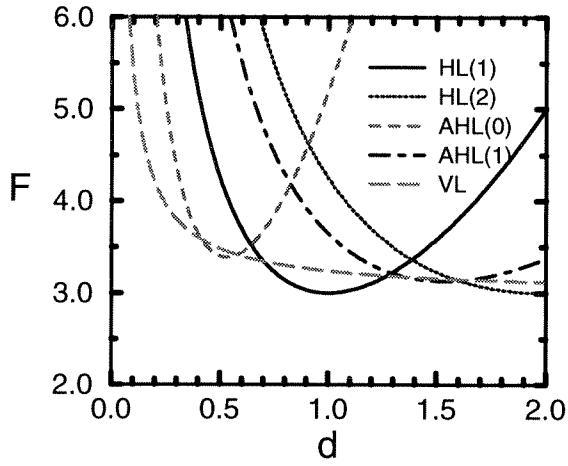

(a)

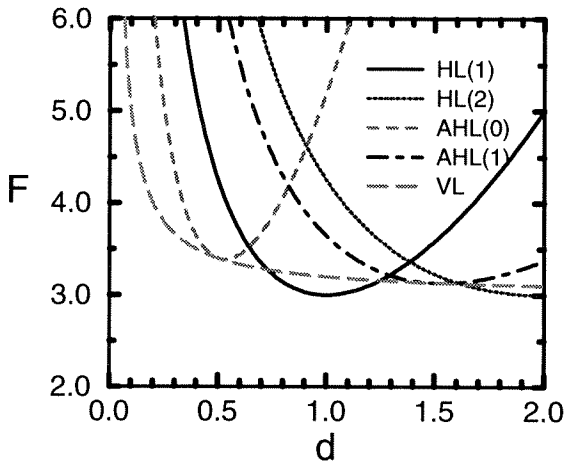

(b)

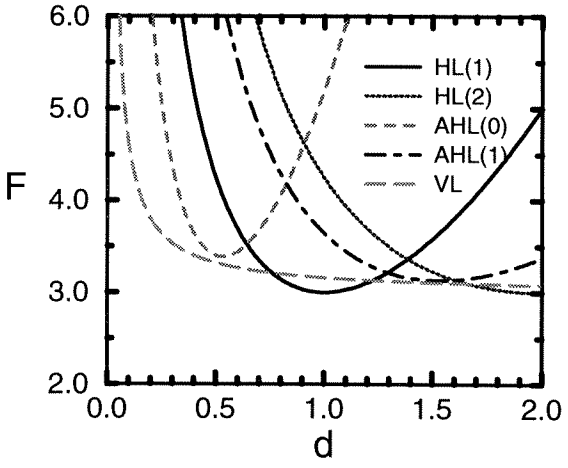

(c)

Figure 4.4: Free energy of diblock copolymer melt confined between the two identical plates as a function of the normalized distance d. The volume fractions of the diblock copolymers are (a) $f = 0.4$; (b) $f = 0.5$; (c) $f = 0.6$. $HL(1)$ (solid), $HL(2)$ (dotted), $AHL(0.5)$ (dashed), $AHL(1.5)$ (dot-dashed)

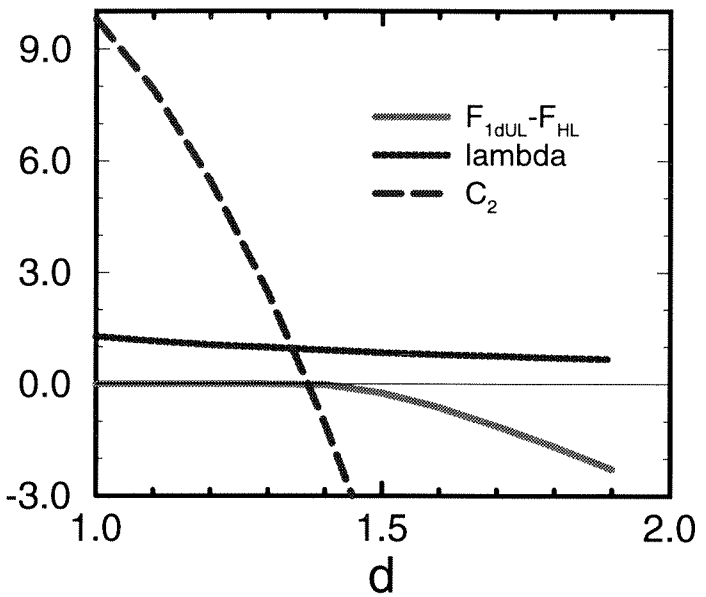

Figure 4.5: The free energy difference between $1dUL$ and HL (solid line), the period of interface profile λ (dotted line), and the quadratic order coefficient C_2 (long dashed) as functions of the normalized distance d for diblock copolymer melt with volume fraction $f = 0.5$

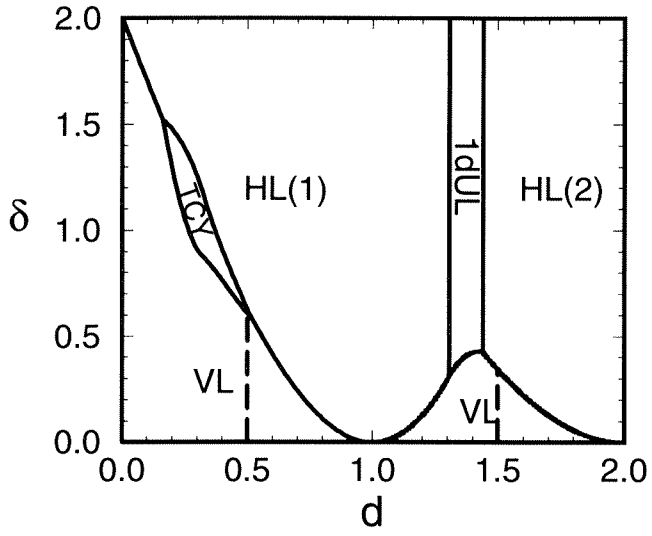

(a)

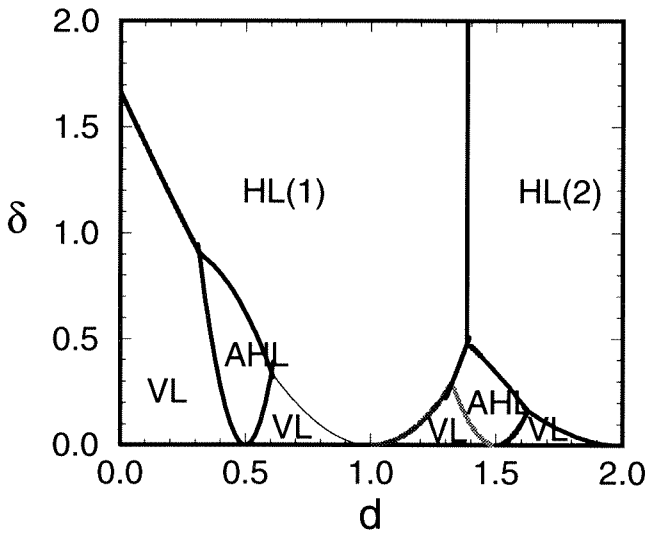

(b)

Figure 4.6: Phase diagram for (a) symmetric diblock copolymer melt, (b) nearly symmetric diblock copolymer melt ($f = 0.4$) confined between two identical walls. The interfacial parameter $\delta = 0.2$

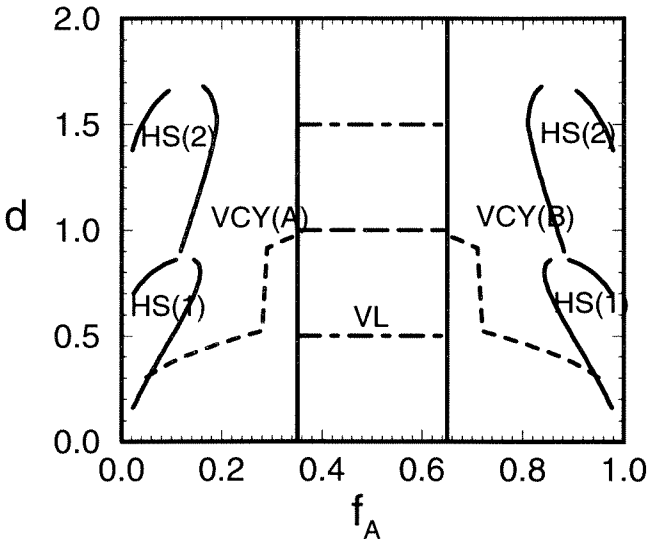

Figure 4.7: Phase diagram for a diblock copolymer melt confined between two identical plates with interfacial paramter $\delta = 0.0$. The solid lines are phase boundaries, the horizontal long dashed line and the dot-dashed lines indicate the coexistence of the VL/HL and VL/AHL phases, the other two dashed lines indicate the coexistence of the VCY/TCY phases.

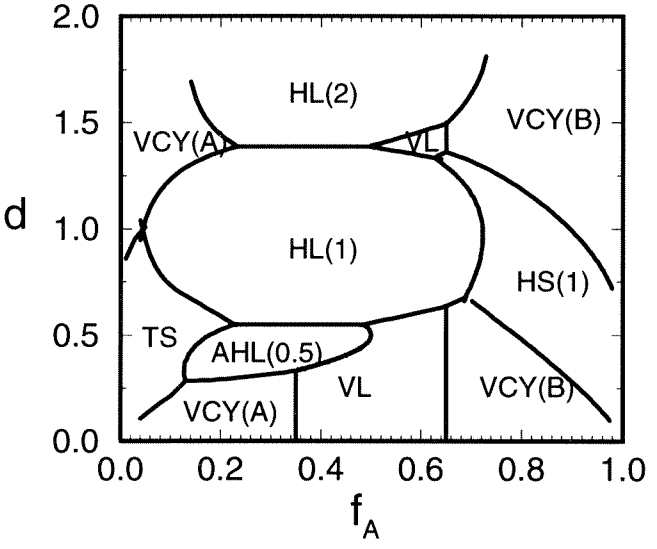

Figure 4.8: Phase diagram for a diblock copolymer melt confined between two identical plates with interfacial paramter $\delta = 0.5$.

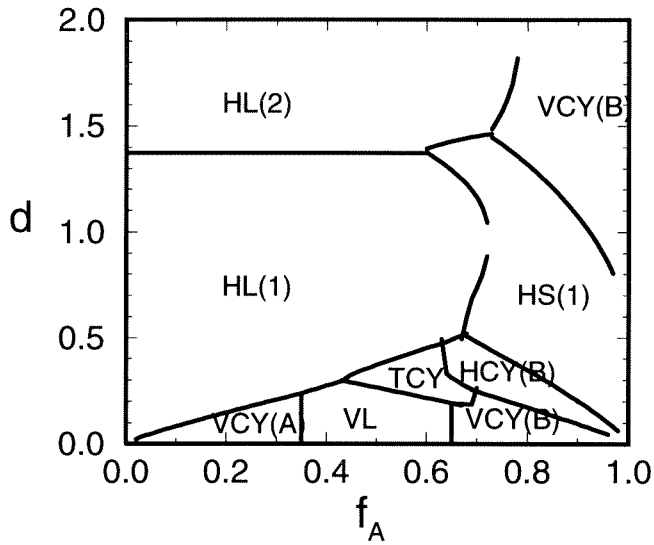

Figure 4.9: Phase diagram for a diblock copolymer melt confined between two identical plates with interfacial paramter $\delta = 1.0$.

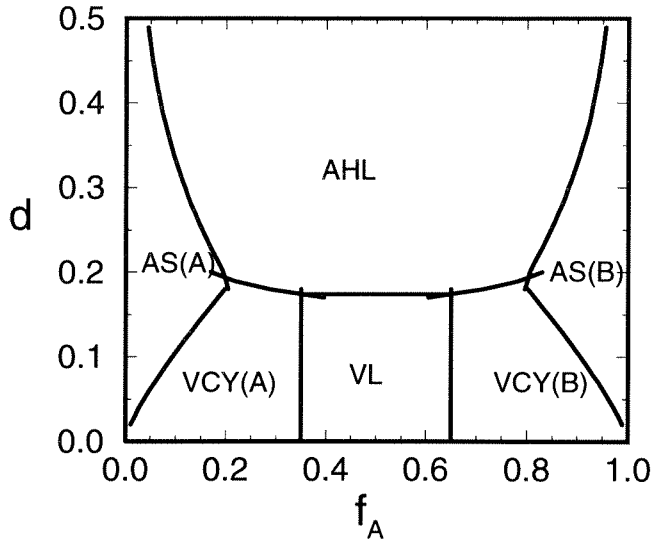

Figure 4.10: Phase diagram for a diblock copolymer melt confined between two distinct plates. One of the plates attracts block A and other attracts block B. The interfacial parameters are $\delta_1 = 0.5$ and $\delta_2 = -0.5$

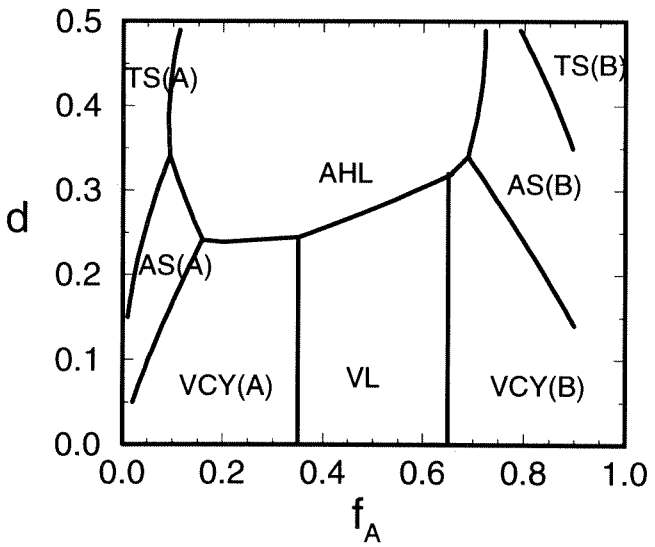

Figure 4.11: Phase diagram for a diblock copolymer melt confined between two distinct plates. One of the plates attracts block A and other does not have preferential affinity for either A or B blocks. The interfacial parameters are $\delta_1 = 0.5$ and $\delta_2 = 0.0$

Bibliography

[1] *Processing, Structure, and Properties of Block Copolymers*; Folkes, M. J., ED; Elsevier: New York, **1985**

[2] *Developments in Block Copolymers -1*; Goodman, I., Ed; Applied Science: New York, **1982**

[3] Leibler, L *Macromolecules* **1980**, *13*, 1602

[4] Fredrickson, G.H. and Helfand, E. *J. Chem. Phys* **1987**, *87*, 697

[5] Helfand, E.; Wasserman, Z.R. *Macromolecules* **1980**, *13*, 994 and the earlier refeerences cited therein.

[6] Semenov, A. N. *Sov. Phys. JETP* **1985**, *61*, 733.

[7] Ohta, T., Kawasaki, K. *Macromolecules* **1986**, *19*, 2621

[8] Ohta, T., Kawasaki, K. *Macromolecules* **1990**, *23*, 2413

[9] Meier, D. J. *J. Polym. Sci., Part C*, **1969**, *26*, 81

[10] Hong, K. M. and Noolandi, J. *Macromolecules* **1981**, *14*, 727; ibid **1981**, *14*, 736; Hong, K. M. and Noolandi, J., ibid **1982**, *15*, 482; ibid **1984**, *17*, 1531; Whitmore, M. D., and Noolandi, J., ibid **1988**, *21*, 2972.

[11] Muthukumar, M., Melenkevitz, J., *Macromolecules* **1991**, *24*, 4199

[12] Muthukumar, M., *Macromolecules* **1993**, *26*, 5259

[13] Schick, M., Matsen, M. W., *Macromolecules* **1994**, *27*, 7157

[14] Olmsted , P. D., Milner, S. T., *Phys. Rev. L* **1994**, *72*, 936; ibid **1995**, *74*, 829

[15] Bates, F. S. Fredrickson, G. H. *Annu. Rev. Phys. Chem*, **1990**, *41*, 525

[16] M. W. Matsen and F. S. Bates *Macromolecules 29.* 1092 (1996), and refrence within.

[17] Hasegawa, H. and Hashimoto, T., *Macromolecules* **1985**, *18*, 589.

[18] Henkee, C. S., Thomas, E. L., and Fetters, L. J., *J. Mat. Sci.* **1988**, *23*, 1685

[19] Coulon, G., Russell, T. P., Deline, V. R., and Green, P. F., *Macromolecules* **1989**, *22*, 2581.

[20] Coulon, G., Collin, B., Ausserre, D., Chatenay, D., Russell, T. P., *J. Physique* **1990**, *51*, 2801

[21] Russell T. P., Coulon, G., Deline, V. R., and Miller, D. C., *Macromolecules* **1989**, *22*, 4600.

[22] Anastasiadis, S. H., Russell, T. P., Satija, S. K. and Majkkrzak, C. F., *Phys. Rev. Lett.* **1989**, *62*, 1852

[23] Anastasiadis, S. H., Russell, T. P., Satija, S. K. and Majkkrzak, C. F., *J. Chem. Phys.* **1990**, *92*, 5677

[24] Coulon, G., Ausserre, D., and Russell, T. P., *J. Phys. France* **1990**, *51*, 777.

[25] Fredrickson, G. H., *Macromolecules* **1987**, *20*, 2535.

[26] Brown, G., and Chakrabarti, A., *J. Chem. Phys* **1994**, *101*, 3310

[27] Kikuchi, M., Binder, K., *J. Chem. Phys* **1994**, *101*, 3367.

[28] Brown, G., and Chakrabarti, A., *J. Chem. Phys* **1995**, *102*, 1440

[29] Walton, D. C., Kellogg, G. J., Mayes. A. M., *Macromolecules* **1994**, *27*, 6225.

[30] Turner, M.S., *Phys. Rev. Lett.* **1992**, *69*, 1788

[31] Turner, M. S., Rubinstein, M., Marques, C. M., *Macromolecules* **1994**, *27*, 4986

[32] K. R. Shull *Macromolecules* **1992**, *25*, 2122

[33] Zheng, W. and Wang Z. G. *Macromolecules* **1995**, *28*, 7215

[34] de Gennes, P. G. *The Physics of Liquid Crystals* Clarendon, Oxford, 1974

[35] Wang, Z. G. *J. Chem. Phys* **1994**, *100*, 2298